Non-destructive and Geotechnical Testing of Railway Track Bed Ballast

Max Clark
BEng(Hons)

PhD
The University of Edinburgh
2001

To Father and Mother

Declaration

This thesis, the work discussed and results reported were carried out solely by myself unless otherwise stated within the text.

Max Clark

Edinburgh, December 2001.

Abstract.

The worldwide expenditure on railway track bed is over £3 billion per annum. For example, in the U.K., Railtrack (group) plc is planning to spend £661 million for the year March 2000 – March 2001 on rail track maintenance. One of the causes of the high outlay is the ballast inspection technique they are currently employing i.e. visual inspection of the track with trial pits to identify problem areas. This thesis examines two other techniques to identify the condition of rail track ballast: ground penetrating radar (GPR) and infra-red thermography.

These methods were investigated scientifically and the findings discussed and compared with the current approach and other recognised practices including, conductivity and falling weight deflectometer, to determine their potential to characterise the composition of the track bed ballast.

Basic work was undertaken on ballast durability using the slake durability test.

Laboratory work using (GPR) was undertaken and the dielectric properties of rail track bed ballast were evaluated, using clean and spent ballast with various moisture contents. This was the first study of its kind. These results were examined and verified on a prototype track bed at The University of Edinburgh, where the conditions were known. This showed that GPR could be used to characterise the composition of in-situ railway track bed ballast. GPR was then used in a full-scale working track situation and different areas of clean and spent ballast successfully identified.

Similar laboratory work was also undertaken using infrared thermography on samples of clean and spent ballast. It was found that clean and spent ballast changed temperature at different rates, which agreed with theoretical models. The work undertaken on the prototype track bed and the full-scale working track confirmed these findings. Also the areas of clean and spent ballast identified with GPR were confirmed with infra-red thermography.

This research has shown that GPR and infra-red thermography are appropriate techniques to obtain the characteristics of the composition of railway track bed ballast. Both techniques found the same anomaly on the full-scale working track: a patch of spent ballast within an area of clean ballast. These techniques are faster and more cost effective than current methods of ballast investigation.

Acknowledgements

Firstly I would like to thank Prof. Mike Forde for his insight and guidance throughout this project. His constant encouragement has been appreciated.

The constant support and expert advise of my second supervisor Prof. Dave McCann on his many visits to Edinburgh and at other times by telephone and e-mail contact.

I am very grateful to the British Geological Survey for lending the slake durability test equipment.

Thanks must go out to the colleagues from my department who have encouraged and advised me, over a number of issues, Kevin, Mike and David. To Justin who has been a good friend throughout my time at Edinburgh University.

I wish to express my thanks to Jason, Gina, Simon and Susan for having to put up with painstakingly proof read my work through these last months.

I would also like to thank Susan for her constant companionship and friendship throughout my PhD.

Table of Contents

Chapter 4: Non Destructive Techniques

Table of Figures

Table of Tables

Chapter 1.

Introduction.

1.1 Development of the Rail Network

The railways in the United Kingdom (UK) were originally built in the 1830s and 1840s. They were designed to carry trains travelling at speeds no faster than 50mph. However, on the UK's busiest rail route (West Coast Main Line (WCML) operated by Virgin Rail Group ltd), which handles more than 2,000 vehicles per day, modern InterCity passenger trains regularly travel at over twice this speed. The Victorian design of the WCML is characterised by tight curves, unlike the East Coast Main Line (operated by Great North Eastern Railway ltd), which is characterised by straighter and faster track. In the UK, Railtrack (group) plc and Virgin Rail Group ltd plan to decrease the journey time and increase reliability on the WCML. To do this, significant improvements need to be made to the existing track and foundations. Other rail networks across the world are facing similar problems.

Although the current UK railway network dates back to 1830, the first railway lines were built in 1604-05 for transporting coal from the pit face to navigable water. Examples of these lines have been found at Wollaton, Nottinghamshire and at Broseley in Shropshire. Timber rails were used on all these early lines, although some had thin iron plates laid over the rail surface for protection. The first wholly iron rails were used at Coalbrookdale in Shropshire in 1767. These enabled trains to carry heavy loads. The trains were moved by horses, men or under gravity. It was not until 1804 that the first locomotive was designed by Richard Trevithick, although

this proved to be too heavy for the delicate track. Eighteen years later in 1822, George Stephenson demonstrated convincingly that railways could be operated, at least in part, by locomotives. By 1835 the railway network had been constructed to transport passengers in addition to goods. The network grew throughout the 1830s and 1840s. In 1836 the Eastern Counties Railway was built, from London to Colchester. This was considered to be one of the worst of the early train services. In the early years of the rail network, independent companies built the railway lines in order to return a profit.

By 1843, a number of small companies were in operation, such as the Liverpool & Manchester, London & Birmingham, Grand Junction and Stockton & Darlington. These small companies started to merge into larger companies, but each operated on different gauge lines. For example, the Great Western railway had a 7ft gauge, the Eastern Companies a 5ft gauge, while Ireland had a 5ft 3in gauge, which remains today. This caused much annoyance as passengers had to change trains and goods were damaged in transportation. The wide gauge of 7ft was advantageous as the ride was more comfortable and the trains could run faster. If this gauge was standard today there would be less speed limitation to the train.

In 1846, Parliament decided that 4ft 8½ in should be the standard gauge and all new track should be built to this specification. 1852 saw the completion of all the principle main lines of the modern railway system of England and work on the Great North of Scotland line began. In 1862 Parliament passed a law forbidding further mergers of train companies. The last of the new main lines to be constructed was the

Great Central Line, built in 1899 from London to Sheffield and Manchester. While this new line was never profitable it was part of a greater concept, linking Manchester to Paris through London and Dover.

Throughout the twentieth century, unprofitable parts of the railway network were 'cut-off' and fell into disrepair. In 1938, the Great Western Company considered electrifying its main line from Taunton to Penzance. This was rejected just before the outbreak of the World War II. Under the Labour Government in 1947, the railways were compulsorily purchased by the State and the British Transport Commission was born. This expanded the network in Scotland as well as in Wales, which was initially built before the 2nd World War. (Simmons J (1961)).

Following privatisation in the 1990s, Railtrack plc was created. It owns all 32,000 km of track in the UK.

1.2 Use of Aggregate as Ballast

Currently, over the UK network, more than 400 million tonnes of aggregate are used as ballast. Railtrack plc plans to spend £1,340 million on track renewal over the year March 2000 – March 2001. 648 km of ballast will be renewed and £661 million will be spent on maintenance in this period.

Ballast is an important factor in efficient operation of railways, as it affects the performance of track foundations. On the WCML, large sections of ballast need to be replaced each year. The current method of determining the condition of the

ballast is visual identification by local 'permanent-way' staff walking the length of the track looking for anomalies. When these anomalies are identified, the 'permanent-way' staff schedules a date to return to the site up to 6 months after the initial survey to dig a trial pit for further investigation. As a result, many trial pits are dug along the length of the track, enabling the in-situ condition of the ballast to be assessed. There are two main problems with this method of visual inspection; it is time consuming and the ballast is only inspected on the surface. The anomalies will only appear on the surface when the condition of the ballast has deteriorated significantly. Trial pits are dug at night to lessen the impact on the operational timetable of the line. However this still causes disruption, as even during the day trains must reduce speed over the inspected track while the disturbed ballast compacts. In addition to being reactive and condition driven, this method of detecting anomalies is very expensive, as the work is conducted at night. This increases the cost of the inspection. The permanent way staff also have a limited 'time window' to conduct the track inspection before the trains recommence operations.

Once an anomaly in the ballast has been identified, a timetable for tamping and stoneblowing is drafted. Tamping and stoneblowing involves maintenance machines. They pack the ballast under the sleepers and blow fresh ballast under the sleepers respectively. Historical ballast inspection was similar to the current practices apart from the replacement of ballast. They had to pick up the rails manually and shovel the ballast in place, this was very labour intensive.

It can take 6 months before any anomalies are examined, and rectified. Therefore the total time from identifying the anomalies to repairing the track could be over a year, increasing the need for ballast replacement, as the degree of ballast deterioration may not be amenable to tamping. It follows that the rail industry requires a modern, inexpensive and efficient scientific technique to measure objectively, the condition of the ballast.

Anomalies within the ballast tend to occur in areas where the ballast has degraded and deteriorated, becoming 'spent' or 'dirty'. This spent ballast results from:

- The ballast particles rubbing together and abrading as the train runs over the track.
- Infiltration of soil particles from the surrounding area.
- Mud pumping and capillary action from below.
- Waste from the train.
- Other items from the train such as brake dust.

These create small particles (fines) which affect the quality of the ballast. Fines fill up the air voids between the large ballast particles.

The ballast gives the track a level and uniform surface to support the train, resulting in a safe and comfortable ride. If the surface of the track varies there is a danger that the train will derail at greater speeds.

Air voids in the ballast allow water to drain away. If fines build up within these voids, water can collect there. This leads to an increase in pore water pressure, resulting in a decrease in the overall strength of the ballast layer.

In spent ballast the shear strength in total stress may be described using the Mohr-Coulomb equation:

$$\tau = c + \sigma \tan\phi$$

Where: τ = shear strength

c = cohesion intercept

ϕ = angle of shearing resistance

σ = normal stress on the failure plane

In saturated conditions, under immediate undrained loading it can be shown (Bishop and Henkel, 1962) that

$$\phi_u = 0$$

where the subscript *u* refers to undrained condition.

Therefore: $$\tau = c_u$$

From Terzaghi's principle of effective stress (Terzaghi, 1943) for saturated soils, the effective normal stress can be described as the total normal stress minus the pore water pressure:

$$\sigma^1 = (\sigma - u)$$

where u = pore water pressure

Thus in terms of effective stress in fully drained conditions (Bishop and Henkel, 1962)

$$\tau = c^1 + \sigma^1 \tan\phi^1$$

where: c^1 and ϕ^1 are the shear strength parameters in terms of effective stress.

For a remoulded soil or ballast, where any cementation or stress history is destroyed,

$$c^1 = 0$$

Therefore: $$\tau = \sigma^1 \tan\phi^1$$

Therefore: $$\tau = (\sigma_0 - u)\tan\phi^1$$

Where: σ_0 = initial total normal stress

Assume a total normal stress increment ($\Delta\sigma$) is imposed upon the spent ballast by one wheel of a train. So as the first wheel passes over the saturated ballast the additional total normal stress is carried on the pore water:

$$\tau = ((\sigma_0 + \Delta\sigma) - (u_0 + \Delta\sigma))\tan\phi^1$$

After the first wheel has passed some plastic shearing occurs resulting in a build up of pore water pressure. Which may be described as follows:

$$\tau = (\sigma_0 - (u_0 + a_1 \cdot \Delta\sigma))\tan\phi^1$$

After the second wheel passes over the ballast, further build up of pore water pressure occurs:

$$\tau = (\sigma_0 - (u_0 + a_{11} \cdot a_1 \cdot \Delta\sigma + a_2 \cdot \Delta\sigma))\tan\phi^1$$

Where: a_1 = the residual pore pressure factor after the first pass

a_{11} = the residual pore pressure factor to be applied to the residual pore pressure factor after the first pass - after the second pass.

a_2 = the residual pore pressure factor resulting from the second pass alone

The above simple deduction indicates decreasing shear strength with increasing number of passes. This may led to a weakening of the ballast.

1.3 Purpose of Research

According to Huille, & Hunt, (2000) problems with the track bed are 70% due to the subgrade and 30% due to the ballast. This thesis focuses on the ballast rather than the subgrade and will concentrate on non-destructive testing (NDT) aspects and techniques, as well as the aggregate testing of ballast to determine the compositional properties rather than the stiffness of the ballast.

The overall objective of this work was to produce a method of high-speed assessment of railway track ballast in-situ. Thus the overall hypothesis to be tested is that NDT techniques can discriminate between clean and spent ballast both in a laboratory environment and in the field.

In Chapter 2, reviews current UK and international practice in the engineering assessment of the track structure. It introduces some areas of ballast identification which we researched in more detail later in the thesis.

In Chapter 3, focuses on ballast used in the laboratory experiments reported in this thesis. Various classification tests are reported, although some of the results (such as

density) are not a prerequisite to the main NDT thrust of the thesis. The slake durability test data is of special interest, as is the proposed new specification for Railway Ballast both new and renewal.

In Chapter 4, the most appropriate NDT methods are reviewed, namely ground penetrating radar (GPR) and infra-red thermography.

In Chapter 5, reports on laboratory modelling of radar and infrared thermography. For the first time data is made available on the electrical permittivity of ballast.

In Chapter 6, reports NDT work undertaken on the pilot scale railway track which was built, to the current Railtrack standards, at the University of Edinburgh.

In Chapter 7, the findings from the laboratory calibration and test track experiments, were tested in a full scale field trial at Ingatestone, East Anglia.

Finally Chapter 8,.contains the conclusions and recommendations for further work.

Chapter 2

Current Practice In Engineering Assessment of The Track Structure.

2.1 Track Components.

Figure 2.1 illustrates the main components of a typical track structure. These components can be divided into two groups:

i) the superstructure which consists of the rails, fasteners and sleepers.

ii) the substructure which consists of the ballast, subballast and the subgrade layers.

The functions of each of these components are described in sections 2.1.1 and 2.1.2.

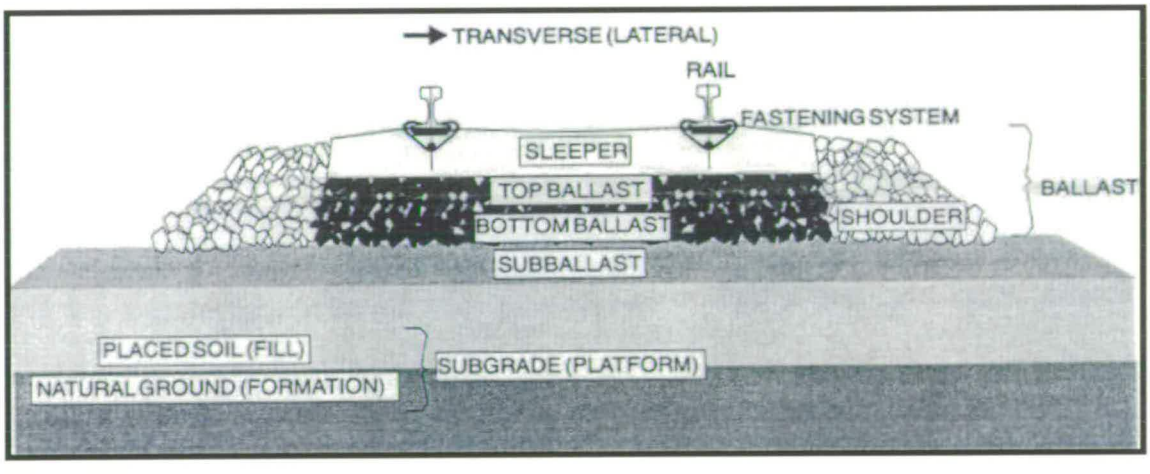

Figure 2.1 - Track Structure Components (based on Selig & Waters (1994)).

2.1.1. Superstructure

- Rails - The rails are the steel members which guide the train wheels evenly and continuously along the track. Welding or bolting connect these steel members

together but, either way, the rail must provide sufficient stiffness to carry and distribute the concentrated wheel loads evenly to the sleepers without causing excessive deflections. Defects in the rail profile can result in dynamic loads (see section 2.3.1) where the wheel applies a continuously varying load as it travels along the track. Ultimately, this can cause differential track settlements and possible derailments.

- Fastening System - The fastening system connects the sleeper and rails, providing them with the ability to resist vertical, lateral and longitudinal rail movements. Such rail movements are caused by the application of wheel loads as well as the thermal expansion and contractions resulting from temperature fluctuations. The fastening system also damps the vibrations induced by the wheel loads.
- Sleepers - The main role of the sleepers is to distribute the loads from the rails evenly into the ballast layers at acceptable stress levels. Additionally they also hold the fasteners and rails at the specified gauge (the spacing between the inside faces of the rails) during periods of loading, as well as resisting lateral, longitudinal and vertical rail movement by anchoring the superstructure into the ballast layer. In the United States sleepers are referred to as ties (tying the rails together).

2.1.2 Substructure

2.1.2.1 Ballast

In the Introduction, it was stated that the ballast must perform many important functions. The most important of these are summarised in Selig & Waters (1994) and Bonnett, (1996) as follows:

- Reduce stresses applied to the weaker subgrade.
- Resist vertical, lateral and longitudinal forces applied to the sleepers and maintain track position.
- Provide a source of damping and resilience to the track.
- Facilitate track maintenance operations such as tamping, stone blowing and ballast cleaning (see section 2.4.2).
- Provide immediate drainage of water from the track structure.
- Provide large voids in which fouling material can be stored.

Other important functions of ballast are the alleviation of frost problems by enabling the drainage of water, prevention of vegetation growth and the provision of electrical resistance between rails.

The preferred choice of ballast is generally crushed angular stone. However, proper subgrade conditions are required before ballast conditions can be optimised. As stated in the "Introduction" section, considerations of the subgrade are outwith the scope of this thesis.

During service, traffic load and the environment breakdown the original gradation of ballast into a wider range of sizes. To minimise these effects, a hard durable rock with particle sizes in the range of 19 mm to 64mm is generally considered ideal. The larger sizes are required for stability, the smaller sizes for reducing the contact forces

between particles. While this is a commonly adopted size range, traditional distributions are generally more well graded than would be regarded as ideal. More uniform ballast has a higher porosity and so can accommodate more fines before fouling decreases performance. However, the well-graded ballast tends to collect fines more easily. The main disadvantage of a wider gradation is particle segregation during maintenance and handling.

The durability characteristics of ballast are assessed by index tests such as impact resistance, crushing value and hardness. Each railroad has a set of ballast specifications which stipulates limits for the values from the index tests.

The ballast layer may be subdivided into four groups, some of which may be seen in figure 2.1.

i). Top Ballast - This is the upper region of ballast, which is disturbed by tamping.

ii). Bottom Ballast - This is the lower region of ballast which is generally the most fouled portion.

iii). Shoulder - The material beyond the sleepers which extends to the bottom of the ballast layer.

iv). Crib - The ballast material between the sleepers.

Despite the importance of ballast, much is still unknown about the factors, which affect its performance. As a result, choice of ballast type, gradation and layer thickness are often governed by tradition, availability of material or simplified guidelines which may not always encompass all of the important factors.

2.1.2.2 Subballast

The subballast is the layer between the ballast and the subgrade. Its main functions are:

- Reduce traffic-induced stresses from the ballast layer and distribute them into the subgrade.
- Provide frost protection to the subgrade.
- Reduce the required thickness of the more expensive ballast material.
- Provide an interface which reduces the migration of fines from the subgrade to the ballast layer.
- Intercept water from the ballast layer and direct it away from the subgrade to ditches located at the side of the track.

2.1.2.3 Subgrade

The main function of the subgrade is to provide a stable foundation to the track structure, which is capable of carrying the stresses distributed to it by the subballast. The stiffness of the subgrade influences the rate of ballast, rail and sleeper deterioration. Additionally it is also a source of differential settlement (Huille, and Hunt. (2000)).

2.2 Fouled Ballast.

Degradation or fouling of ballast is a result of breakage due to mechanical wear and vibration by the train mechanisms, chemical wear due to pollution and weathering and an infiltration of fines from the surface to the subgrade. As the voids in the original clean ballast become filled with particles of 0.075mm diameter or less (fines), the ability of the ballast to fulfil its requirements satisfactorily will diminish. In the advanced stages of this process, when fines account for around 10% of the total mass, the ballast is said to be spent. The most commonly observed problems due to fouling are restriction of drainage and interference with track maintenance. However, as the voids become completely filled with fines the ballast begins to take on the characteristics of these fines. For example, during wet conditions the fines begin to take the characteristics of mud resulting in the bed softening and deforming. When such wet fouled ballast freezes, resiliency is lost. Moreover, when the fines dry, they tend to bind with the crushed rock particles, again resulting in a loss of resiliency, this is known as cemented ballast. (Selig & Waters (1994))

Figure 2.2 - Comparison Between Spent and Clean Ballast.

Figures 2.2a and 2.2b provide a visual comparison between spent and clean ballast respectively. The spent ballast is gap graded (see section 2.3).

From a series of analytical modelling and laboratory box tests undertaken at the University of Massachusetts, it was found that, for a ballast mass applied with a repeated axle load, the ballast degradation and settlement increased as the average particle size was increased (Selig, 1985). Degradation mostly occurred in the 6 inches beneath the sleepers and increased with increasing wheel load. However, the maximum amount of fine particles generated in the tests was c.1.6% of total ballast mass. This suggests that mechanical wear alone is insufficient to cause fouling.

2.3 Compaction and Settlement of Ballast.

2.3.1 Principles

When track maintenance is required to correct irregularities, the spent ballast is in a dense state, particularly beneath the sleepers.

Traffic is the most effective means of compacting clean ballast under the sleepers, but this takes time and can result in differential settlements. Settlement of ballast is highly variable, even under strict test conditions where samples are carefully prepared and identical loads are applied, i.e. since ballast is a random arrangement of stones, the settlement that occurs under a given load is also random. Figure 2.3 shows the vertical profile along one rail of a typical section of track.

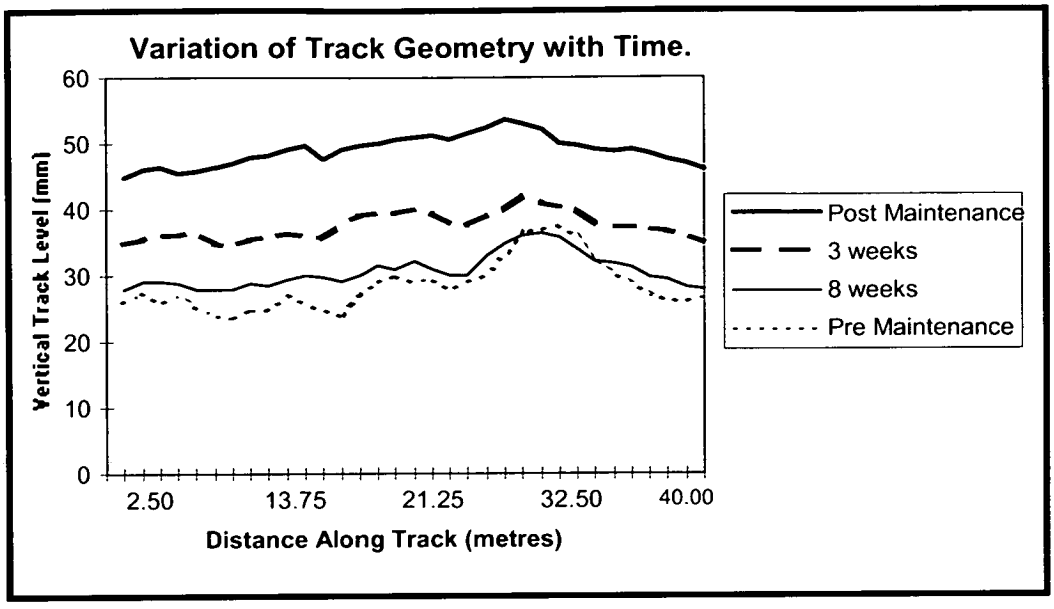

Figure 2.3 - Variation of Track Geometry with Time (Shenton (1975)).

Each of the lines in figure 2.3 indicates the profile at a given time. The track movements are greatest in the period soon after maintenance using tamping machines. After this first rapid movement, the rate of settlement and deterioration reduces. In general, a given section of track will have a tendency to deteriorate towards a given shape. This could be attributed to the "inherent quality" of the track which is determined during the early part of its life by the quality of construction work and materials used (Shenton (1984)).

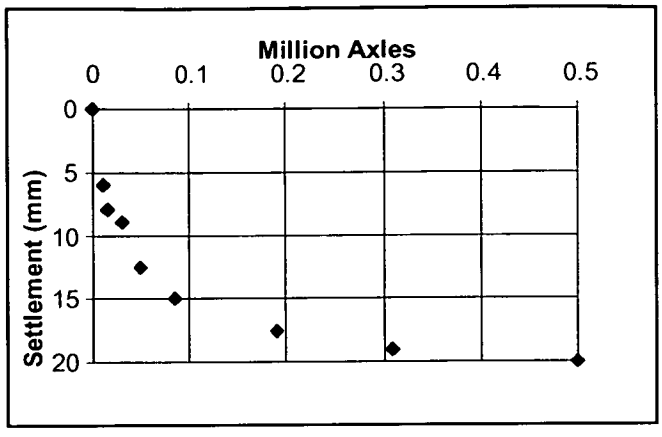

Figure 2.4 - Variation with Traffic Intensity (Shenton (1975))

Figure 2.4 illustrates the principles of this settlement time relationship more clearly in terms of traffic density. The rapid settlement following tamping and the decreasing rate of settlement thereafter is clearly evident. After approximately half a million axles passes, additional settlement is barely noticeable (Shenton (1984)). It was not possible to achieve this level of compaction in the laboratory tests, as it was not possible to run trains over the test-rig.

In addition to the frequency and intensity of load cycles, there are many other factors which influence the total amount of differential settlement.

- Substructure - Differential settlements may be caused by deterioration in the deeper ballast and the sub grade. These settlements are usually negligible as long as the foundation has been adequately designed. Shenton (1975)
- Dynamic Forces - A continuously varying vertical load from a wheel along the track bed can occur due to irregularities in the running surface of the wheel or irregularities in the vertical geometry in the track bed.
- Ballast Type and Condition - From section 2.2 it is clear that as ballast becomes fouled over time, it is no longer able to fulfil its requirements satisfactorily.

Interference with track maintenance, drainage restrictions and loss of resiliency are all problems associated with fouled ballast.

- Rail Shape - Uneven distribution of loads can result from defects in the longitudinal shape of the rail arising during the manufacturing process or from misalignments produced at welds.
- Sleeper Spacing - Within a section of track the closer together the sleepers are spaced, the less load each sleeper will carry, resulting in reduced settlements. Variations in sleeper spacing along the line may also cause non-uniform disruption to the ballast.
- Axle Load – Under normal operational activities settlement is approximately proportional to the axle load. However for very high axle loads, settlement may be approximately proportional to the square of the axle load. The point at which this transition takes place is not known. Shenton (1975)
- Mixed Axle Loads - When there are two axle loads, it is the larger which dominates the ballast deformation. For example if the smaller load is less than 50% of the larger it produces insignificant deformation. Shenton (1975)

Although the above discussion examines the causes of settlements in isolation, there are clearly many interactions to be considered which make settlement predictions very difficult. The settlement of the sleeper can also be determined by calculating the dynamic loads on the section of track. The resulting deteriorated shape of the track can then be used to re-calculate new dynamic loads and by a repetition of this procedure the development of track deterioration can be simulated (Shenton, 1975).

2.3.2 Methods of Track Maintenance.

2.3.2.1 Tamping Machine

Combined tamping and lining machines carry out routine maintenance on most railways. By comparing the attributes of an existing track with those of a designed track, an onboard computer is able to guide the machine in raising the rail and sleepers to a predetermined level using hydraulic arms. The tamping arms penetrate the ballast at the rail/sleeper interface and squeeze up under the sleeper to retain it in the raised position. This tamping process disturbs the compact nature of the ballast and leaves it in a loosened state resulting in renewed settlement as traffic re-compacts the ballast (Coombs. (1971), Selig. & Waters (1994)). This method is particularly suitable for maintenance requiring a large lift associated with long wavelength faults. The latest generation of tamping machines has a higher level of accuracy when re-aligning and is capable of higher speeds (Ehara (1999)). However, since tamped ballast tends to return to its pre-tamped state, tamping machines are unable to perform around junctions as the gaps between the rails narrow and they can buckle the rails (Markine & Esveld (2000)).

2.3.2.2 Stoneblower

The stoneblower adjusts track geometry by adding new ballast to the surface of the existing ballast. The process involves measuring the existing geometry of the track. The precise track lift required at each sleeper to restore the track geometry is determined. The volume of ballast required to achieve such a lift is calculated, i.e. the volume which, when compacted, will provide the required volume increase. The sleeper is then lifted to the required level by hydraulic arms while stoneblowing tubes are driven down alongside the sleeper. The measured quantity of ballast is blown down the tubes and into the voids underneath the sleeper. The stoneblowing tubes are removed and the sleeper replaced. This method is particularly suitable for low lifts associated with short wavelength faults. (Coombs (1971), Selig & Waters (1994)). The major advantage of stoneblowing is that the effects of stoneblowing last longer than that of tamping (Collinson (1998)), however stoneblowers cannot lift the rails more than 50mm. Additionally, as stoneblowing inserts smaller rock particles into the ballast, rendering it heterogeneous, it is not possible to tamp a stoneblown track Selig & Waters (1994).

2.3.2.3 Ballast Cleaner

As previously mentioned, the ballast becomes increasingly fouled with dirt over time until it is either necessary to clean the ballast or replace it. The ballast cleaner has an excavation chain which, as the cleaner moves forward, removes the ballast from beneath the track. The ballast is directed by the excavation chain to a series of vibrating screens, which separate the dirt from the ballast. The dirt is then conveyed away and the clean ballast returned to the track (Coombs (1971)).

2.4 Track Stresses

Because the ballast mass is composed of relatively large diameter particles and behaves more like a complete structure than its individual components, the distribution of stresses developed beneath the sleepers is difficult to determine. If, for example, a 300mm deep layer of ballast comprising of 25-50mm diameter particles is acted upon by a sleeper of 250mm width, the number of particles involved in supporting the sleeper is relatively small. Only 100-200 contact points may support a sleeper that has been in the track for some time. As a result, measurement of accurate pressures in the ballast is extremely difficult. The stress conditions were measured rather than defined, by using pressure cells mounted along the base of a sleeper and load cells buried just below the bottom of the ballast layer. These measurements were made for a range of different depths (Shenton (1975)). Figure 2.5a illustrates these findings.

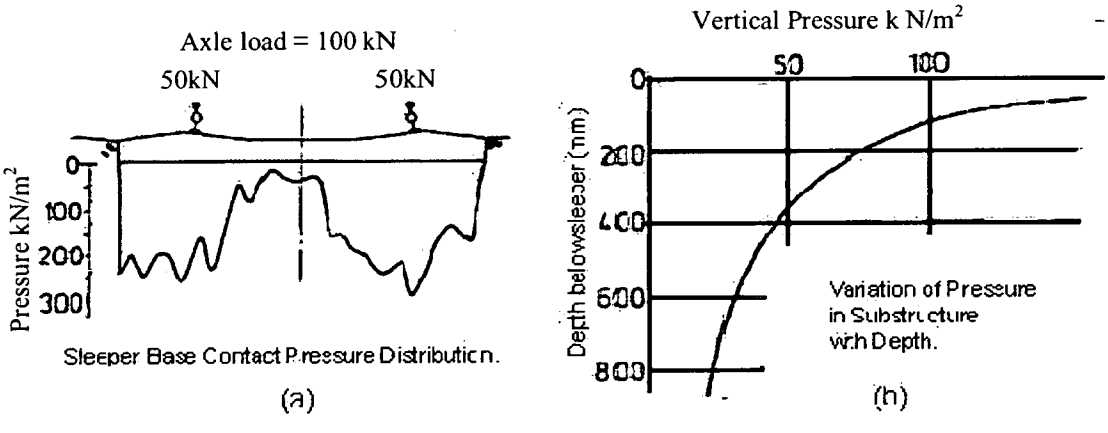

Figure 2.5 - Typical Pressure Distributions (Shenton (1975))

The contact pressure distribution is very erratic and varies greatly from test to test. However, the concentration of ballast packing under the rail-foot area (the normal maintenance practice), can usually be observed. Variation of vertical pressure with depth in the ballast mass can be approximated from Fig 2.5b. This has been found to closely follow the Boussinesq stress distribution (Shenton (1975)).

2.5 Improvements in Track Performance.

It is possible to construct beds with low rates of deterioration assuming that there are no problems with the formation. To achieve this, it is necessary to have ballast with uniform settlement properties and straight rails. By controlling these two factors the variations in dynamic loads for the traffic can be controlled (Selig (1985)). Work on the settlement of ballast has identified the importance of having a properly prepared and consistent track foundation with sufficient depth to limit deflections. On existing tracks, selective packing under the sleepers can reduce differential ballast settlement. For new construction, improved methods of preparing consistent ballast bed are required.

Differential settlements produced by traffic compaction are clearly undesirable. Therefore, construction and maintenance methods are needed which place ballast in the track without segregation and compact it to a state equivalent to the effects of traffic while maintaining surface alignment. Once placed and compacted, ballast beneath the sleeper should be left undisturbed until it needs to be cleaned.

2.6 Strength Parameters of Ballast.

A number of properties of the ballast can be analysed to assess whether or not a section of ballast has passed its useful life. There are many different British Standard tests that can be carried out to determine properties of the ballast. These tests are detailed in table 2.1. While table 2.2 lists similar American Standard tests. It can be seen from table 2.2 that the American Standards have different tests than the British Standards.

Type of Test	British Standard
Density and Absorption	BS 812: part 2: 1995
Particle Size Distribution	BS 812: part 103: 1985
Flakiness Index	BS 812: part 105: 1989b
Elongation Index	BS 812: part 105: 1989a
Moisture Content	BS 812: part 109: 1990d
Aggregate Crushing Value	BS 812: part 110: 1990b
Ten Percent Fines Value	BS 812: part 111: 1990e
Aggregate Impact Value	BS 812: part 112: 1990c
Aggregate Abrasion Value	BS 812: part 113: 1990a
Polished Stone Value	BS 812: part 114: 1989d
Water Soluble Chlorides	BS 812: part 117: 1988b
Sulphate Content	BS 812: part 118: 1988a
Soundness	BS 812: part 121: 1989e
Frost Heave	BS 812: part 124: 1989c

Table 2.1 List of British Standards Relating to Aggregate Testing

Type of Test	American Standard.
Accelerated Polishing of Aggregates Using the British Wheel	ASTM D3319 1997a
Aggregate Durability Index	ASTM D3744 1997b
Bulk Density	ASTM C29/29M 1997c
Degradation of Fine Aggregate Due to Attrition	ASTM C1137 1997d
Index of Aggregate Particle Size and Texture	ASTM D3398 1997f
Lightweight Particles in Aggregates	ASTM C123 1996a
Resistance to Degradation of Large-Size Coarse Aggregate by Abrasion and Impact in the Los Angles Machine	ASTM C535 1996b
Sieve Analysis of Fine and Coarse Aggregates	ASTM C136 1996c
Specific Gravity and Absorption of Coarse Aggregate	ASTM C127 1993
Surface Moisture in Fine Aggregate	ASTM C70 1994

Table 2.2 List of American Standards Relating to Aggregate Testing

One of the most important properties of the ballast is its strength and resistance to crushing. For this reason, five tests (explained below) were selected from the list of British Standards, which determine these properties, and how they vary between clean and spent ballast. These specific tests were selected as the University did not have the appropriate equipment to undertake the other mechanical tests mentioned above. The significance of these five tests is that they all model the wear of the ballast, while some of the others do not. The wear of the ballast is one of the factors that determines the speed of deterioration.

Even though it is not one of the British or American Standard tests, the Slake Durability test was investigated as part of this research because there does not appear to be a durability test which tests the ballast over a long period of time. Additionally the Slake Durability test models the action of the train passing over saturated ballast better than the other standard tests. As the Slake Durability Test (SDT) is a constant abrasion test conducted over runs of over 16 hours, this is similar to the wear of constant train traffic. Bell, Culshaw & Cripps (1999) reviewed selected geophysical test on chalk, including the Slake Durability test, the test methods described and results found were used when deciding what test to undertake as part of this study.

There are many other tests for particle characteristics. Many of these have been undertaken and documented in America and form part of the American Standards in table 2.2, and are summarised and outlined in table 2.3.

Test For Ballast Particle Characteristics
DURABILITY • Los Angeles abrasion • Mill abrasion • Deval abrasion (wet and dry) • Clay lumps and friable particles • Crushing value • Impact
SHAPE AND SURFACE CHARACTERISTICS • Flatness • Elongation • Hericity • Angularity or roundness • Fractured particles • Surface texture
GRADUATION • Size • Size Distribution • Fine particles content
UNIT WEIGHT • Specific gravity • Absorption • Rodded unit weight
ENVIRONMENTAL • Freeze-thaw breakdown • Sulphate soundness
CEMENTING CHARACTERISTICS
IDENTIFACTION AND COMPOSITION • Petrographic analysis • Chemical analysis • X-ray diffraction

Table 2.3 Test for Ballast Particles Characteristics. (Based on Selig & Waters (1994))

The findings of the above tests are that:

"On the basis of strength considerations, broader ballast graduations are better than narrow graduations. However, other factors such as durability, fines storage volume, size segregation and maintenance must also be considered in selecting graduation.

More research on these factors is needed before an optimum grading can be established." (Selig & Waters (1994))

Until 1986, the bases of the AREA (American Railway Engineering Association) specification for ballast limited the amount of flat or elongated particles (length to thickness ratio greater than 5) to 5% by weight. [From 1997 AREA became the AREMA (The American Railway Engineering and Maintenance-of-way Association) when it merged with the other railway support association.] However, only very elongated shapes would be eliminated by this specification. After 1986 the AREA adopted the Corps of Engineering definition of elongated particles to be a length to thickness ratio greater than 3. The percentage of such particles still remains at 5% by weight. This requirement is more restrictive, and therefore better, than the previous AREA requirement. This still does not limit flaky ballast, unlike the British standards B.S. Flakiness Index part 105 (1989b), even though both sets of tests are comparable as shown in Phemister and Markwick (1946).

2.7 Petrographic Analysis

Several investigations have attempted to correlate the results of petrographic analysis of the particles with field degradation. The performance of the rock ballast subject to the physical effects of traffic loading and to the chemical and physical effects of weathering depends, to a great extent, on the characteristics of the rock. This can be readily determined by petrographic analysis. Table 2.4 summarises the characteristics identified by petrographic analysis, which, if present in abundance in a rock, may represent "fatal flaws" and cause the rock to be rejected for use as ballast.

Petrographic Properties That May Represent Fatal Flaws	
Properties of Ballast Rock	Principal Deleterious Effect
MINERALOGICAL	
General high content of very soft minerals (e.g. clays, mica, chlorite)	Rapid physical degradation, clay and fine mica-rich fines
Argillaceous sedimentary rocks (e.g. mudstone, shale)	Rapid physical degradation, clay-rich fines
Mica-rich metamorphic rocks (e.g. slate, phyllite, schist)	Rapid physical degradation, clay and fine mica-rich fines
Igneous with deuterically altered feldspar	Rapid physical degradation, clay-rich fines
Sulphide-rich(> about 2–3%) (e.g. pyrite, pyrrhotite)	Oxidtion of sulphide results in acidic conditions prompting chemical weathering of other mineral components
TEXTURAL	
Poor consolidation (in sedimentary and volcaniclastic rocks)	Rapid physical degradation by abrasion; susceptibility to freeze-thaw
High porosity (>~ 5%) in sedimentary rocks	Degradation by freeze-thaw and abrasion if pores are large and abundant
Vesicularity (in volcanic rocks)	Degradation by freeze-thaw and abrasion
Friable texture in crystalline rocks	Rapid physical degradation by abrasion; susceptibility to freeze-thaw
STRUCTURAL	
Closely spaced joints, bedding partings, foliation	Rapid physical degradation by abrasion; susceptibility to freeze-thaw; generation of unsuitable particle shapes

PARTICLE SHAPE AND SURFACE CHARACTERISTICS	
Smooth particle surfaces (often due to rock texture)	Poor mechanical stability
Unsuitable particles shape	Poor mechanical stability; load fracture or elongated or tabular particles.

Table 2.4. Petrographic properties (based on Selig and Waters (1994))

Table 2.5 shows the ballast standards in various countries around the world. It can be seen that there are very few common tests through all the different countries. None of the international ballast tests concentrate on long term durability as can been seen by table 2.5. Therefore the long term slake durability test will be investigated in this thesis.

	Country					
Standard	UK	US	Australian	German	Sweden	Finland
Particle size Distribution	Yes	Yes	Yes	Yes	Yes	Yes
Flakiness Index	Yes					
Elongation	Yes	Yes	Yes	Yes	Yes	Yes
Aggregate crushing Value	Yes		Yes		Yes	Yes
Wet Attrition	Yes					
Los Angles abrasion		Yes	Yes	Yes	Yes	
Nordic Ball Mill Test						Yes
Resistance to Weathering					Yes	
Weak Particles			Yes			

Table 2.5 Comparison of the International Railway Standards. (Railtrack (1998), CP Rail specification for ballast (1987), Track Access (1998), Waldon,. M., (2000), Banverket, (1996), VR (1995))

2.8 American and Canadian Ballast

There have been substantial tests into the best type of ballast to use for railway track beds in America and Canada, (Raymond, & Diyaljee(1979)). They use a number of different types of rock depending on the location. These include Grenville Marble,

through to St. Isodore limestone, Coteau dolomite, Sudburg slag. The Coteau dolomite is very similar in strength to the granodiorite used in this country. These ballast were then subjected to various tests, some of which were conducted in the laboratory. These were the standard North American tests, mill abrasion and the Los Angles abrasion test. The ballast samples were also tested using a triaxial test. The ballast was further tested by placing 10 samples on 10 adjoining 400 m sections of track and subjected to the same load. From the above experiments it was shown that, for the condition and tests undertaken, the top ballast materials were the nickel ore slag (Sudburg slag) and Coteau dolomite (which was the strongest under repetitive loading), whilst the least suitable for use on railway track bed were the limestones.

2.9 Conclusions

- A railway track consists of
    - Superstructure
    - Substructure
        - Ballast
        - Sub-Ballast
        - Sub-Grade
- Ballast is an important part of the track.
- Ballast deteriorates due to a number of mechanisms.
- Tamping, Stoneblowing and Ballast Cleaners are all tried and tested methods of ballast maintenance, all with different advantages and disadvantages.
- Clean and spent ballast has different particle size distributions.

- Spent ballast is gap graded.
- The British and American Standards for aggregate testing are different and neither are complete.
- Every country has its own set of ballast test standards.

Chapter 3

Specification and Testing of Track Ballast.

3.1 Introduction to Ballast:

The ballast used within this study was quarried from the Cliffhill Quarry, Nuneaton, Leistershire. This quarry is the main ballast stone quarry for ARC and Tarmac ltd. All the ballast that Tarmac supplies to the train maintenance companies comes from this one quarry. Cliffhill quarry has been active for over 150 years, producing mainly kerbstones. Rail ballast has been quarried here since 1850. The ballast stone is a granodiorite, a type of granite, with a chemical composition as described in table 3.1.

	Granodiorite from Cliffhill Quarry (Brewer (1999)) %	Referenced Granodiorite (Le Maitre 1976) %
SiO_2	51.5	66.1
Al_2O_2	15.0	15.7
Fe_2O_3	8.9	1.4
MgO	4.6	1.7
CaO	6.8	3.8
Na_2O	2.3	3.8
K_2O	2.2	2.7
Mg_3O_4	0.2	
CO_2		0.1
H_2O		0.8
TiO_2		0.5

Table 3.1 Chemical Analysis of Granodiorite

The granodiorite quarried from the Cliffhill site has very high magnesium oxide (MgO) and iron II ferric oxide (Fe_2O_3) content. This contamination of the granodiorite was due to limestone dust being present at the quarry.

There are other sources of railway ballast in the U.K., one of them being the Meldon Quarry, near Okehampton, Devonshire. This quarry and the surrounding geological area has been thoroughly investigated by Dearman & Butcher (1959), Dearman & El Sharkawi (1965) and Dearman (1958, 1960, 1962 & 1974) to name but a few. Near the granite dyke that runs through the quarry there are many other rock types

particularly limestone, slate and shale & quartzite. Work has been undertaken to investigate the weathering properties of the dolerite found at the Meldon quarry (Dearman (1974)). The granite in that region has a unit density (dry) of 2.61 g/cm^3, a uniaxial compressive strength (dry) of 282 MPa and a porosity of 0.3%.

Igneous rocks, of which granodiorite is one, are formed by the solidification of hot molten rock which has ascended from hot lower levels below the solid crust of the earth. For example, the lava from a volcano is molten rock, which has been forced up to the earth's surface. As one lava-flow is poured out over another, great lava-fields are built up covering hundreds, in some places thousands, of square miles. This process is still occurring today; for example in the shaping of Iceland, but the same process has operated in many areas and at many periods during the history of the earth. In the United Kingdom there are ancient extensive lava outcrops in Snowdonia, the Lake District and in Scotland. Different factors affect the lava as it cools; such as the pressure exerted upon it, the original temperature and the chemical composition of the surrounding rocks, etc. These factors determine the type of granite the cooled lava produces. (Phemister, J and Markwick, A.H.D. (1946), Hall, A (1987), Cox, K.G., Bell, J.D. and Pakhurst, R.J. (1979))

The Cliffhill quarry claims that the granodiorite quarried there has the following values (Brewer (1999)):

Wet attrition values:	3.2-3.6 (max 4)	
Compressive strength	124 MPa	
Uniaxial compressive strength	151 MPa	
Aggregate impact value	13	
Water absorption	0.4	
Aggregate abrasion value	4.3	
Polish Stone Value	55	
Specific Gravity	2.84	(2.72 (Hall, A (1987)))
Loss on ignition	7.2%	

3.1.1 Scanning Electron Microscope Test on Ballast

An investigation was undertaken into determining the nature of the fines in the spent ballast. A representative sample of the fines within the spent ballast was taken. It was washed in an ultrasonic bath and then washed with hydrogen peroxide to dissolve the organic material. It was found that 70 % by weight was organic. The sample was carbon coated and placed in a Scanning Electron Microscope (SEM). In the SEM X-rays were bombarded against the sample and the reflected electrons and backscatter, were imaged. A variety of materials were found within the sample of fines and ballast.

Large amounts of calcite calcium carbonate, quartz, iron rich calcium and clay minerals were found. These chemicals probably came from weathering of the ballast

or were other weathered particles brought in by wind and rain. Other materials found were asbestos (from the brakes of trains), iron and steel (from the trains' wheels) and titanium. The following figure 3.1, figure 3.2 and figure 3.3 are pictures of the fines and ballast samples generated by the Scanning Electron Microscope, while figure 3.4 and figure 3.5 are graphs identifying the sample materials.

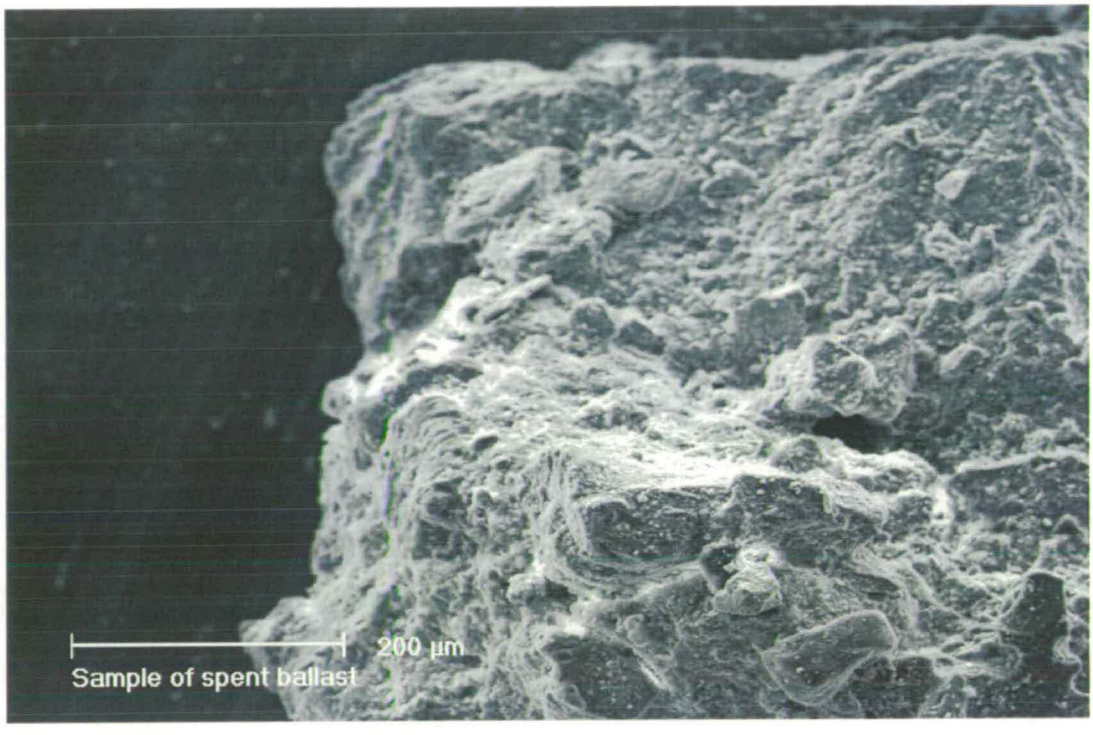

Figure 3.1 SEM picture of a ballast particle

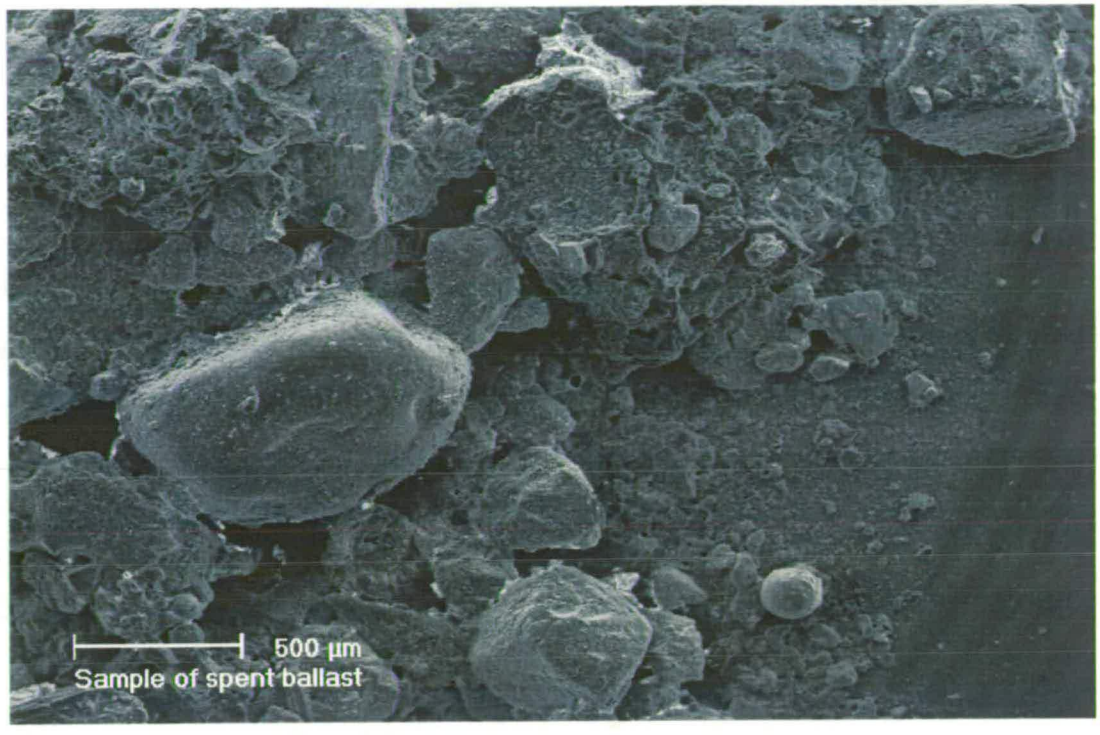

Figure 3.2 SEM picture of ballast particle including metal fragments

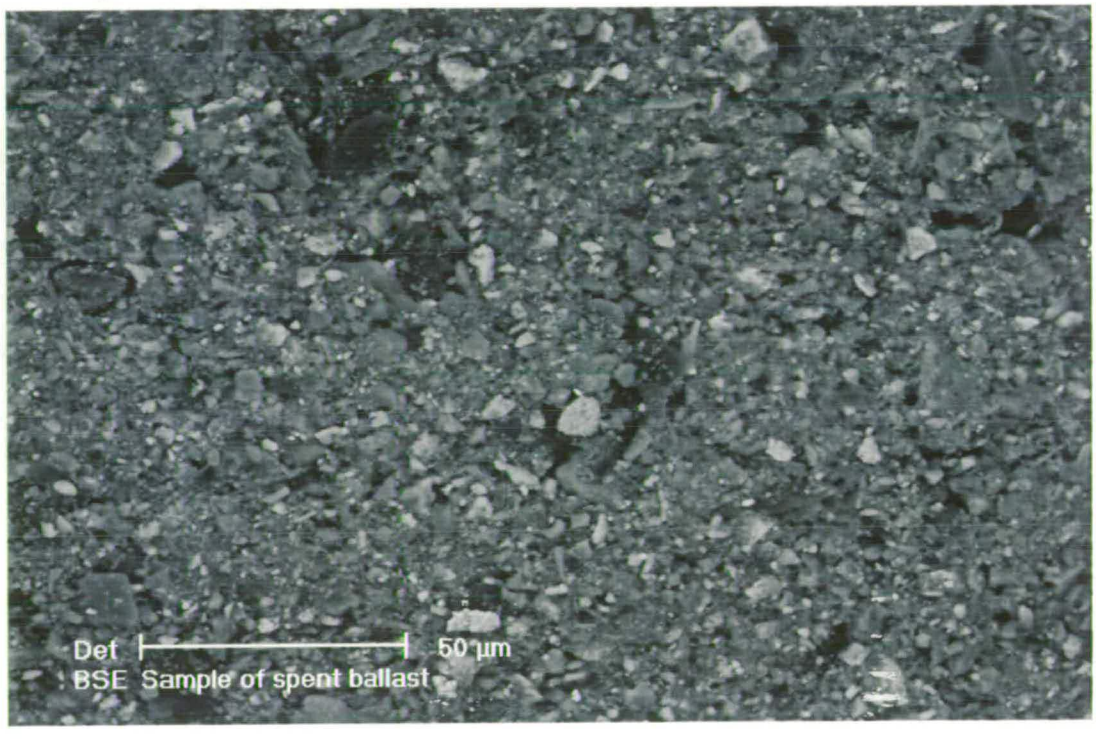

Figure 3.3 SEM picture of the surface of a ballast particle

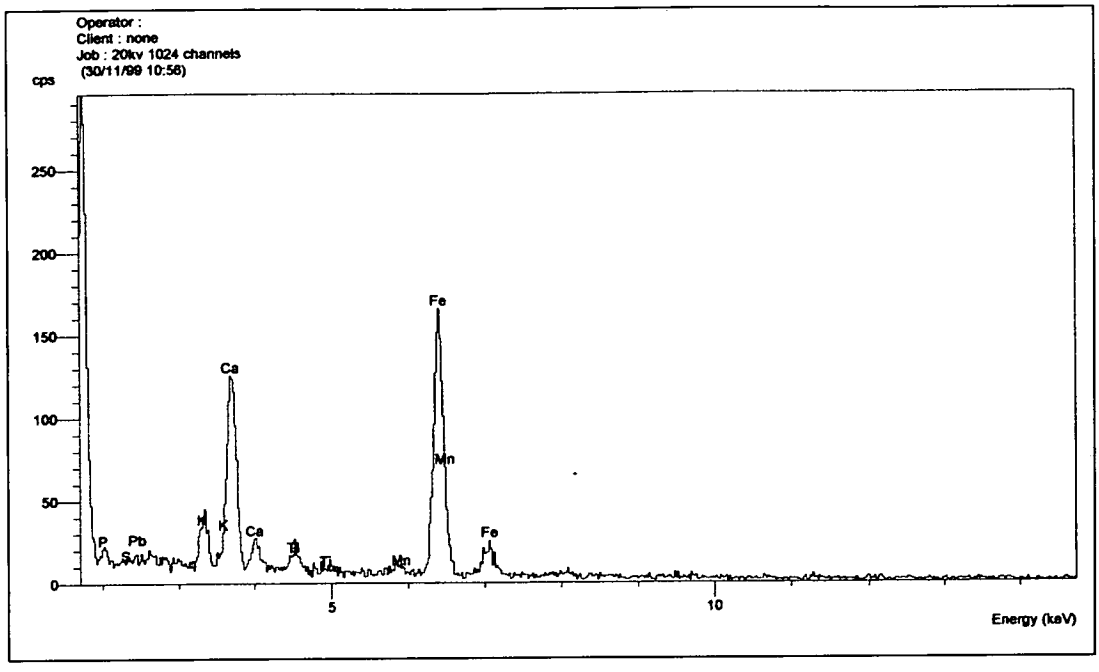

Figure 3.4 Graph of the chemical composition of some of the fines

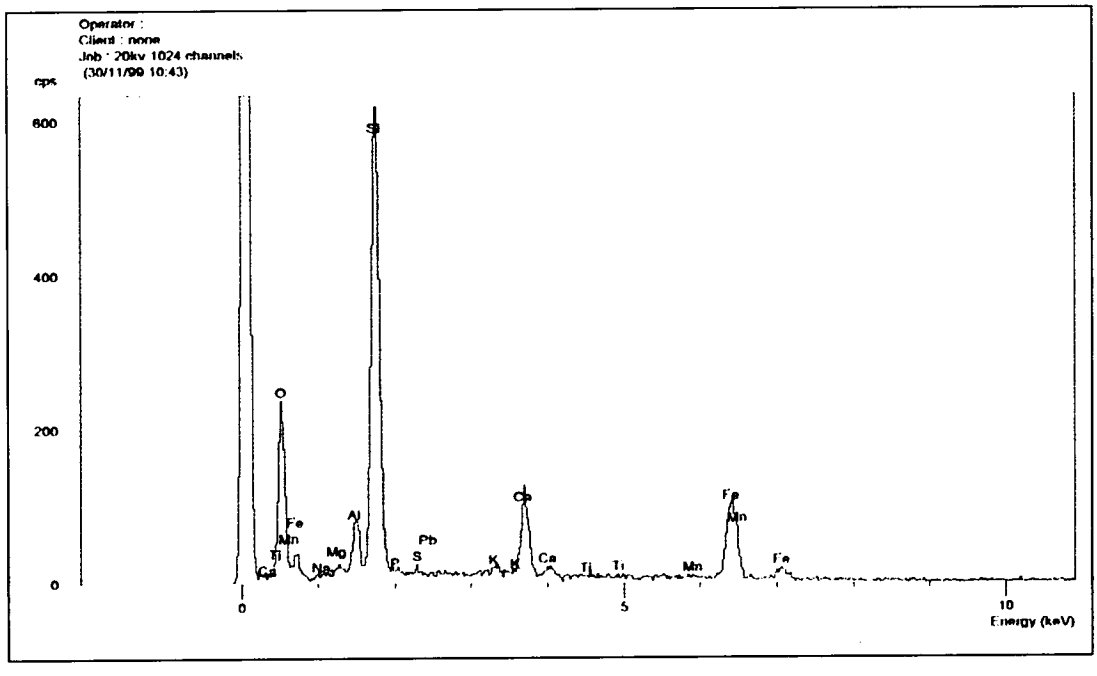

Figure 3.5 Graph of the chemical composition of some of the fines

3.2 Ballast Specification

All the following tests were carried out on ballast obtained from the UK. The current specification for the stone used as ballast of railtrack line, relies on dimensions, flakiness, elongation, aggregate crushing and wet attrition. The current specifications split into two areas; new track ballast (Railtrack Line Specification (1998)) and ballast returned by an automatic ballast cleaner (Railtrack Line Specification (1996)). All the tests carried out in this thesis were undertaken using the current practices and standards. There are new methods that could tell the size, shape and roughness of aggregates based on a 3-d-laser-digitising techniques (Lanaro, Tolppanen, Illerström & Stephansson (2000)) but this was not investigated further as part of this thesis as they cannot calculate the strength of the aggregate. The tests undertaken are specified as follows:

3.2.1 Dimensions

As we have seen in section 2.1.2 and the Introduction, the ballast must perform many different functions, some of which are: reduce stresses applied to the weaker subballast, resist vertical, lateral, and longitudinal forces applied to the sleepers to maintain track position, and to provide drainage of water from the track structure. The sample of ballast used in the laboratory work reported in this thesis, was granite crushed to the specific grading used on the track.

The granite used for ballast in general has a hard abrasiveness resistance value, a high aggregate toughness value as well as a specific gravity (bulk) of about 3.4.

As the name suggests, clean ballast is ballast that is in a new state and condition, and has not been used on the track. Clean ballast is uniformly graded and can be classified as coarse gravel. Clean ballast is also free from all kinds of dirt including oils.

The ballast shall have a consistent mixture of sizes mainly between 28mm and 50mm to conform to the following limits shown in table 3.2:

Square Mesh Sieve (mm)	**Railtrack standard.** Cumulative % by weight passing BS Sieve	**Clean Ballast.** Sample of ballast used in experiments. Cumulative % by weight passing BS Sieve	**Spent Ballast.** Sample of ballast used in experiments. Cumulative % by weight passing BS Sieve
63	100	100	100
50	100-97	97	98
37.5	65-35	50	85
28	20-0	10	65
14	2-0	0	40
1.18	0.8-0	0	0

Table 3.2 Ballast particle size distribution standards

These results may be interpreted more easily on the particle size distribution charts (figure 3.6, figure 3.7 and figure 3.8). All sieve tests were completed as specified in BS812 Section 103 (1985). The actual test weights are to be found in Appendix A.

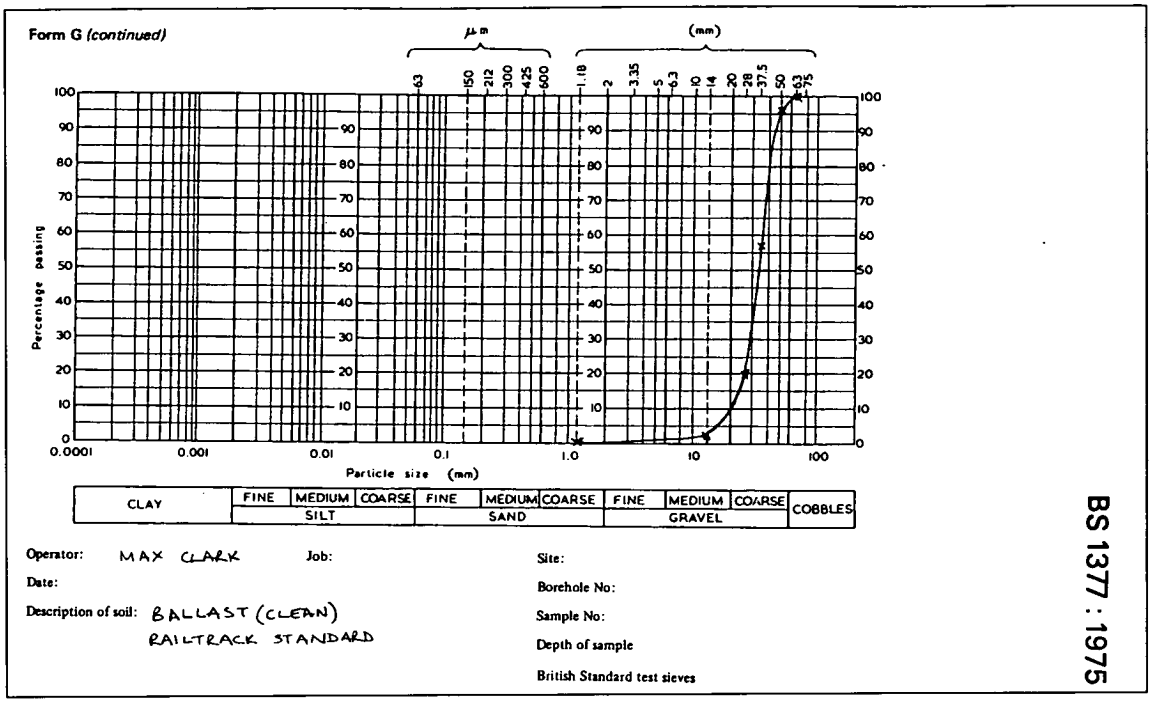

Figure 3.6 Railtrack standard particle size distribution for clean ballast.

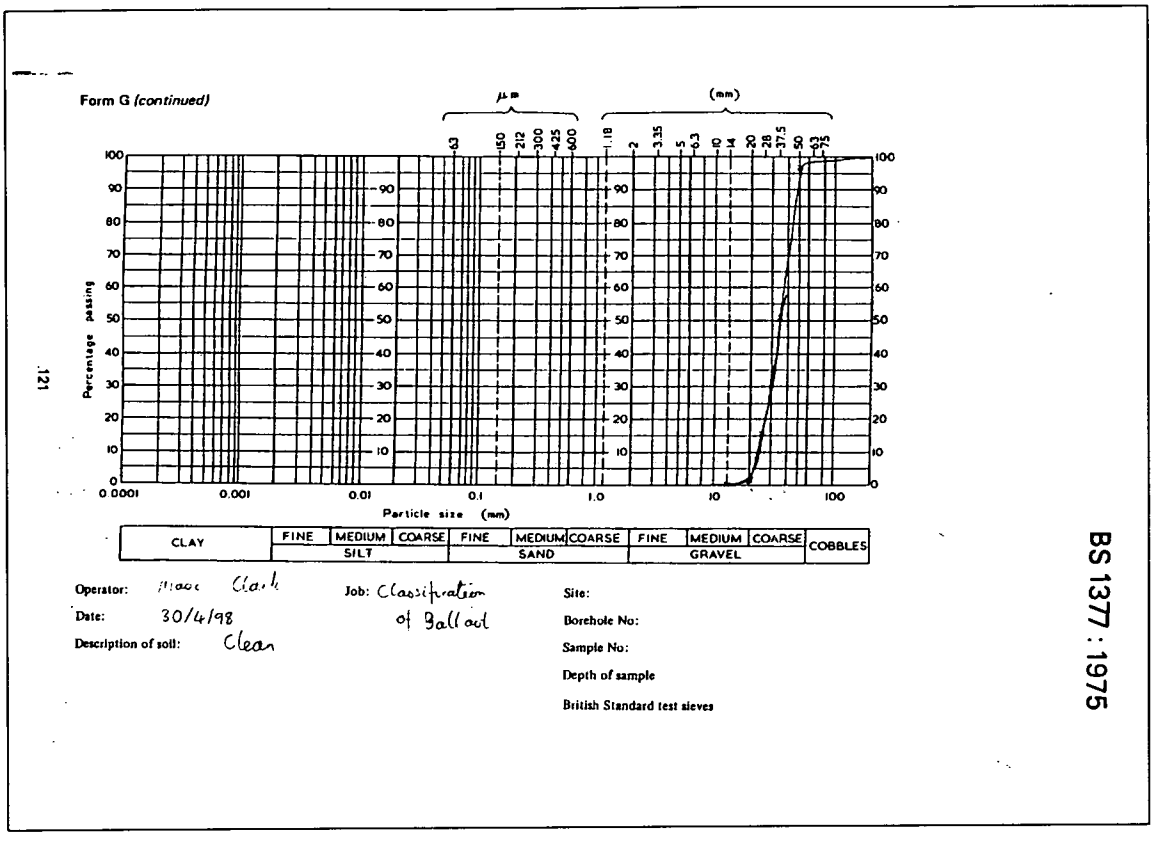

Figure 3.7 The particle size distribution for the clean ballast used in the experiments in this thesis

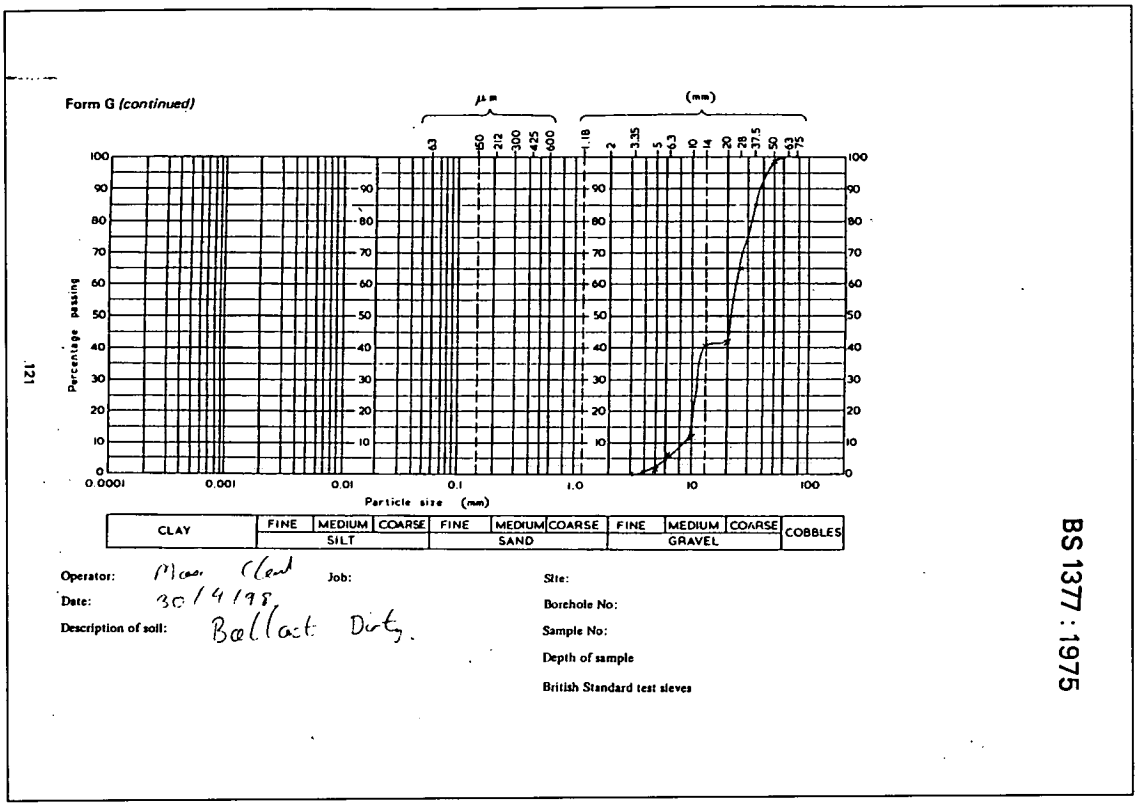

Figure 3.8 The particle size distribution for the spent ballast used in the experiments in this thesis

Spent ballast can be described as ballast that can no longer fulfil the requirements of the job for which it is being used. This is usually when the mass of fines contained within the ballast makes up 10% of the total mass of the ballast, and as a result the ballast is gap-graded gravel as can be seen by the sieve analysis figure 3.8. The spent ballast used in the current experimental programme came directly from the WCML and was deemed to be at the end of its usable life.

The particle size distribution of spent ballast showed a gap-grading, of the ballast. This result was repeatable and shows a paucity of stones in the 20-14 mm size bracket. This may be due to a number of factors. Perhaps this size of stone was subjected to more crushing forces due to its position within the ballast structure, or

perhaps this was due to the greater area this size of stone exposed to chemical breakdown compared with the larger stone size.

Within the railway industry they use two words to mean ballast that has come to the end of its lifespan, fouled and spent ballast. A general definition of fines is 0.075mm or less in diameter. These small particles are formed as the individual particles within the ballast break down. This is caused by mechanical wear from the vibrations and loads from passing trains, chemical wear caused by pollution and the effect of the weather eroding the larger particles away. As can be seen from the results of the sieve analyses, it is clear that the clean ballast has a far better and more uniform gradation than the spent.

3.2.2 Flakiness index

The flakiness index should not exceed 40% as measured by the test specified in BS812 Section 105 (1989b)

3.2.3 Elongation Index

The elongation index should not exceed 50% as measured by the test specified in BS812 Section 105 (1989a).

3.2.4 Aggregate Crushing Value

The aggregate crushing value (ACV) shall not exceed 22% (ACVP22%) using the test specified in BS812 part 110 (1990b) on particles of 14-10mm. Potential suppliers are required to provide ACV data covering the past 6 months' production, stating average and standard deviation of ACV.

The ACV of an aggregate is a relative measure of the resistance of it to crushing under a gradually applied load.

3.2.5 Wet Attrition Value

The wet attrition value (WAV) shall not exceed 4.0 % using the test specified in the superseded BS812: 1951 Clause 25.

3.2.6 Standard for the Ballast Returned by a Ballast Cleaner

The above tests to determine the suitability of ballast are only applicable for new ballast. For ballast that is returned by automatic ballast cleaners, the only requirements are a dimension test, where:

Square Mesh Sieve (mm)	Railtrack standard. Cumulative % by weight passing BS Sieve
50	100-97
28	20-0
14	5-0

Table 3.3 Particle size distribution for ballast returned by a ballast cleaner.

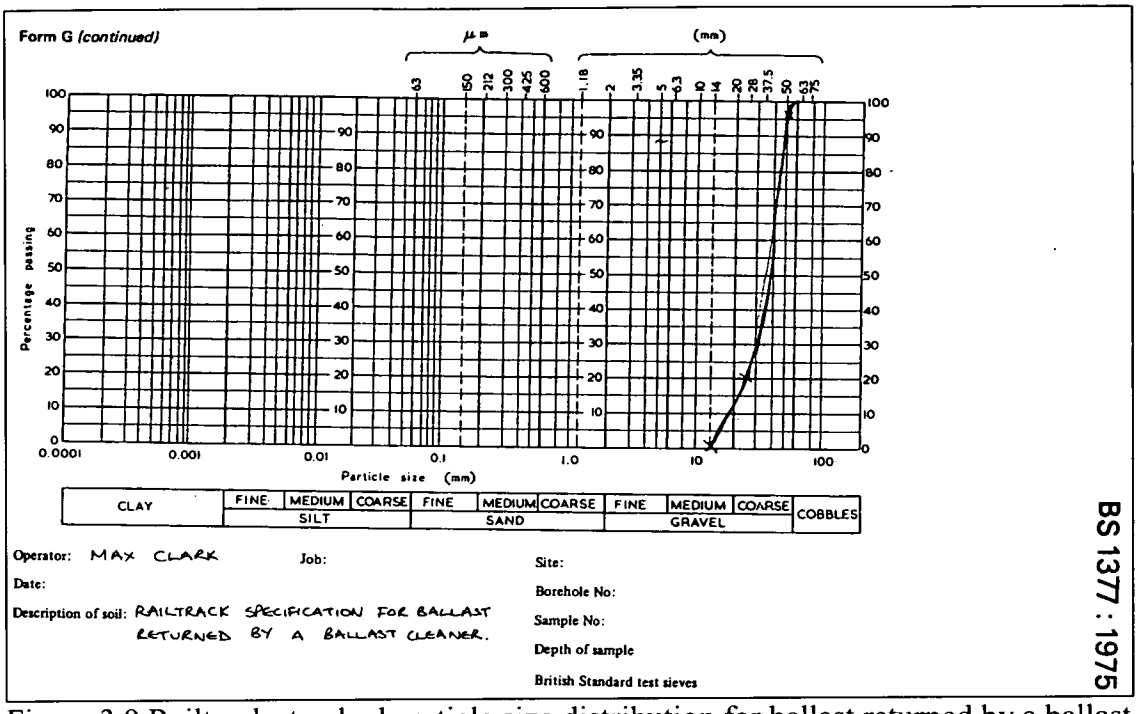

Figure 3.9 Railtrack standard particle size distribution for ballast returned by a ballast cleaner.

3.2.7 Current Inspection Method

The present method to determine whether the ballast is spent or not is by visual inspection of the ballast. As can be seen from the aggregate crushing test (see section 3.4.1), the spent ballast conformed to the specification laid out in the Railtrack specifications, even though this ballast was classified as spent ballast, and taken off the track.

3.3 Limitations

The tests outlined in the track specification only describe the shape of the material, particle size distribution of the material, as well as simple crushing and attrition tests. The problem with the above approach to testing of materials for use as ballast, is that all the experiments are static. That is, they do not dynamically test the durability of

the ballast. In the track specification of ballast it states that the ballast should be hard, durable, natural stone, but does not say how durable the ballast should be. If it were possible to test the durability of the ballast in a laboratory experiment, it might be possible to predict the life expectancy of the ballast. A more relevant test is the Slake Durability Test, see below in section 3.4.5.

3.4 Experiments

3.4.1 Density of Ballast

The density of the ballast was found by following BS 812 part2 (1995). The dimension of the box used was, 0.52 m x 0.585 m x 0.36 m.

Density of Ballast = (Mass of Ballast)/(Volume of Container).

$\rho = m/V$

Using the above equation, the density of spent and clean ballast was found to be the actual data can be found in appendix A:

Clean Ballast Density = 1608 ± 2 kg/m^3

Spent Ballast Density = 1803 ± 6 kg/m^3

The experimental data can be found in Appendix A. The density classification was undertaken in a large box for accuracy, but this precluded the opportunity to easily undertake multiple classification tests. This was considered acceptable practice in this instance as the data was not used for further calculations. The spent ballast is of noticeably higher density than the clean ballast. This is because the spent ballast contains a larger number of small particles than the clean, allowing the spent ballast to be compacted to a greater extent, with more of the voids in the material filled.

3.4.2 Aggregate Crushing Value (ACV)

The ACV of an aggregate is a relative measure of the resistance of an aggregate to crushing under a gradually applied load. This test provides useful information as to how the ballast would react if a stationary or slow moving load were applied to it.

Experimental Method

The ACV test was conducted in accordance with BS 812: part 110: 1990b. Three samples of clean and three samples of spent ballast were tested with each sample being air-dried. Each of the samples were loaded into the mould in a series of three layers, with each layer being tamped 25 times from a height of 50mm using the appropriate tamping rod. Each sample was loaded into the crushing machine, and a load of 400kN was applied over a period of 10 minutes

Figure 3.10 Sample loaded into mould

Figure 3.11 Crushing machine

Each sample was then sieved using a 2.36 mm sieve. The amounts passing and retained by the sieve were then weighed to the nearest 0.1g.

The experimental values of ACV were calculated using the following formula:

$$ACV = \frac{M2}{M1} \times 100$$

Where M1 = Total mass of test specimen (kg)

M2 = Mass of material passing 2.36 mm sieve (kg)

Material	ACV (%)
Clean Ballast	18
Spent Ballast	21

Table 3.4 The ACV for clean and spent ballast

The values in table 3.4 are the mean values of all the data which can be found in appendix A. As can be seen from the results of the tests conducted the ACV of the spent ballast was higher than that of the clean ballast. This shows that as a load is gradually applied to the ballast, the spent ballast breaks up more readily than the clean, indicating that the spent ballast has a weaker structure. This could be due to the spent ballast having been previously subjected to heavy loads, and as such, the particle breakdown had already commenced as a result of stress fractures. The ACV test is more relevant to slow moving trains than high speed trains- as the load is applied very slowly in this test, which would simulate a slow moving train such as a freight train, rather than a fast moving train which might be modelled by an impact load on the ballast. Therefore it would be more useful for the assessment of ballast on industrial lines, freight routes, or in areas where trains are stood on the track. The one limitation of this test is that the load applied had to be 400 kN. In the context of the railway lines this will not always be the case as the axle loads exerted onto the ballast by a train can be anything from 100–400 kN

3.4.3 Aggregate Impact Value (AIV)

The AIV of an aggregate gives a measure of the relative resistance of aggregate to sudden shock or impact. This measure is important in the context of ballast, as the effect of a high-speed train passing over the ballast is similar. It is therefore important to understand how the ballast will react to a sudden shock.

Experimental Method

The AIV tests were conducted in accordance with BS 812: part 112: 1990c. Three samples of clean and three samples of spent ballast were tested with each sample being air-dried. Each of the samples was loaded into the mould in a series of three layers, with each layer being tamped 25 times from a height of 50mm using the appropriate tamping rod. Using the standard testing machine, each sample was given a total of 15 blows at an interval of not more than 1 second.

Figure 3.12 Aggregate impact testing equipment.

The sample was then passed through a 2.36 mm sieve, and the mass of fines passing measured to the nearest 1g.

The experimental results for the AIV were calculated using the following formula:

$$AIV = \frac{M2}{M1} \times 100$$

Where M1 = Total mass of test specimen, (kg)

M2 = Mass of material passing 2.36 mm sieve, (kg)

Material	AIV (%)
Clean Ballast	9
Spent Ballast	12

Table 3.5 The AIV for clean and spent ballast

The values in table 3.5 are the mean value all the data which can be found in appendix A. The results of the AIV tests show that the AIV for the clean ballast was 25% lower than that of the spent ballast. This means that as the ballast ages and comes to the end of its useful life, the resistance of the ballast to crushing under impact decreases. As the ballast is used and worn, the strength of the individual particles decreases, allowing more fines to be removed from the particles. This could be critical to how well the ballast supports the rails, and ultimately, the train passing over it. The AIV is more relevant to high-speed passenger trains than freight. This is due to the shock exerted from high-speed trains being more instantaneous than that

of the slower freight trains. This causes more of an impact loading to be put on the ballast, rather than the crushing loading exerted by a slower train. From the results obtained it is impossible to say at exactly what speed of train either the ACV or the AIV test should be used. However if slow trains are running i.e. below 30mph the ACV should be used and if the trains are running at over 100 mph the AIV test should be used.

3.4.4 Ten Percent Fines Value (TFV)

The TFV of an aggregate gives the relative resistance of an aggregate to crushing under a gradually applied load. Essentially the TFV measures the same properties as the ACV test, but slightly differently. The differences between the two tests are that in the ACV test, the load was pre-determined, and the mass of fines measured. In the TFV test, the opposite is true, i.e. the mass of fines is pre-determined, and the loading required to produce this must be found.

Experimental Method

The TFV test was conducted in accordance with BS 812: part 111: 1990e. A number of clean and spent ballast samples were tested with each of the samples being air-dried. Each of the samples were loaded into the mould in a series of three layers, with each layer being tamped a total of 25 times from a height of 50mm, using a tamping rod. Each sample was then loaded into the crushing machine, as used in the ACV test and steadily loaded to the required force over a period of 10 minutes.

The required force was calculated by:

$$\text{Required Force} = \frac{4000}{AIV}$$

This gave in neither case the correct percentage of fines. The required force for the clean ballast was found to be around 250kN, whilst for the spent ballast, this force was found to be around 145kN.

Each sample was then passed through a 2.36mm sieve, and the mass of the material both passing and retained was measured

The experimental results for the force required to produce 10% fines is calculated by:

$$F = \frac{14f}{m+4}$$

Where:

f= Maximum force (kN)

m= Percentage of material passing through a 2.36 mm sieve. (%)

Material	Force to produce 10% fines (kN)
Clean Ballast	253
Spent Ballast	146

Table 3.6 The TFV for clean and spent ballast

The values in table 3.6 are the mean values all the data can be found in appendix A.

As shown in each of the tests conducted, the strength characteristics of the ballast change as it ages. Using AIV, ACV and TFV tests could provide a quick and easy way of determining ballast age and assessing its condition. Although these methods are not conclusive, they provide useful information on which follow-up tests should be conducted.

Of the three methods of testing used, the AIV test would seem to be the most relevant in the context of high speed railway lines, since the load is repeatedly applied and removed quickly. ACV and TFV tests would be more relevant in the context of industrial or freight lines where traffic moves at a slower pace. For testing on freight lines the TFV test may prove to be more relevant since it measures the load required to produce 10% fines.

3.4.5 Slake Durability Test

The standard Slake-Durability Test was chosen because it is designed to assess the resistance offered by the rock sample to weakening and disintegration when subjected to cycles of drying and wetting. This would simulate the weathering effect as well as the effect from the trains going over the ballast. A lot of research has been undertaken into investigating the effect of weathering on rocks. There are degrees of weathering tests included in BS 5930 (1999). Dearman (1986, 1995) states the current weathering classification of rocks in the U.K.. He specifically relates BS 5930 to the weathering of granites in Australia, Hong Kong and in the U.K. Weathering is considered to be less important than the crushing of the rocks due to the passing of the trains. The Slake-Durability of mudrock has been calculated in other studies (Bell, Entwisle & Culshaw (1997)), and compared with other durability tests, such as the free-swell coefficient, freeze-thaw and heat-cool cycles. This study undertook the standard Slake-Durability test using 2 cycles and found that mudrock had a high Slake-Durability value (according to Brown (1981)).

The Slake Durability test was completed in accordance with the ISRM methods as described in Brown 1981. The Slake Durability test examines the durability of the rocks when rubbed together but does not measure the durability of the material when subjected to the weather. To measure this is more complicated and is explained in Taylor-Firth & Laycock (1999). For the Slake Durability test the sample was placed in a clean drum (comprising a 2.00mm standard mesh cylinder with a length of 100mm and diameter of 140mm). The drum was rotated in a trough of slaking fluid (usually water) at a constant speed of 20 revolutions per minute for 10 minutes. The

material retained on the drum mesh is dried and weighed. The ratio of final mass to initial mass is the Slake Durability index. The drums and the slake durability equipment are shown in figure 3.13. Figure 3.14 shows ballast after 120 hours of testing.

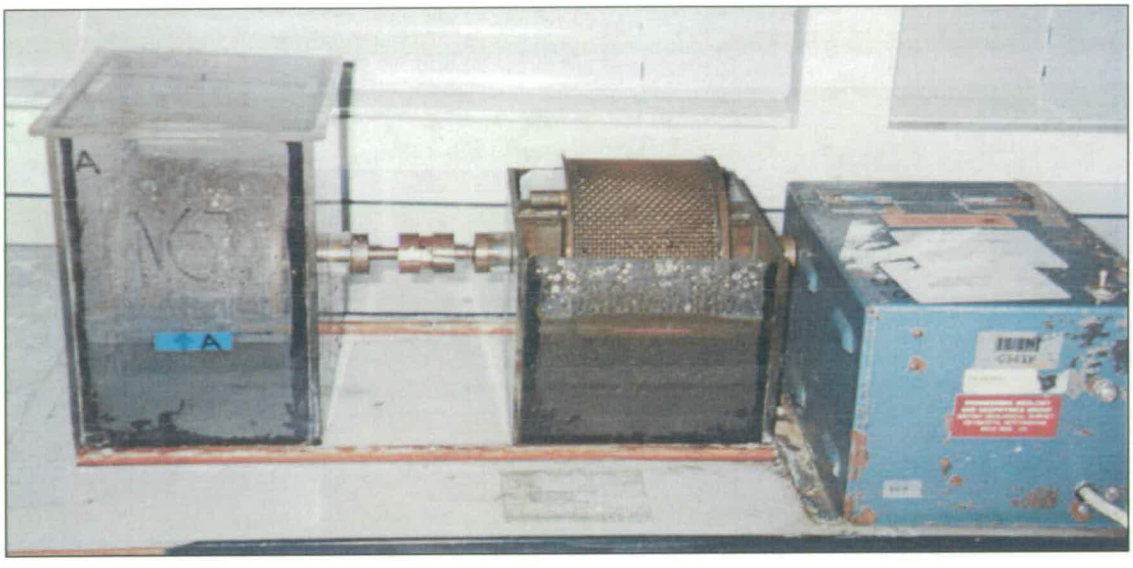

Figure 3.13 The Slake Durability test.

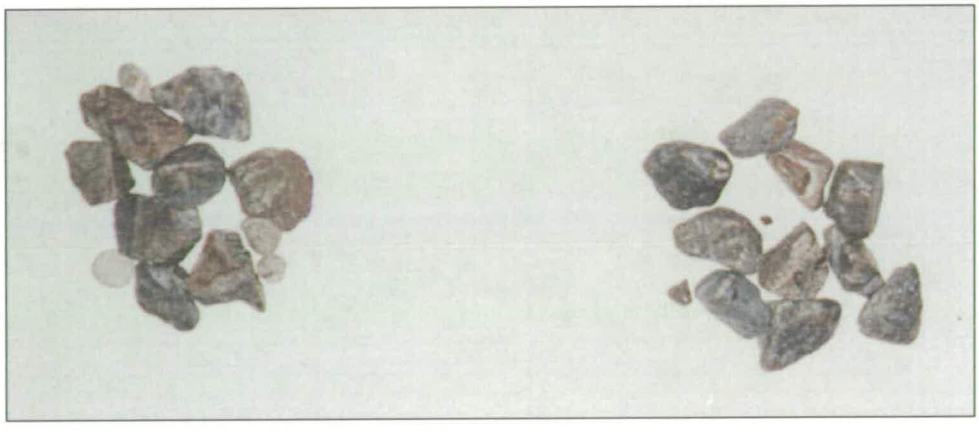

Figure 3.14 Ballast samples after 120 hours of testing.

The results from these tests on the samples of clean and spent ballast at Edinburgh University are shown in table 3.7.

Material	Slake Durability Index %
Clean Ballast	99.6
Spent Ballast	99.2
Hard White Sandstone	93.2
Coarse Red Sandstone	93.6
Silty sandstone	91.5
Mixed Silty Sandstone	77.6
Shale	95
Siltstone	78
Clay shale	20
Mudstone	5

Table 3.7 Slake durability results from a number of different materials.

All the results in table 3.7 were obtained from 2 cycles of the Slake Durability Test, using water as the slaking fluid. From Bell (1992) a slake durability index of over 95% (which includes ballast), is thought to be very high, between 75-95% to be high, 50 – 75% to be medium, 25-50% to be low and below 25% as very low. While anything over 60 % can be called durable.

The differences between the spent and clean ballast are due to the fines on the spent ballast being washed off. It can be seen from comparing the short term Slake

Durability Test results, that ballast has a higher durability index than the other materials tested.

Following this the ballast was subjected to a long term Slake Durability Test. The number of cycles was increased and the time period over which the ballast was tested also increased. The results were compared with those obtained from a geological investigation of the caverns in the Hunterston Peninsula, Ayrshire (Institute of Geological Sciences (1976)). The tests were conducted using four different time periods and two different slaking fluids. Between each time period (cycle) the samples were dried and weighed, and the process was then repeated.

Time Period (Hours)	**Revolutions**	**Slaking fluid**
4	4800	Tap water
16.25	19500	Tap water
16.3	19560	Salt water
64	76800	Tap water

Table 3.8 List of different times and slaking fluid used in the experiments.

3.4.5.1 Results

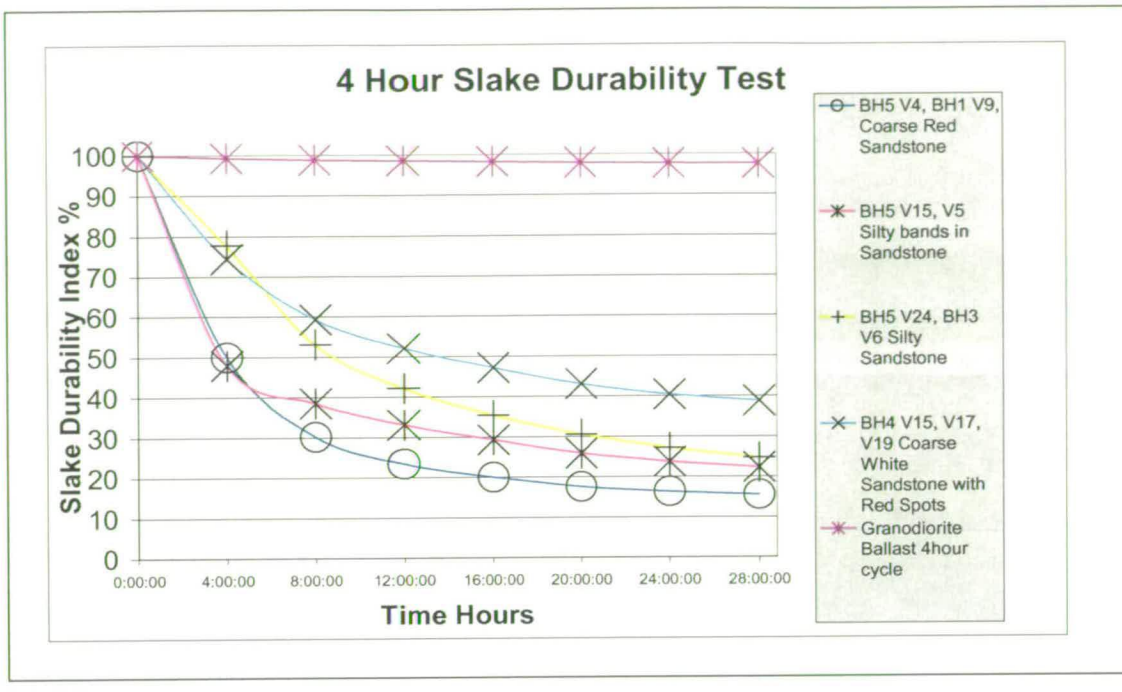

Figure 3.15 Results from the 4hr Slake Durability Test

Figure 3.15 shows the tests ran for over 28 hours in 7 cycles of four hours. Figure 3.15 shows the durability of the ballast compared with coarse red sandstone, banded silty sandstone, silty sandstone and coarse white sandstone with red spots, over a 4 hour cycle period in tap water.

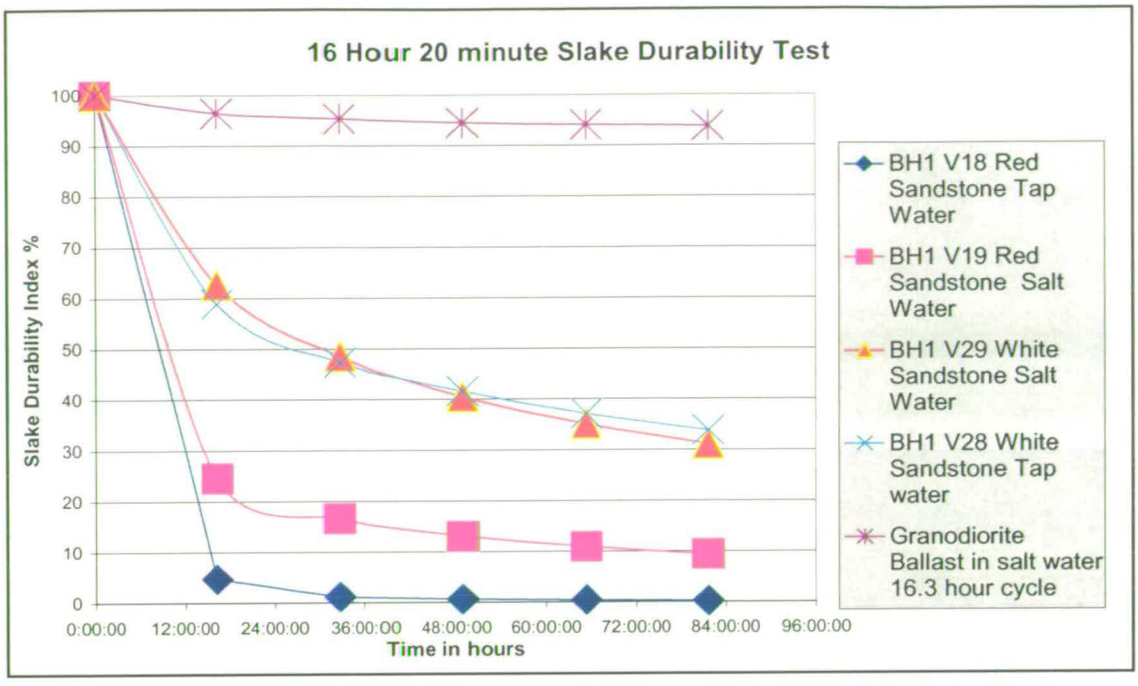

Figure 3.16 Results from the 16hr 20 min Slake Durability Test

Figure 3.16 shows the durability of ballast in salt water compared with white sandstone in salt water, white sandstone in tap water, coarse red sandstone in saltwater and coarse red sandstone in tap water, using a 16 hour 20 minute cycle time period. It can be clearly seen from figure 3.16 that over the five cycles of 16 hours 20 minutes, ballast is more durable than any of the other materials tested.

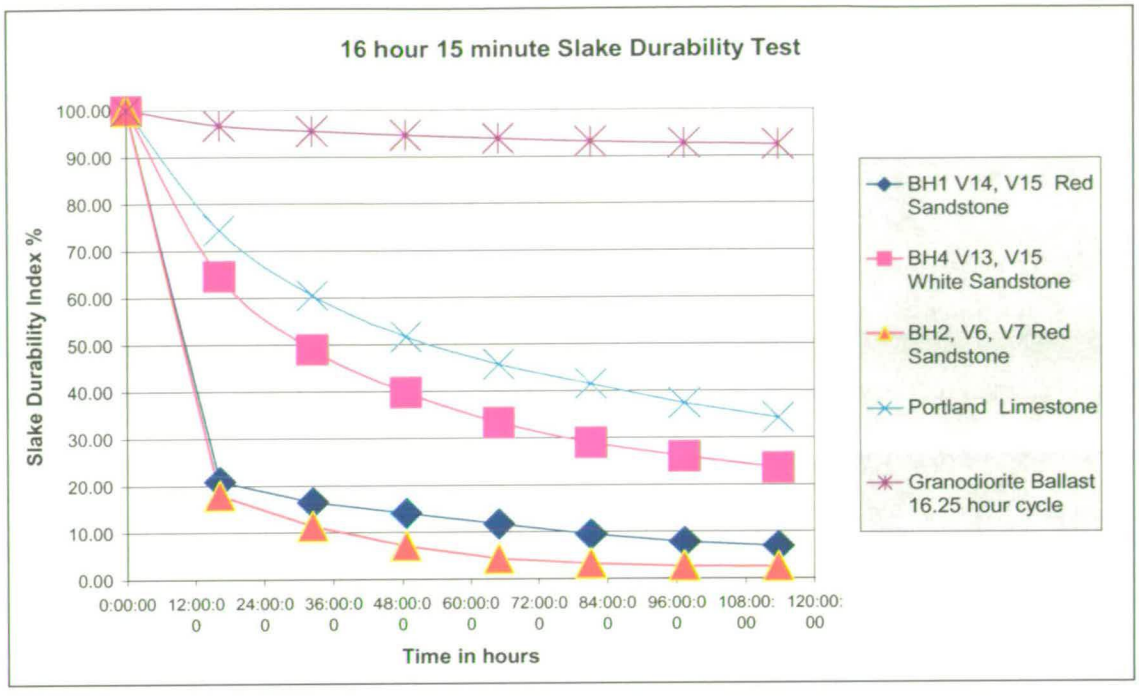

Figure 3.17 Results from the 16hr 15 min Slake Durability Test

Figure 3.17 shows the durability of ballast compared with Portland limestone, white sandstone, red sandstone and silty sandstone, over a time period of 16 hours 15 minutes all in tap water. This test was conducted over 114 hours with seven cycles of 16 hours 15 minutes.

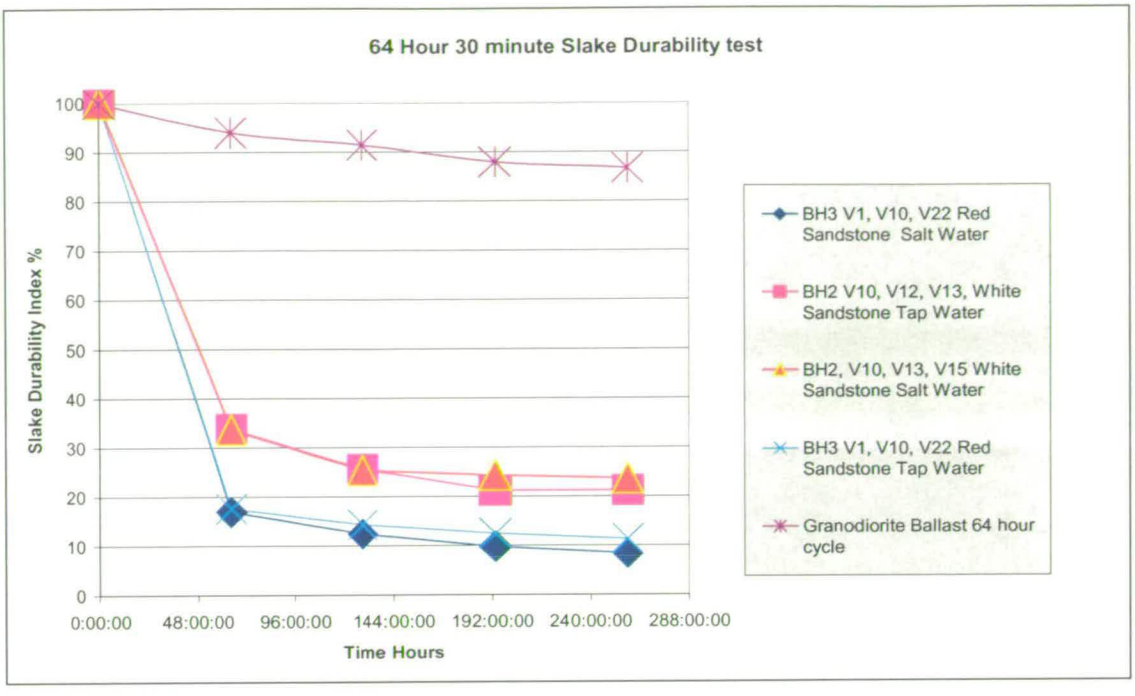

Figure 3.18 Results from the 64hr 30 min Slake Durability Test

Figure 3.18 shows the durability of the ballast compared with white sandstone in tap water and salt water and red sandstone in tap water and salt water. Figure 3.18 showed the results after 258 hours comprising of 4 cycles of 64 hours and 30 minutes.

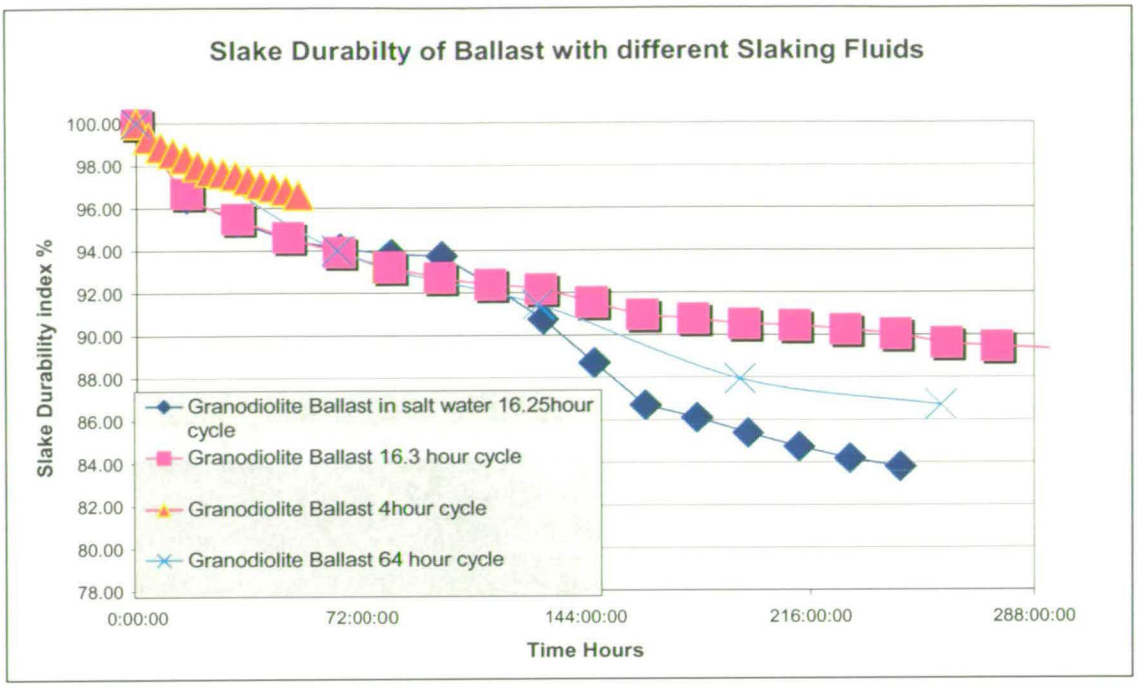

Figure 3.19 Comparison of different times and slaking fluids.

Figure 3.19 shows the durability of ballast tested in different slaking fluids. It can be seen that the slaking fluid has no great effect on the durability of ballast over the first 120 hours. Over a longer time period the salt-water sample showed greater deterioration. Thus, on the track, the ballast should deteriorate more near the coast as opposed to further inland.

The traffic movement can be simulated by the Slake Durability Test. Given the length of a train and the average speed of a train it is possible to calculate the time taken to pass over an area of ballast. Thus using the data produced from the Slake Durability Test, the wear after each passage of trains can be calculated. Two calculations were performed, one based on InterCity trains and one based on freight trains. The number of trains passing a certain spot was assumed to be the worst case

scenario that was given to me in a private conversation with Railtrack plc and was 20 trains per hour. Other assumptions made were; the length of an intercity carriage to be 30.54 m and a freight train carriage to be 10 m, the number of carriages in a intercity train to be 12 and in a freight train to be 60, the speed of the intercity trains to be 100 mph and the freight trains to be 30 mph.

The time taken to travel over an area of ballast was calculated, from the above information and hence the amount of time the ballast was subjected to a dynamic load, can be produced. The time ballast on a intercity track was subjected to a dynamic load is about 50 seconds per hour, while a freight train is subjected to about 40 seconds of dynamic load per hour. To equate the time of dynamic load to wear the initial linear phase from figure 3.16 was used

From these assumptions and initial calculation it was calculated that, with Intercity trains it would take about 2¼ years for the ballast to reduce to 90% of its original mass, while from only freight trains it would take 2¾ years for the ballast to be reduced to the same level. Therefore, the total wear from both freight trains and InterCity trains are similar. Figures 3.20 and figure 3.21 show the number of trains required to reduce the percentage of ballast. It can be seen that it will take just under 400,000 passage of InterCity trains and 70,000 passages of freight trains to produce a 10% loss of ballast mass according to the Slake Durability test.

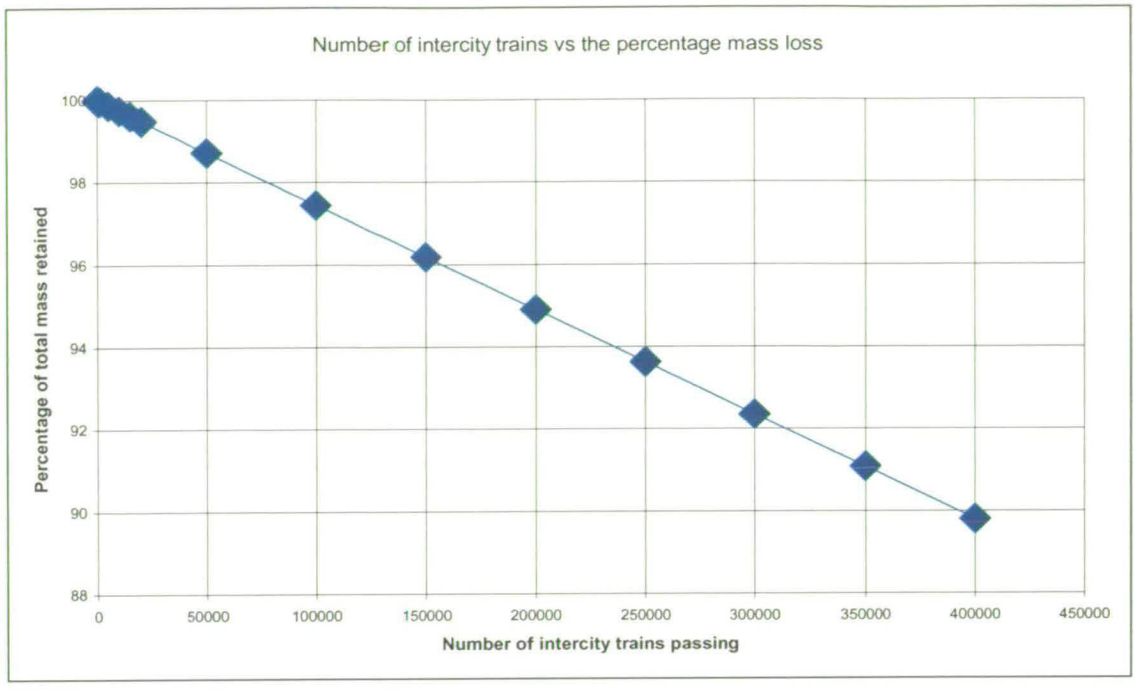

Figure 3.20 Number of InterCity trains passing and resulting percentage mass loss.

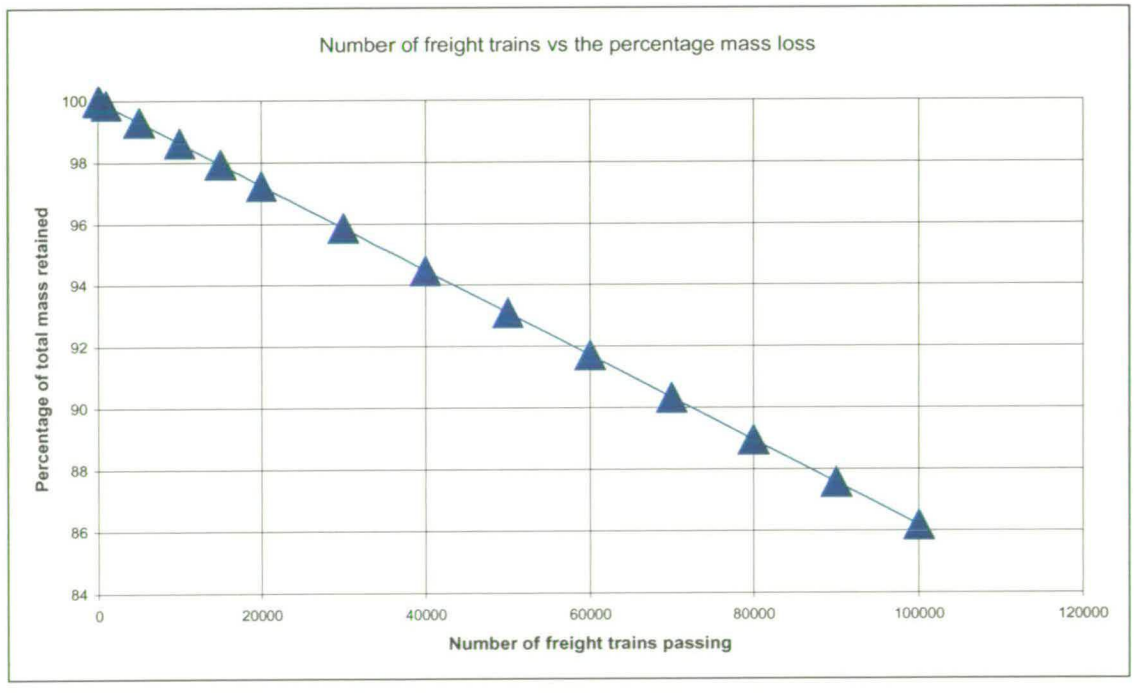

Figure 3.21 Number of freight trains passing and resulting percentage mass loss.

3.5 Proposed New Specification for Railway Ballast, New and Renewal.

Property	**Current Railtrack Specification**	**Proposed New Specification**
Material Property	Hard, durable and angular	Same
Particle Size Distribution	Described in Table 3.2	Same
Shape	Flakiness Index: not exceed 40% Elongation Index: not exceed 50%	Same
Aggregate Crushing Value	≤ 22%	≤ 20%
Wet Attrition Value	≤ 4%	Same
Aggregate Impact Value	-	≤ 10%
Ten Percent Fines Value	-	≥215
Slake Durability Test	-	≥90%

The reasons for the changes of the standards are to have stone that will perform better and thus slow the rate of contamination and the need for constant changing of the ballast.

The new Aggregate Crushing Value is stricter than the current standard. It was shown in the experiments undertaken as part of this thesis, that spent ballast could qualify as clean ballast on the existing standard. This test could be ideal for freight lines.

The aggregate impact value test is ideally suited for high-speed lines as it models the shock induced by high-speed trains.

The ten percent fines value test is ideal as it shows the greatest difference between clean and spent ballast as it exploits the stress fractures within the ballast. This is an ideal test for freight lines.

Slake Durability Test is an ideal test for high-speed lines as it models trains constantly running over the ballast. This test is flexible so that it can also model tracks near the coast as salt water can be used as the slaking fluid.

3.6 Conclusion

It has been shown that using the standard tests there is a difference between the strength of the spent and the clean ballast. This is perhaps due to the fact that there are already stress fractures within the spent ballast, which occurred while it was on the track. It was shown with the Slake Durability Test that granodiorite (ballast) is a very durable rock and using salt water increases the deterioration. Over 2400 hours the ballast only deteriorated to 80%, with no salt water.

A new specification has been put forward for new and renewal ballast, based on the experimental work undertaken as part of this thesis. This new specification has 4 new areas an increase in the aggregate crushing strength, introduction of the aggregate impact test, the ten percent fines test and the slake durability test.

Chapter 4

Non Destructive Techniques

4.1 Introduction

The current method of ballast assessment is to dig trial pits at regular intervals along the length of the track. The total length of track in the U.K. is over 20,000 miles, so there is a need for a rapid assessment of the track. In the light of recent disasters, which have occurred in the rail industry, this need for rapid non-destructive assessment of the network has never been more important, especially as there is an expected 50% growth in passenger traffic and 80% rise in freight traffic over the next ten years (ICE report 2000). This necessitates a cost-effective mode of ballast inspection which does not disrupt the normal service of the rail network.

Various non-destructive techniques were investigated to determine which method is suitable to measure the in-situ characteristics of the ballast.

4.2 Geophysical Techniques

There are five fundamental questions which must be answered prior to undertaking a geophysical survey (Annan & Cosway (1992)).

- What is the target depth?

Clearly, if the target is located at a depth greater than the penetration capabilities of the non-destructive technique this can be ruled out as a possible survey method.

- What is the target geometry?

The height, width, length and orientation of the target should be determined as accurately as possible.

- What are the electrical properties of the target? (Only applicable to radar)

In order to obtain useful results, the target should present a contrast in electrical properties to the surrounding (host) materials so that the electromagnetic signal will be reflected. The electrical properties of a material are the dielectric permittivity and conductivity.

- What is the contrast in the physical properties? (Only applicable to radar)

Not only should the permittivity and conductivity of the host material be quantified but the degree of heterogeneity of these properties throughout the mass should be estimated. If variations in these host materials are similar to those of the target, the target may not be recognizable.

- What is the signal to noise ratio?

Non-destructive systems are highly sensitive pieces of equipment and the received signal can be adversely affected in the presence of electromagnetic sources or transmitters. Accessibility and the presence of hazards should also be taken into consideration.

4.3 Principles of Ground Penetrating Radar (GPR).

GPR is a non-destructive technique that is often used to investigate the composition of materials beneath the surface such as rock formations, soils and gravel as well as analyzing man-made materials such as masonry and concrete. It can be used to determine the depth of strata, determine the location of the water table and is

effective in detecting anomalies and hidden objects such as pipes, cables, sewers, steel reinforcement, foundations and voids. Daniels (1989) states GPR is generally regarded as being the best technique for the detection and identification of subsurface anomalies and as such its use in industry is increasing. One of the most important aspects of a geophysical survey is to define the problem and decide which technique(s) will be effective.

4.4 Ground Penetrating Radar Concepts.

Figure 4.1 shows the basic principles of radar. The fundamentals of GPR are described in Daniels (1989). GPR systems work by emitting short pulses of electromagnetic energy, typically of frequencies in the range of 25 to 2,000 MHz, into the transmission medium by means of an antenna. The pulse length can range from 1ns to 10ns depending on the type of material and the resolution required (see table 4.2).

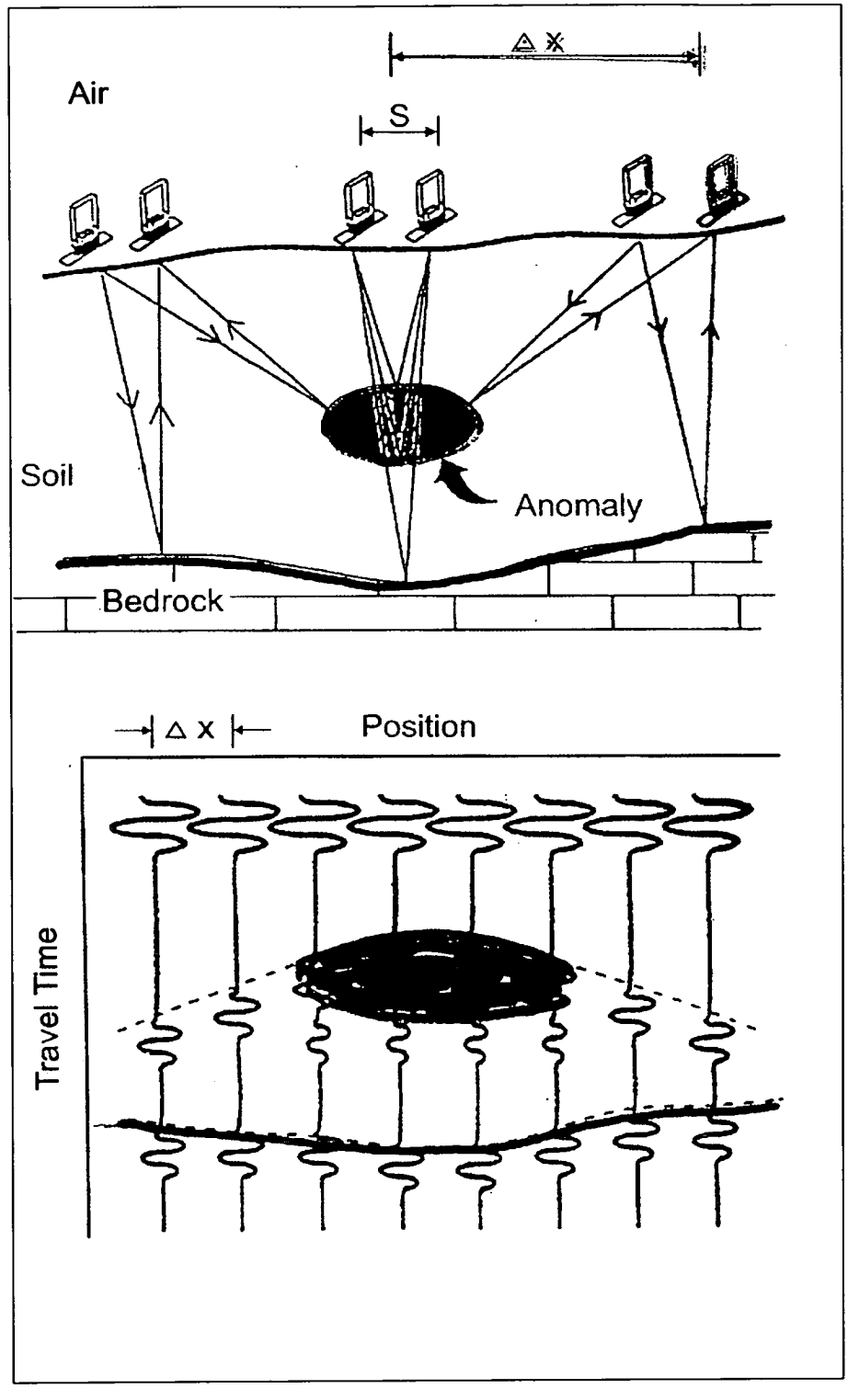

Figure 4.1 Basic Principle of Radar testing.

The signals transmitted into the medium of interest are partially reflected on encountering a change in the electrical properties of that medium. The reflected signal is recorded at a receiver while the transmitted part continues through the new material. This process is repeated when further electrically different media are met by the transmitted signal. The series of reflections recorded at the receiver allow an image of the interior structure to be built up. The Design Manual for Roads and Bridges (Anonymous (1994)) includes the technique's usage for the investigation of pavement defects and also covers the basic theory.

In most practical applications, geological and building materials are classified as low loss materials at radar frequencies and therefore the general equation for wave velocity is often simplified to:

$$v = \frac{c}{\sqrt{\varepsilon_r}} \qquad (4.1)$$

c= Speed of light (m/s)

v= Velocity of the radar signal (m/s)

ε_r= Dielectric constant which is independent of frequency and conductivity.

The depth is determined from the time it takes the reflected wave to be detected at the receiver. Knowing the velocity of the wave through the relevant media the depth is calculated using the equation 4.2 below:

$$d = v\left(\frac{t}{2}\right) \qquad (4.2)$$

where: d = Depth of reflector (m)

v = Velocity of electromagnetic wave (m/s)

t = Two-way travel time. (s)

The two-way travel time is defined as the time it takes for the signal to travel from the transmitter to the reflector and back to the receiver, covering twice the distance (d) under investigation

Figure 4.2 illustrates the partial transmission and reflection of an electromagnetic wave as it passes through an interface where the dielectric properties of the material changes. This is similar to the situation of the ballast on the rail track where the top layer is ballast and GPR is being used to examine the interface between the ballast and the bottom layer of soil or clay (subgrade).

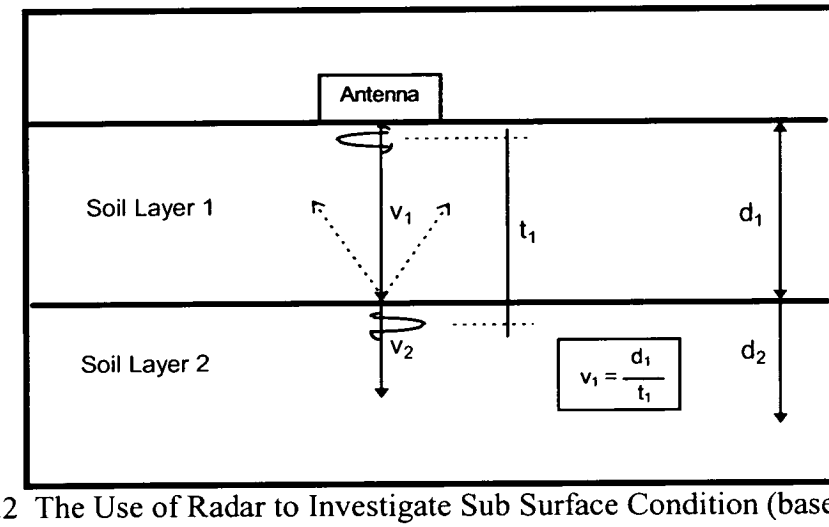

Figure 4.2 The Use of Radar to Investigate Sub Surface Condition (based on Forde & McCavitt (1993)).

The signal attenuation is given by:

$$\alpha = \omega\left[\frac{\mu\varepsilon'}{2}\left(\sqrt{1+\tan^2\delta}-1\right)\right]^{1/2} \qquad (4.3)$$

where: α = attenuation coefficient

$\omega = 2\pi f$ - angular frequency (rad s^{-1})

π = ratio of the circumference to the diameters of a circle

f = centre frequency of the transmitted signal (Hz)

$\mu = \mu_r\mu_o$ - magnetic permeability (H m^{-1})

μ_r = magnetic permeability of the material

μ_o = magnetic permeability of free space

$\varepsilon' = \varepsilon_r\varepsilon_o$ - real part of dielectric permittivity

ε_r = relative permittivity of the material or dielectric constant

ε_o = permittivity of free space

$\sigma = \varepsilon''\omega$ - conductivity

ε'' = imaginary part of the complex permittivity

$\tan^{TM} = \frac{\varepsilon''}{\varepsilon'} = \frac{\sigma}{\omega\varepsilon'}$ - loss tangent (or dissipation factor)

The material dielectric permittivity is a complex function:

$$\varepsilon = \varepsilon' - j\varepsilon''$$

ε'': commonly referred to as loss factor, is frequency and conductivity dependent.

$j = \sqrt{-1}$

The amplitude reflection, r, and transmission, t, coefficients for the electromagnetic waves are:

$$r = \frac{Z_2 - Z_1}{Z_2 + Z_1} \qquad \text{and} \qquad t = \frac{2Z_2}{Z_2 + Z_1}$$

where Z_1 is the impedance of the first material,

Z_2 is the impedance of the second material

and for low loss dielectrics the impedance Z is given by:

$$Z = (\mu_o / \varepsilon_o \varepsilon_r)^{0.5}$$

where: μ_0 = magnetic permeability of free space

ε_0 = permittivity of free space

In the case of oblique incidence it will be:

Perpendicular polarisation

$$r = \frac{Z_2 \cos\theta_i - Z_1 \cos\theta_t}{Z_2 \cos\theta_i + Z_1 \cos\theta_t} \tag{4.4}$$

$$t = \frac{2Z_2 \cos\theta_i}{Z_2 \cos\theta_i + Z_1 \cos\theta_t} \tag{4.5}$$

Parallel polarisation

$$r = \frac{Z_2 \cos\theta_t - Z_1 \cos\theta_i}{Z_2 \cos\theta_t + Z_1 \cos\theta_i} \tag{4.6}$$

$$t = \frac{2Z_2 \cos\theta_i}{Z_2 \cos\theta_t + Z_1 \cos\theta_i} \tag{4.7}$$

The electrical conductivity has the greatest bearing on the degree of signal attenuation; i.e. on the extent to which the signals penetrate into the ballast, see equation 4.3. The higher the conductivity the greater the attenuation and the less the depth of penetration. The power of the emitted radiation from the transmitter is also a

factor and as the lower frequency antennas produce more powerful signals, these antennas can penetrate to greater depths. However, there is a trade off; lower frequency antenna give poorer resolution.

A typical 900 MHz dipole antenna, manufactured by GSSI, is shown in figure 4.3. A radar antenna produces signals which emerge in a complex pattern as is shown in figure 4.4, which indicates the form of radiation pattern emitted by a dipole antenna. There is another type of antenna, a horn antenna, which produces a more focused beam though the general pattern of radiation is similar.

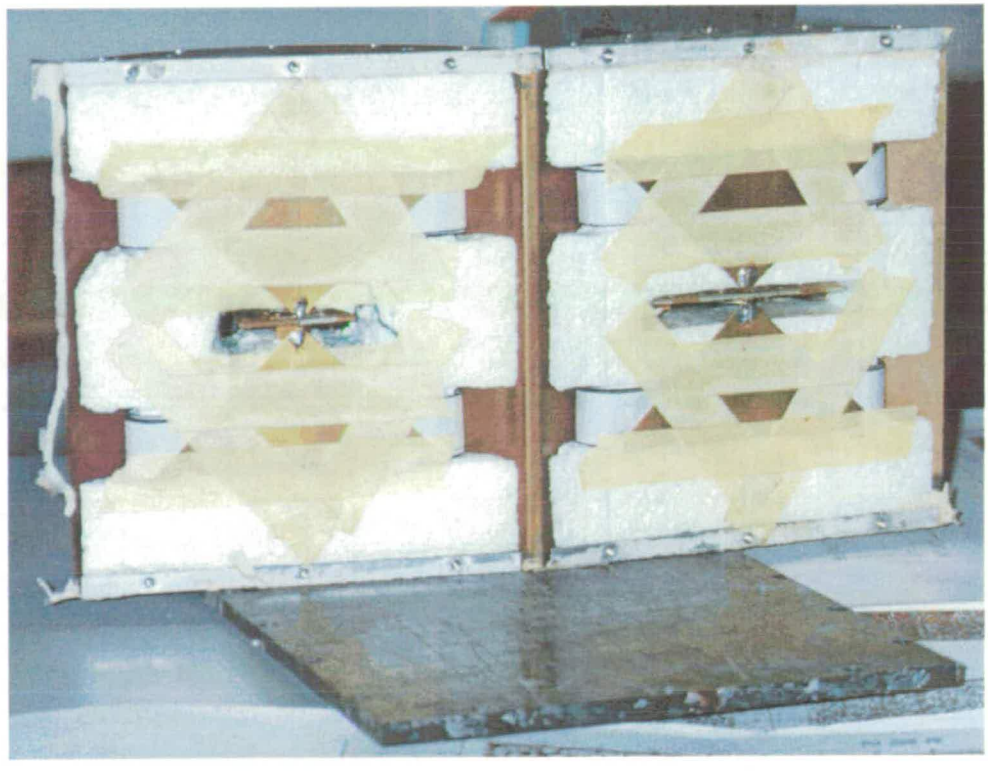

Figure 4.3a - Front of bow-tie antennae in 900 MHz commercial antenna showing transmitter/receiver separation.

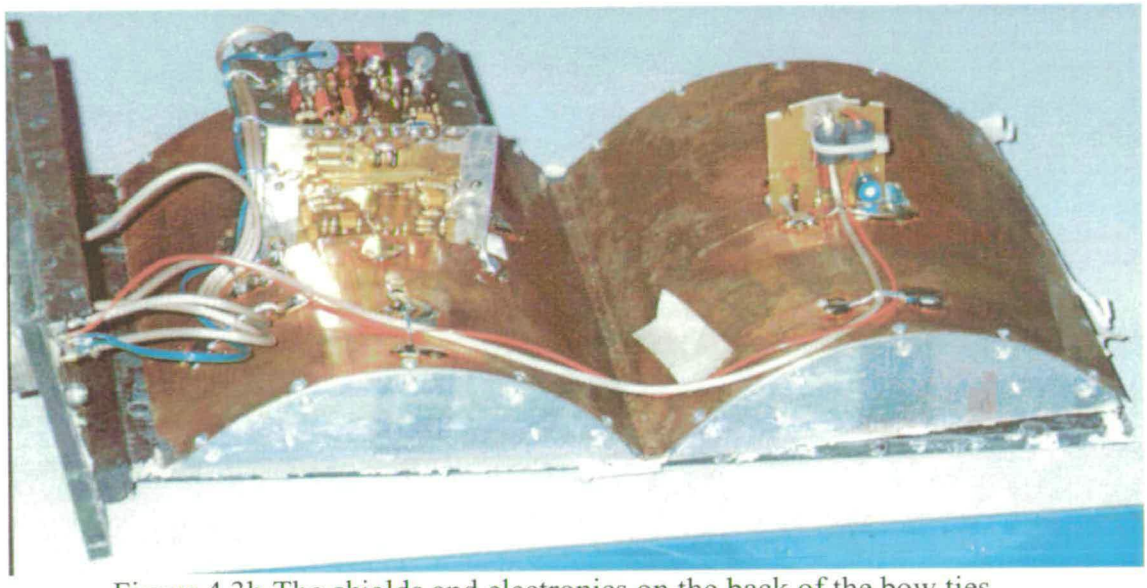

Figure 4.3b The shields and electronics on the back of the bow ties.

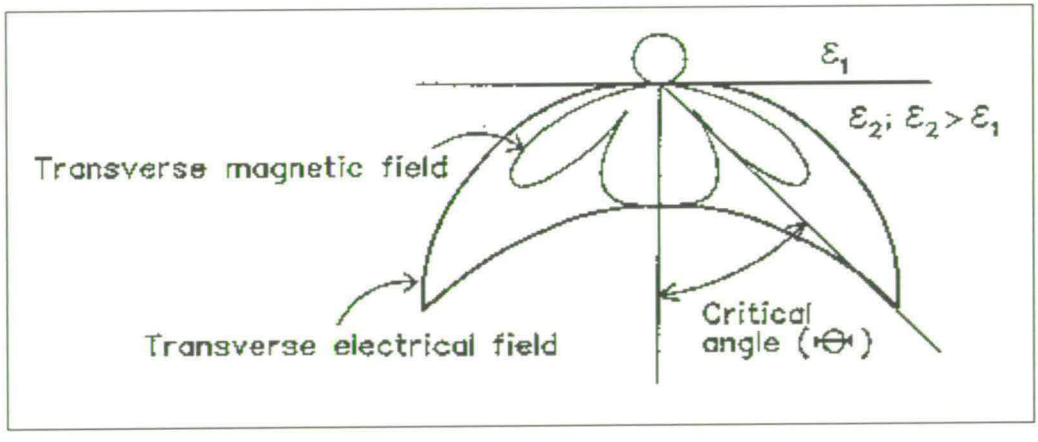

Figure 4.4 Radiation pattern from a dipole antenna.

As the radiation emerges over an area, rather than being a narrow beam, reflections may be received from objects in front of, behind and to the side of the antenna.

4.4.1 Permittivity and the Dielectric Constant.

The dielectric constant is a dimensionless measure of the capacity of a material to store a charge when an electric field is passed through it. Like a perfect conductor, a

perfect dielectric material is one in which no energy is lost when the electric field is passed through it. Conversely, an imperfect dielectric material acts as an insulator where energy losses occur in the form of heat. Many materials exhibit both properties, changing character throughout their mass. Dry bulk density primarily influences the dielectric constant of dry materials. In partially saturated or fully saturated soil the dielectric constant is primarily determined by the water content, salinity and porosity. The effect of water on the dielectric constant is described in Wensink (1993), while the effects of a changing water content during a survey is described in Greaves, Lesmes, Lee & Toksöz (1996). Table 4.1 shows typical values for some common materials. Generally, the permittivity of a material rarely exceeds 11. In comparison, the relative permittivity of water is substantially greater at 81. Therefore the dielectric properties of wet soil tend to be dominated by the characteristics of the water. The presence of salts (electrolytes) in solution further increases the conductivity of water.

Material	**Dielectric Constant, ε_r**	**Electromagnetic Wave Velocity, V_m (m/s)**
Air	1	3.00×10^8
Asphalt	3 – 5	$17.34 \times 10^8 - 13.42 \times 10^8$
Concrete	4 – 11	$13.00 \times 10^8 - 9.04 \times 10^8$
Granite	4 – 7	$13.00 \times 10^8 - 11.22 \times 10^8$
Masonry	6	1.22×10^8
Water	81	0.33×10^8

Table 4.1 Typical Values of Dielectric Constant and Velocities for Common Materials.

When two materials are mixed together, the factors affecting the permittivity of the mixture include the permittivity of the individual substances, their volume fractions,

the distribution and shape of the particles and their orientation relative to the incident electromagnetic waves.

The velocity, V_m, at which electromagnetic waves propagate through a low loss material is related to the dielectric constant, ε_r, and can be expressed as follows:

$$V_m = \frac{c}{2\sqrt{\varepsilon_r}} = \frac{d}{t} \tag{4.8}$$

where,

c = velocity of light = 3 x 10^8 metres per second [m/s]
d = depth of the material layer [m]
t = time taken for electromagnetic wave to travel a distance [d]

4.4.2 Considerations when using Radar

Radar signals are sensitive to changes in material conductivity. In areas of high conductivity the range and resolution of radar decreases (Colla, McCann, Forde, & Das (1997)). Therefore, on the railway, if the conductivity of the ballast is high, the radar signal will identify the ballast / soil interface. If the radar does not identify the interface or an object, it does not mean that it is not there. It has been shown that the size and depth of an object can determine whether it is identified using radar (Martin, Hardy, Usmani & Forde (1995), Padaratz. & Forde (1995), McCann & Forde (2000)). It was shown from McCann & Forde (2000) that the minimum object depth for radar detection is a third of the wavelength while for other non-destructive techniques such as impact echo (I-E) it could be as much as half of the wavelength. For use on the track bed this is irrelevant as the depth of ballast is half a metre and small objects within the ballast are of no interest. Another problem to be considered

when using radar in the rail environment is that of clutter. The shorter the wavelength the more it will be scattered by the ballast particles. It has been shown by Padaratz, & Forde (1995) that for the electromagnetic energy not to be scattered when passing a material with particles of 50mm diameter average size, e.g. ballast, the frequency of the antenna should not exceed 500MHz. From Padaratz, Hardy & Forde (1997), it has been shown that when the antenna is coupled with the surface, the signal frequency decreases. As the frequency decreases, the wavelength increases - assuming the velocity through a material is constant (see equation 4.9). This may not be valid in geotechnical radar surveys using low frequency antennae where the conductivity is high (Padaratz & Forde (1995)).

$$v=\text{constant} = \lambda_0 * f \qquad (4.9)$$

f= frequency (Mhz)

λ_o= wavelength (m)

When the antenna is coupled with the surface of the material the frequency of the signal decreases by about 40%, leading to an increase in the wavelength. This reduces the resolution of the signal (a half the wavelength), making shallow targets harder to identify.

There are several techniques that have been used to model the predicted image from the radar antenna, such as ray tracing (Colla, Burnside, Clark, Broughton & Forde (1998)) and using finite-difference time domain (FDTD) (Giannopoulos (1997), Nelson (1994) and Lee & Suh (1997)). These techniques and others (Olhoeft (1993))

have been used to simulate the radar image to improve the interpretation of the radar images, and to see if radar is a suitable technique for a given scenario before field tests are conducted.

4.4.3 Antennae.

Surface penetrating radar systems have the ability to use a variety of antennae based on different frequencies for different applications. The centre average frequency of an antenna is a measure of how sensitive it is to a range of frequencies around this average. Propagation losses, antenna size, material type and the size of the object to be detected dictate the choice of frequency of operation and therefore the resulting penetration and resolution of the measurements. For example, an antenna with a centre frequency of 500 MHz can typically penetrate to depths of 2 metres in clays with a corresponding resolution of 5 cm (about a half of a wavelength [$\lambda/2$]). Table 4.2 shows the propagation and resolution through ballast, concrete and masonry.

Material	ε_r	Frequency (MHz)	Velocity (cm/ns)	Wavelength (cm)	Resolution (cm)	Z_{min} (cm)	Penetration (cm)
Masonry	5.69	900	12.55	13.9	7	4.6	Low
Concrete	9	900	10	11.1	5.6	3.7	Low
Ballast	3	900	17.32	19.2	9.6	6.4	Low
Masonry	5.69	500	12.55	25.1	12.6	8.4	Medium
Concrete	9	500	10	20	10	6.7	Medium
Ballast	3	500	17.32	34.6	17.3	11.4	Medium
Masonry	5.69	100	12.55	125.5	62.8	41.8	High
Concrete	9	100	10	100	50	33.3	High
Ballast	3	100	17.32	173.2	86.6	57.2	High

Table 4.2 GPR Propagation and Penetration through Concrete, Masonry and Ballast (Based on McCann & Forde (2000))

An antenna of higher frequency will operate with a higher resolution providing increased clarity, but the depth of penetration is proportionately reduced. Conversely, a lower frequency antenna will provide greater penetration but less clarity. Materials with a high conductivity such as wet clays and soils containing a large amount of dissolved salts are the most difficult to penetrate whereas materials such as granite and sandstone are relatively easy to penetrate. In regions where soils of high conductivity such as clay exist, penetration may be reduced to the point where radar may no longer be the preferred method of testing. An important consideration when choosing equipment for an application is to determine the exact trade off between suitable resolution, antenna size and the penetration required. As a guideline, "it is better to trade off resolution for penetration. There is no use in

having great resolution if the target cannot be detected!" (Annan A P & Cosway S W, (1992)).

Targets which possess a dielectric constant similar to that of their surroundings may be difficult, perhaps impossible, to identify using radar equipment. Conversely, because electromagnetic waves are unable to penetrate metallic objects, large reflections can usually be detected.

4.4.4 Controller and Display.

On site, the operator needs to be able to view the radar data, to configure the radar for the particular site under investigation and to record the received data. There are three approaches to acquire radar data:

- An analogue system in its entirety e.g. OYO Georadar 1, GSSI Sir 3 and Sir 8
- An analogue anetenna and cable with digitisation by an A/D card in its mainframe e.g. GSSI Sir 10 and Sir 2
- Fully digital with digitisation at the antenna e.g. Pulse Echo 1000

At Edinburgh University we have a type 2 system the Geophysical Survey Systems (GSSI) SIR SYSTEM-10B. This is a computer controlled multi-channel radar system, which is used to automatically display, process and record subsurface profiles. The system incorporates an in-built video monitor, which can display real time images in colour, grey scale or provide the operator with an oscilloscope trace (O-Scope) and wiggle plots. Also, to allow the operator to obtain the best results possible, the system includes real time digitally controlled gain and filtering functions to provide high signal to noise data quality. The system can simultaneously record signals from up to four antennae, greatly improving survey

efficiency and flexibility while a large capacity of storage space allows data to be rapidly stored for later post-processing on the GSSI RADAN for Windows package. This software allows data to be manipulated into a more easily interpreted format (see section 4.3.5).

4.4.5 Radar Data and Image Processing.

The signals recorded by the radar receiver create a section of time (or depth) to distance profiles which can be interpreted as an image. Radar images are relatively easy to interpret if the following point is noted. The radar assumes that the reflected signals are coming from directly beneath the antenna, but, as the radar antenna operates with a "conical beam of approximately 35°" (McCann, Jackson & Fenning (1988)), it will detect targets which are not directly beneath the antenna. As a result, the radar sees the target from a number of different angles as it passes over the surface of the ground producing a hyperbolic signature in the radar image. The shape of the hyperbolic signature depends on the wave propagation velocity in the medium and on the position of a buried object relative to the radar path. Similarly, the presence of walls in a structure can result in diagonal "swipes" extending from top to bottom.

Post-processing is generally undertaken to enhance the raw data to improve the quality and presentation of the data supplied to the operator. Before using post-processing software the user should determine whether or not an interpretation can be made from the raw data and if not, determine how much processing is likely to be required. For example, changing the colour transform may be sufficient, but for

more difficult images, sophisticated filtering techniques may be required. The most common reasons for processing are as follows:

- To provide displays to the users that are easier to understand than the raw data.
- To convert the time-scale on the image into terms of depth.
- To examine aspects of the data which may provide insights which are otherwise not apparent in the raw data.
- To remove noise and interference from the data and hence improve data interpretation.
- To correct for geometrical errors and provide more accurate depth interpretation.
- To compensate for increasing signal attenuation with depth.

However, only limited improvement can be made to the images due to the unpredictable nature of interference. Similarly, applying a gain to weak signals also results in the amplification of the background noise and interference, providing the operator with a "noisy" result.

4.4.6 Discussion

GPR is an extremely versatile technique (Hobbs, Temple, Hillier, Silk & Tattersall (1993)) and in some applications is the only technology which can be used successfully for the location of hidden features. For instance, GPR has been used to investigate roads, (Gordon, Broughton & Hardy(1998) and Hugneschmidt, Partl & De Witte(1998)) and to find archaeological remains (Goodman & Nishimura (1992)). GPR has also been used in association with other techniques as shown in Binda, Saisi

& Tiraboschi (2000) where radar was used to assess earthquake damaged towers in Italy. In this study, they also used a geometrical survey, static and dynamic monitoring, soil surveys, infra–red thermography, sonic testing as well as drilling cores. Flint, Jackson and McCann (1999) and Colla, McCann, Forde, & Das, (1997) show that GPR can be used on masonry arch bridges, to determine the internal state. There has been a European Union (E.U.) study undertaken (Göttel & Flohrer (1999)) to compare the suitability of various commercial antennae and systems, for work on post-tensioned bridges, this work also involved some radar modelling as well. From this E.U. study the GSSI radar system that Edinburgh University own is identified as highly competitive with the other systems. Radar is a cost-effective method, it is easy to use and can be employed for various materials and locations, whilst clays, metals and saline solution give problems. Improvements in GPR systems as a whole should enable better performances to be achieved in the future, while the interpretation of radar images will also improve as computer processing power increases.

The potential problems that may be encountered when using radar on railway track bed are interference from the rails and the sleepers, penetration problems from scatter due to the large particles of ballast and attenuation due to the conductivity of the ballast.

4.5 Electrical Conductivity

4.5.1 Principles of Electrical Conductivity

The electrical conductivity method is a cost effective, non-destructive technique that is capable of mapping terrain rapidly. The electrical conductivity of a material is a measure of the ease with which an electrical current can be made to flow through it and is similar to the method used to detect magnetic fields (Duffin (1990)). The technique involves using equipment such as the Geonics EM-38 where a transmitter coil, T_x, introduces an artificially-generated alternating current into the ground (see Fig 4.3). The penetration of the emitted current is directly related to the intercoil spacing, s (m).

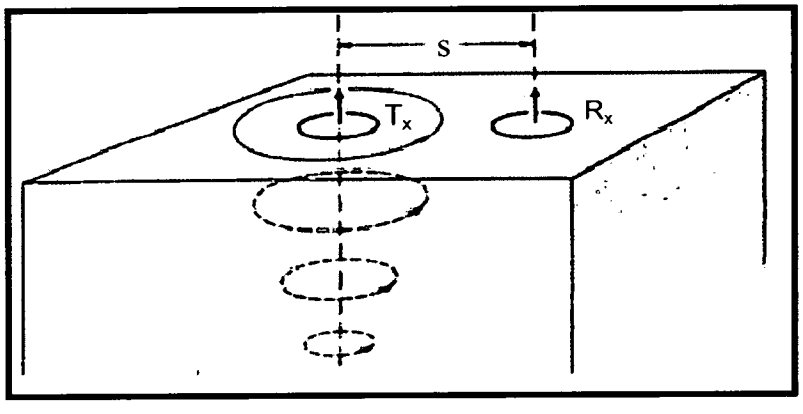

Figure 4.5 - Induced Current Flow (based on McNeil (1980))

These currents induce very small currents in the earth that generate a secondary magnetic field, H_s. This secondary magnetic field is measured with the primary field, H_p by a receiving coil, R_x. In general, the secondary magnetic field is a function of the intercoil spacing, ground conductivity, σ (mS/m) and operating

frequency, f (Hz). The secondary magnetic field can be shown in equation 4.10 (McNeil J D, 1980):

$$\frac{H_s}{H_p} \approx \frac{i\omega\mu_0\sigma s^2}{4} \tag{4.10}$$

where $\omega = 2\pi f$
μ_0 = permeability of free space
$i = \sqrt{-1}$

This ratio of the secondary to the primary magnetic field is linearly proportional to the electrical conductivity. Therefore, given Hs/Hp, the apparent conductivity (σ_a) is determined by the equipment as defined in equation 4.11:

$$\sigma_a = \frac{4}{\omega\mu_o s^2}\left(\frac{H_s}{H_p}\right) \tag{4.11}$$

If the electrical properties of two layers of material are sufficiently different, then a different field strength will be measured by the meter. Conversely, if there are insufficient differences between the properties, then no field strength variation will be measured. Deviations from the expected pattern of conductivity from homogeneous ground can provide information on the presence of subsurface anomalies. This technique is particularly suited to finding the location of cavities and buried mineshafts, exploration of archaeological sites (e.g. a wingwall of a 100 year old masonry arch bridge (Denton (1995)).

There are two methods of measuring the conductivity of a material, measuring the in-phase or quad-phase conductivity. The EM–38 has 2 coils of wire – the receiver and transmitter. The two methods are characterised by whether the receiver and transmitter are co-planar, co-axial or at right angles to each other (orthogonal). Induced currents and the associated secondary magnetic fields differ in phase from

the primary field, and detected signals can, therefore, be resolved into components which are in-phase and 90° out of phase with the primary field. In-phase components are sometimes termed real, as opposed to imaginary, quadrature or simply out of phase. These different components are the two different modes in which the EM-38 is able to measure (Milson, J. (1996)).

4.5.2 Factors Affecting Conductivity

Many factors can potentially affect the ground conductivity, however, at a given location, relatively few of these are dominant. Most rocks and soils are electrical insulators demonstrating high resistances. In general, conductivity is electrolytic and is determined by the constituents of the material, its structure and the moisture content. The conductivity of rocks and soils is therefore determined by the following: (McNeil (1980))

- The porosity of the material: shape and size of pores, number, size and shape of interconnecting passages. The compaction of the material will affect this parameter.
- The extent to which these pores are filled with water (moisture content). The moisture content is influenced by the location of the water table and climatic conditions; i.e. rate of rainfall and evaporation as well as the time after which the rain has stopped.
- Concentration of dissolved electrolytes in the moisture.
- Temperature of the pore water.
- The amount and composition of suspended matter within the moisture.

4.5.3 Advantages and Limitations

Conductivity meters such as the Geonics EM-38 are lightweight and easily manoeuvrable and can be used by a single operator to rapidly survey a large area of terrain non-intrusively and cost effectively. The EM-38 has a depth penetration of between 1.5m and 2m.

As with all geophysical instruments there are some limitations in using terrain conductivity techniques, some of which are as follows:

- With low values of terrain conductivity, it becomes difficult to induce sufficient current in the ground to produce a detectable magnetic field at the receiver coil. Conversely with high values of conductivity the received magnetic field is no longer linearly proportional to terrain conductivity.
- Calibrating and maintaining the "instrument zero". It is necessary that the zero setting is accurately maintained over long periods of time and over the wide variations in temperature which may be encountered in the field. Further influences along the survey line such as the presence of intermittent metal objects can disrupt readings significantly.

4.5.4 Data Processing.

Although terrain conductivity data can be analysed visually, i.e. regions may contain subsurface anomalies where higher or lower values than expected were obtained, more sophisticated techniques are nevertheless available. PC based commercial software packages such as the Geonics Mapping System are designed to process the terrain conductivity data and create a variety of report quality maps. These maps can take the form of:

- Shaded relief maps
- Contour maps
- Colour image maps

The Geonics system works with one or more readings (Z values) obtained from known (x,y) co-ordinates. There are two Z-values; Z_1 is the ground conductivity (or in-phase) in milliseimens/m (mS/m) whereas Z_2 is the magnetic susceptibility (or quadphase), measured in parts per thousand (ppt) - see Fig 4.6.

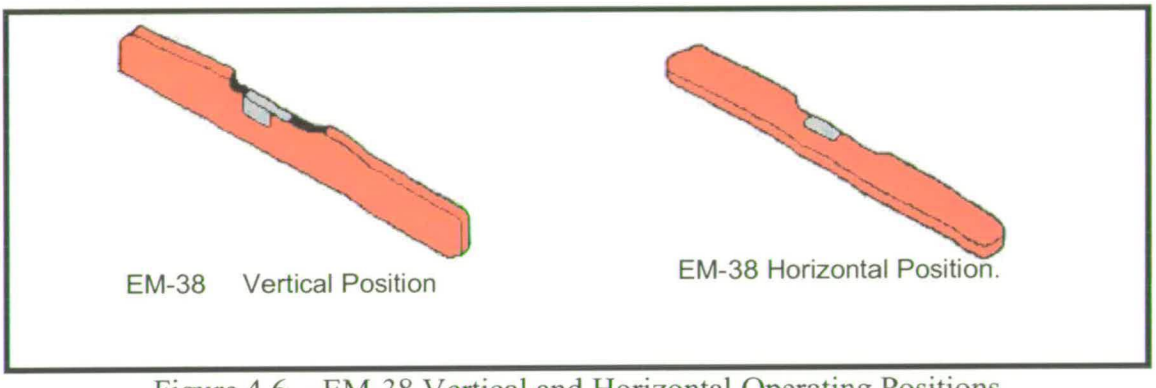

Figure 4.6 - EM-38 Vertical and Horizontal Operating Positions

(based on Milson, J., (1996))

4.6 Infra –Red Thermography

4.6.1 Introduction

Most materials absorb infra-red radiation in a wide range of wavelengths, causing an increase in the temperatures of the materials. All objects with a temperature greater than absolute zero emit infra-red energy, and even glowing objects usually emit far more infra-red energy than visible radiation.

Thermal imaging is a technique for converting a thermal radiation pattern, which is invisible to the human eye, into a visual image. To achieve this, an infra-red camera is used to measure and image the emitted infra-red radiation from an object. Since this radiation is dependent upon the object surface temperature, it makes it possible for the camera to calculate and display this temperature. However, radiation measured by the camera does not only depend on the temperature of the object, but also its emissivity and its absorption by the atmosphere. Further radiation (e.g. reflected from the sun) may be introduced by the surroundings, which may be reflected on the object.

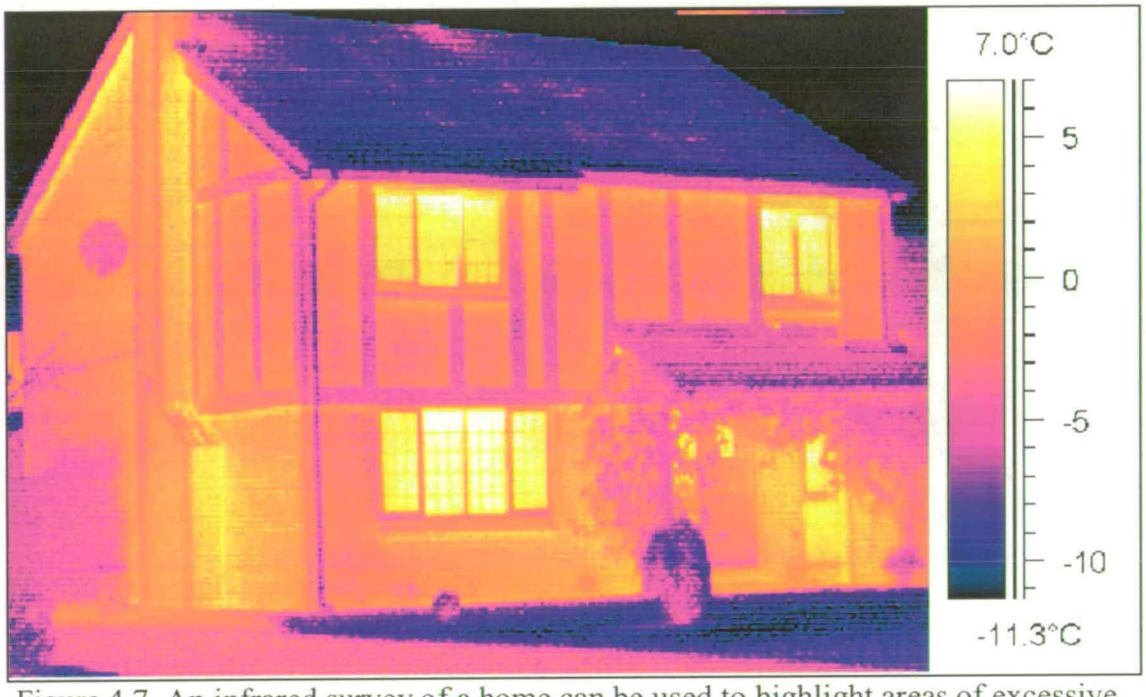

Figure 4.7 An infrared survey of a home can be used to highlight areas of excessive heat loss (Agema Infrared Systems, (1997)).

Infra-red radiation has many applications such as civil, industrial, medical, scientific and military. The use of thermal imaging to detect heat loss form a house is shown in figure 4.7.

4.6.2 The Electromagnetic Spectrum.

Electromagnetic radiation can be characterised by its frequency or wavelength. When electromagnetic waves are ordered in accordance with their frequency or wavelength, this ordered arrangement is called the electromagnetic spectrum (see Fig 4.8). A source of radiation never produces just one frequency of electromagnetic waves, but emits a mixture of waves of many different frequencies.

The electromagnetic spectrum extends from zero, the short wavelength limit of the spectrum (gamma-rays), to infinity, the long wavelength limit of the spectrum (radio waves). Visible light occupies a narrow band extending from about 0.4 μm to 0.7 μm. The coloured components of this band can be seen when a beam of light is passed through a glass prism extending from red at the long wavelength end to violet at the short wavelength end. The radiation dispersed by the prism extends further in both directions but the human eye cannot detect light outside this range.

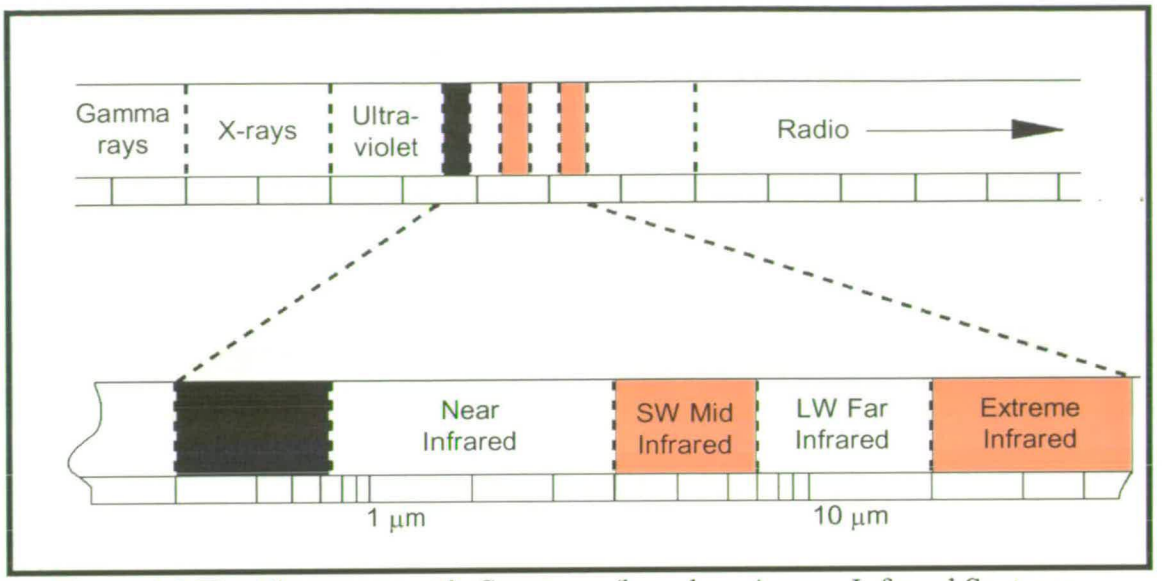

Figure 4.8 The Electromagnetic Spectrum (based on Agema Infrared Systems, (1997)).

The infra-red spectral region is important in thermography. Infra-red radiation is the region of the electromagnetic spectrum between visible light and microwaves, containing radiation with wavelengths ranging from 0.75 μm to 10 μm. This infra-red region is often further subdivided into arbitrary sub-regions (see Table 4.3).

Sub-region.	Wavelength (μm)
Near Infra-red	0.75 - 3
Middle	3 - 6
Far Infra-red	6 - 15
Extreme	15 - 100

Table 4.3 – Infra-red Sub-regions.

4.6.3 Thermal Emission.

All objects are continually emitting radiation with a wavelength distribution and at a rate that depends upon the temperature of the object and its emissivity, $\varepsilon(\lambda)$. Table 4.4 shows typical emissivities for a variety of common materials.

Material	Temp °C	Emissivity, ε
Dry Concrete	35	0.95
Common Red Brick	20	0.93
Dry Soil	20	0.92
Saturated Soil	20	0.95
Distilled Water	20	0.96

Table 4.4 Typical Emissivities of Common Materials

(based on Agema Infra-red Systems, (1997)).

4.6.4 Blackbody Radiation

A surface which absorbs all radiation incident upon it is called a blackbody, i.e. its absorptivity is 100% efficient, $\alpha(\lambda) = 1$. From Kirchoff's law, for any body, the ratio $\varepsilon(\lambda)/\alpha(\lambda) = 1$, therefore, the emissivity of a blackbody must also be unity, $\varepsilon(\lambda) = 1$. Therefore the energy emitted by a blackbody is the maximum theoretically possible for any given temperature. The total spectral radiant emittance of a blackbody, $E_b(\lambda)$ may be described by Planck's radiation law. (Drysdale (1997))

$$E_b(\lambda) = \frac{10^{-6} \times 2hc^2\pi}{\lambda^5}\left[e^{\frac{hc}{kT\lambda}} - 1\right] \quad [\mathrm{W/m^2.\mu m}] \tag{4.12}$$

Where:

$E_b(\Leftrightarrow)$ = Total amount of energy per unit area by a block body (J)

c = Velocity of light (m/s)

h = Planck's constant

k= Boltzmann's constant

T = Absolute temperature (K)

$\Leftrightarrow$ = wavelength (μm)

Figure 4.9 shows a family of curves obtained by plotting Planck's formula for various temperatures. It can be clearly seen that for any curve, the emittance is zero at λ = 0m, increasing rapidly to a maximum at a wavelength λ_{max} after which it approaches zero again at very long wavelengths. As the temperature increases, the

amount of energy emitted at any wavelength increases, and the wavelength of peak emission decreases (given by Wien's displacement law).

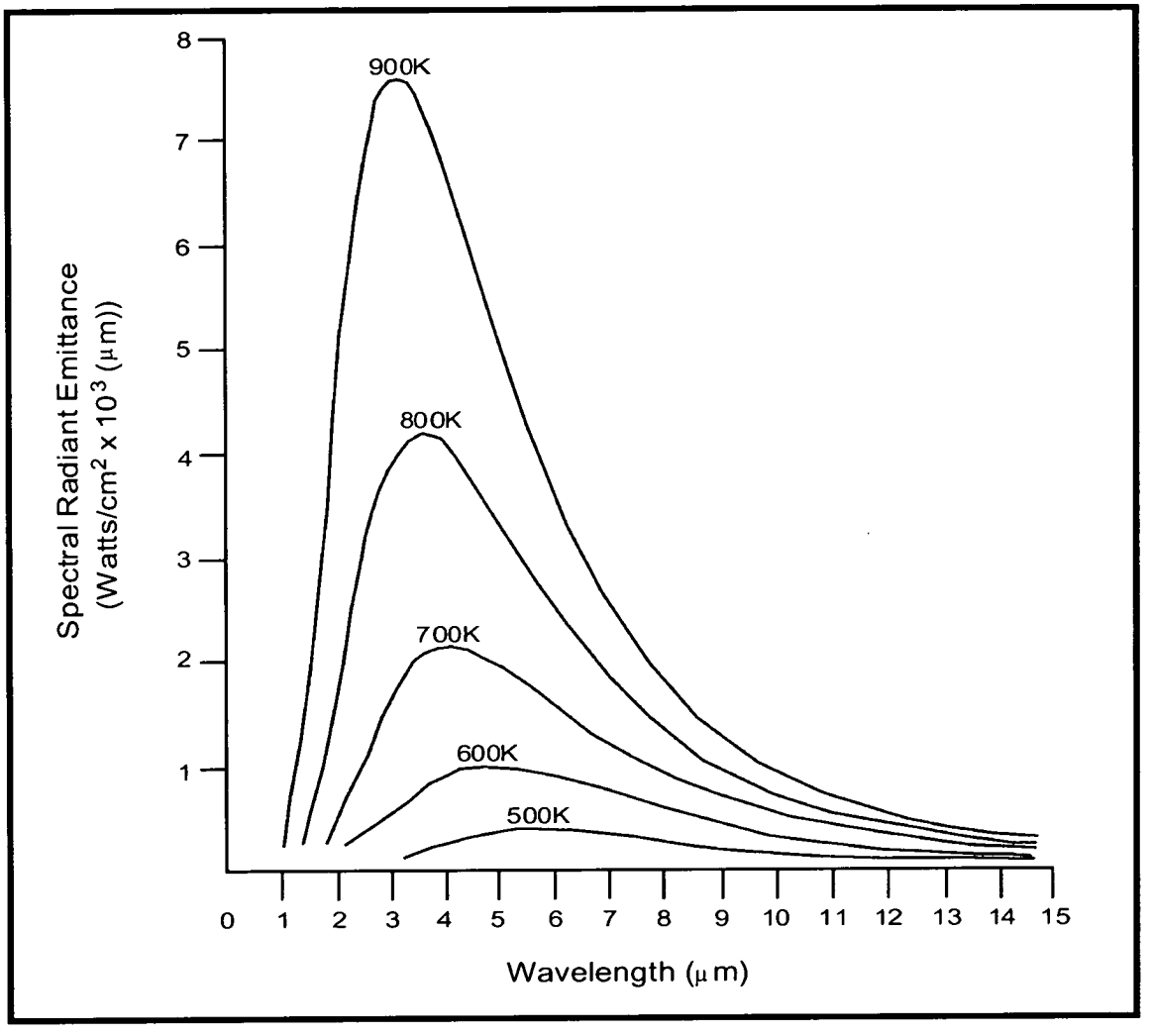

Figure 4.9 Variation of blackbody emissive power with wavelength and temperature according to Planck's law (based on Holman (1992)).

If Planck's formula is differentiated with respect to λ, the maximum wavelength λ_{max} may be obtained from Wien's displacement law: (Drysdale (1997))

$$\lambda_{max} = \frac{2898}{T} \qquad [\mu m] \tag{4.13}$$

This formula expresses, in mathematical terms, the observation that colours vary from red to yellow as the temperature of a radiator increases where the wavelength of the colour is the same as the wavelength calculated for λ_{max}. For example, at room temperature (≈300K) the peak emittance lies at $\lambda_{max} \approx 9.66$ μm, in the far infra-red. The dotted line shown on Fig 4.10 represents the maximum emittance at each temperature calculated from Wien's displacement law.

By integrating Planck's formula in the region λ=0 metres to $\lambda = \infty$, the total radiant power, E_b, of a blackbody can be expressed as the Stefan Boltzmann law: (Drysdale (1997))

$$E_b = \sigma T^4 \quad [\text{Watts}/\text{m}^2] \tag{4.14}$$

Where: $\sigma = 5.67 \times 10^{-8}$ W/m^{2}k^4

This formula states that if the temperature, T, is doubled, for example from 273K to 546K, then the radiated energy increases 16 times. Large amounts of energy must therefore be supplied to achieve high temperatures because of the high loss by radiation. Graphically, E_b, represents the area under the Planck's curve for a particular temperature.

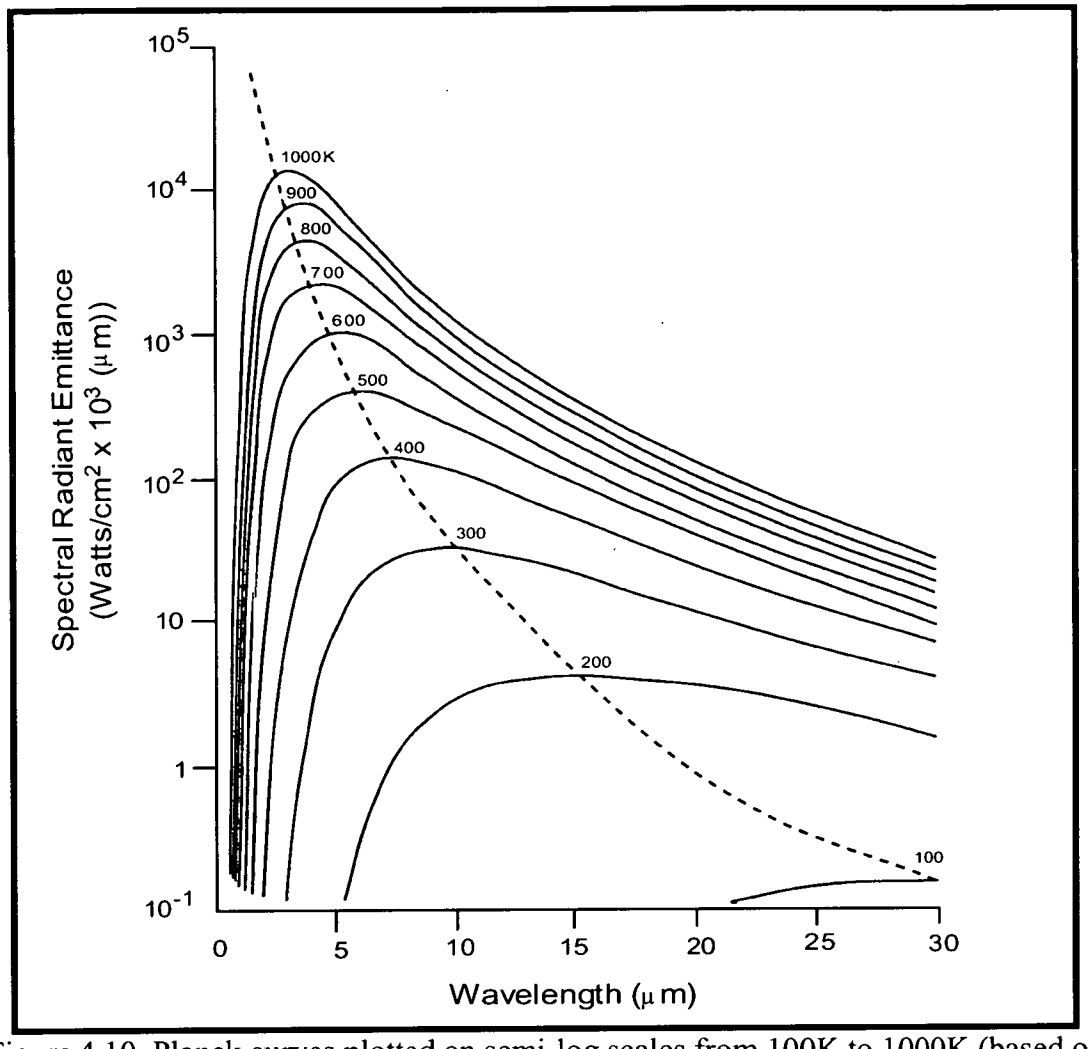

Figure 4.10 Planck curves plotted on semi-log scales from 100K to 1000K (based on Holman (1992)).

4.6.5 Behaviour of Real Bodies.

In reality, surfaces are less efficient absorbers and emitters than blackbodies (i.e. $\alpha<1$, $\varepsilon<1$) due to three wavelength dependant factors. Of the radiation incident upon a surface, a fraction α_λ may be absorbed, a fraction R_λ may be reflected and a fraction T_λ may be transmitted. Clearly the sum of these three factors must always total one at any wavelength (equation 4.15): (Drysdale (1997))

$$\alpha_\lambda + T_\lambda + R_\lambda = 1 \qquad (4.15)$$

Further, the emissivity ε_λ may be defined as the ratio of the spectral radiant power from an object to that from a blackbody at the same temperature and wavelength, (equation 4.16): (Drysdale (1997))

$$\varepsilon(\lambda) = \alpha(\lambda) = \frac{E(\lambda)}{E_b(\lambda)} \tag{4.16}$$

Where:

$\varepsilon(\lambda)$ = emissivity

$\alpha(\lambda)$ = absorptivity

$E(\lambda)$ = Emissive power of the real surface

4.6.6 Grey Bodies

A grey body is defined as one for which emissivity and absorptivity are independent of wavelength. The total emissive power of a greybody is the same as a blackbody at the same temperature reduced in proportion to the value of, ε, from the greybody, where: (Drysdale (1997)

$$E = \varepsilon\sigma T^4 \quad \text{Watts /m}^2 \tag{4.17}$$

Where

E= radiation (W/m^2)

T= temperature (K)

σ= Stefan Boltzmann constant (5.67 x 10-8 W/m^2K^4)

ε = emissivity

4.6.7. Further Material Properties.

As mentioned previously, thermal imaging systems provide a means of determining the variation of temperature within a "scene". This information may be of direct importance or may be used to determine other information about the scene or object. Properties of materials and the variations of the property for different materials can be calculated from the thermal data.

4.5.8 Heat Capacity

The heat capacity of an object is the amount of heat energy required to raise the temperature of an object by one Kelvin (J/kg.K). Similarly, specific heat is the amount of heat necessary to raise a unit of material by one degree of temperature (J/K). The heat capacity for a given volume of material is the product of the volume, specific heat and the density.

Specific heat and density vary for different materials and thus the temperature obtained by the materials for a given heat input will also vary. Similarly, objects with different heat capacities which lose heat at the same rate will change temperature to varying degrees. The specific heat of most materials remains essentially constant over the common range of temperatures, but, at extremely low temperatures, the value of the specific heat becomes smaller.

4.5.9 Thermal Conductivity.

Conduction heat transfer is the rate of flow of thermal energy through a material, q. For instance, if one end of a metal bar with uniform thermal conductivity is held in a flame, heat will be conducted evenly along the bar as long as a temperature difference is maintained between the two ends. This conduction is due to the excitation of molecules at the hot end of the bar. The excited molecules then collide with other molecules, exciting them also, thus passing thermal energy along the length of the bar. There are two modes by which thermal energy may be transported in solids: lattice vibration and transport by free electrons. In good conductors a large number of free electrons move about in the lattice structure of the material, carrying with them thermal energy from a high temperature region to a low temperature region.

The rate of heat transfer by conduction through a material is dependant upon its thermal conductivity coefficient, k_t (W/m.K). The defining equation (equation 4.18) for the thermal conductivity can be expressed in terms of the rate of heat transfer (Fourier's Law): (Drysdale (1997))

$$\dot{q}'' = -k_t \frac{\partial T}{\partial x} \quad \text{[Watts]} \tag{4.18}$$

$\dot{q}''$ = One directional heat flow W/m^2

k = Thermal conductivity W/mK

T = Temperature K

x = Distance m

In reality, the thermal conductivity of a material is unlikely to be uniform throughout its mass. For example if a sheet of material which possesses a varying thermal conductivity is heated to a constant temperature on one surface, then the temperature on the other surface will be higher in areas where the thermal conductivity is greatest. A thermal image would highlight those areas of varying thermal conductivity.

4.6.10 Convection Heat Transfer.

Convection heat transfer is the movement of gases or liquids in response to a non-uniform temperature distribution. Figure 4.11 shows a heated plate allowed to cool in still air at room temperature.

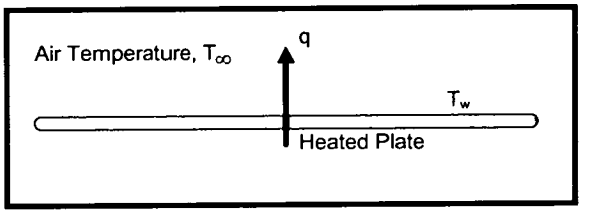

Figure 4.11 Convection Heat Transfer from a heated plate (based on Holman (1992)).

The temperature of the plate is T_w, and the temperature of the air is taken as T_∞. Heat applied to the air causes it to expand in the region closest to the heat source. This region now has a lower density than surrounding regions and, under the influence of gravity, travels upward. Conversely, an area of fluid or gas that has been cooled becomes more dense and travels downward under the influence of gravity. In either case, a convection current is established that travels through the body of the fluid, transferring heat and causing a temperature redistribution.

Newton's law of cooling expresses the overall effect of convection in equation 4.19: (Drysdale (1997))

$$q = h_t A\left(T_w - T_\infty\right) \quad \text{[Watts]} \tag{4.19}$$

q = rate of heat transfer W

h = Convective heat transfer coefficient W/m^2K

A = Area perpendicular to the x-direction m^2

T = Temperature K

Here the rate of heat transfer is related to the temperature difference between the plate and fluid and the surface area, A.

4.6.11 Application of Infra–Red Thermography

The technique of infra-red thermography has been successfully applied in a number of areas; e.g. to measure the conductive heat loss of infants in the medical industry (Adams, Gill, EK & Nelson (1998)), in the quality assessment and design of semiconductors (Talwar, Jogai & Loehr (1998)), in the printing industry to determine when the ink is dry (Can (1998)), in concrete structures in India (Kulkarni (1996)), identification of buried mineshafts (Donnelly & McCann (2000)), identification of canal seepage (Engelbert, Hotchkiss & Kelly (1997)) as well as various other civil engineering applications (Burnay, Williams & Jones (1988)). As well as many different applications of infra–red thermography there are many different methods of using thermography; e.g. one dimensional heat-flux sensing (which the majority of applications utilise), the quasisteady technique and measuring heat transfer in wind tunnels (Yang (1989)).

In a number of cases infra–red thermography has been used in collaboration with other techniques and has proved successful. Examples of these cases are Moropoulou, Koui, Tsiorva, Kourtele & Papsotiriou (1997), where infra–red thermography was used with digital image processing and fibre optic microscopy to assess and evaluate weathering damage on the Medieval City of Rhodes. Another example involved infra–red thermography, electrical resistivity sounding and borehole drilling was used to determine the seepage of a canal in Nebraska (Engelbert, Hotchkiss and Kelly (1997)). Infra-red thermography, acoustic imaging, radiography tomography and GPR have been used together to determine the location and depth of various anomalies in concrete structures (Büyüköztürk (1998)). Washer (1998) states that radar and infra–red thermography can be used together to identify cracks in highway bridges in the USA, and that infra-red is a useful tool to test areas which the radar cannot reach. In the USA the D4788 (1997) standard states the appropriate methodology to conduct an infra–red survey of Bridge Decks. Various works have been undertaken to quantify infra–red imagers. Offermann, Bissieux & Beaudoin (1998) have done this by statistical methods.

Thermal imagers offer an excellent means of making a qualitative determination of the temperature of a surface, but absolute temperature measurement is fraught with difficulties. The radiation received from an object is a function of its temperature, spectral emissivity, and reflections from its surroundings along with atmospheric transmission. This means that practical measurements should be undertaken in a temperature-controlled environment allowing time for the object to reach thermal equilibrium with its surroundings. Consideration needs to be given to the fact that, outdoors, many factors alter the surface temperature of the object under

investigation. The weather can have a major effect. Sunlight may increase the temperature and wind may decrease the temperature of an object. Rain will lower the temperature of an object through both conductivity and evaporation, it will also cause a change to the emissivity.

4.7 Other NDT Techniques

4.7.1 Falling Weight Deflectometer.

The falling weight deflectometer (FWD) is a test method which was developed to provide detailed information on the structural response of a highway pavement to simulated traffic load. The FWD applies an impulse load to the pavement and the velocity response is measured using a number of geophones (Sharpe & Collop (1998)). The velocity of the received signal at the geophones is used to calculate the elastic moduli of the various layers in the pavement. An assessment is then made comparing the calculated results with laboratory results (Sharpe & Collop (1998)). It has been shown that the FWD can be used to measure the stiffness of railway track (Fortin (1983)). The load was applied to a sleeper. The clips holding the rail to the sleeper were released on 3 adjacent sleepers so the track response could be measured using the geophone set-up, see figure 4.12.

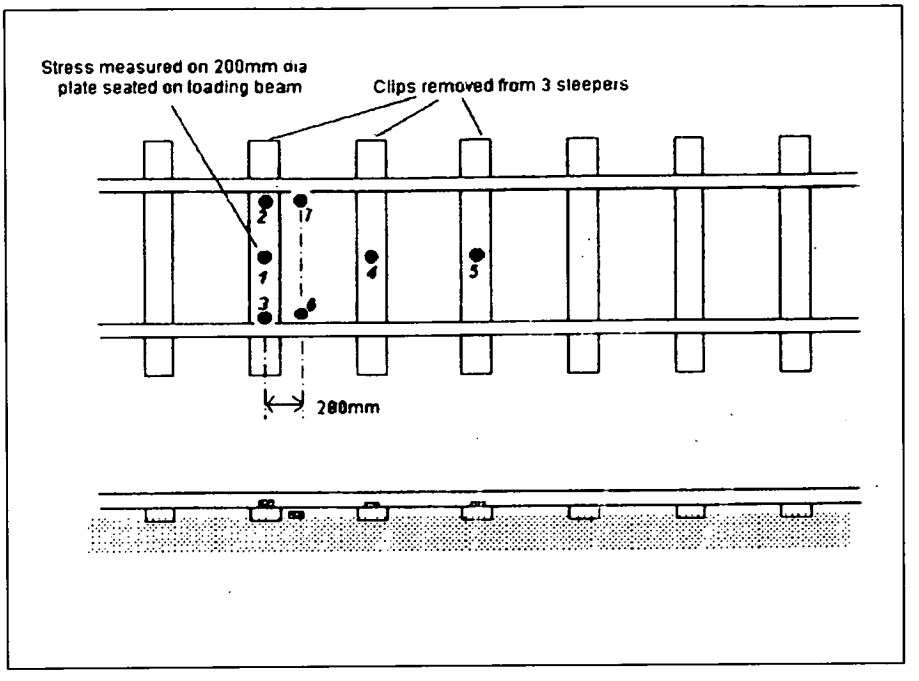

Figure 4.12 FWD Geophone arrangement (based on Sharpe & Collop (1998))

From the results of the FWD the track stiffness can be calculated (Sharpe (1996)). It has been shown that a discontinuity in track stiffness leads to a geometrical irregularity (Huille & Hunt (2000)).

The disadvantage of the FWD is that it is slow, requiring the sleepers to be unclipped. Track stiffness leads to geometric irregularities, but the condition of the ballast is only one of many factors leading to the deterioration of track stiffness, therefore, other methods need to be used in conjunction with FWD to identify the condition of the ballast.

4.7.2 Gamma Ray Spectrometer

This method is commonly used as a tool for a wide range of applications including ground radiometric surveys for uranium, portable vehicle surveys for hydrocarbons,

small airborne survey systems, laboratory data analysis and core logging. This system was used on ballast to identify the presence of potassium as a radioactive isotope. This was tested as it was assumed that the fines in the ballast would contain potassium from a nearby field, as agricultural fields will contain potassium-rich fertilisers.

This method was tested on both the test-rig at Edinburgh University [see chapter 6] as well as with field tests of the radar and infra-red thermography [chapter 7]. Unfortunately, this technique showed no significant differences between the gamma count for both clean and spent ballast.

4.7.3 Seismic

This method is commonly used in geophysical surveys to detect hydrocarbon deposits and differences in the rock strata. The method is based on the generation of seismic waves at, or below, ground level and the measurement of the time taken by the waves to travel from the source, through the medium, to a series of geophones laid out in a line from the source. The seismic signal can be generated by a number of sources including a sledgehammer and plate, falling weight, detonator and explosives. The resultant ground motion at the surface is detected by the geophones. This method picks up interference from the proximity to road and rail traffic and is normally used for surveys where a depth of penetration over 10m is required, as the resolution tends to be limited to 1m. The geophones need a good contact with the ground material and a couplant is often used, which is a time consuming process. The method was not considered suitable for the determination of ballast depth and condition as it did not have sufficient resolution and was time consuming.

Additionally the coupling between with the ballast and geophones was considered to be inadequate, as ballast is a granular material.

4.7.4 Magnetic

The magnetic method involves the measurement of variations in the magnetic field of the earth caused by local differences in the magnetisation of the surface. A magnetic survey is quick and easy to conduct and can be surveyed with a close grid spacing of 1m at low cost. Diurnal variation (the changing magnetic field of the earth over time caused by other heavenly bodies) may need to be subtracted from the recorded data and is normally recorded throughout the survey. This can be avoided by the use of a magnetic gradiometer survey. This technique employs two magnetometers at a fixed distance in the vertical plane and measures the gradient of the magnetic field. It is mainly used to locate buried mineshafts and pits, but has also been used to locate pipelines, cables and sunken vessels. This method is not suitable for the examination of ballast as the track, reinforcing bars and overhead cables do all cause interference and the magnetic properties of the clean and spent ballast would not vary significantly.

4.7.5 Ultrasonic

This method uses the transmission of high frequency sound waves into a material to detect imperfections within the material or changes in its properties. Pulse echo is the usual ultrasonic method and involves the introduction of sound waves into the object. The reflections (echoes) are returned from differences and internal imperfections of the material. The ultrasonic method was not considered useful in this evaluation as the transmission of the sound waves relies on a good contact with the surface, which would both be time consuming and a good surface may not be available due to the granular nature of the ballast.

4.7.6 Gravimeter

Gravity surveying involves the measurement of the Earth's gravitational field, which is a function of:

- Distance from the centre of the Earth.
- Centrifugal acceleration due to the Earth's rotation.
- The distribution of the mass, which is controlled by the presence of hills and valleys in the vicinity of the observation point and changes in the density in the rocks in the Earth.

There are many complicated corrections, which need to be applied to the data before it can be mapped. The application of this method in the engineering field has been limited, with greater use in the investigation of deep structures. The gravity method was not thought to be of use for application to railway ballast.

4.8 Summary of NDT Techniques for Use on Railways

Many of the techniques and applications mentioned have come from a geophysical background, where radar, conductivity and thermography have been used over the past 20 years with great success. Traditionally geophysical techniques have been used to undertake site investigations. One of the aims of this project was to take the knowledge that has been gained over the years from geophysical surveys and apply it to the classification of ballast. McCann, Culshaw & Fenning (1997) review the current geophysical techniques and explain the best practice to undertake a geophysical survey. McCann, Jackson & Culshaw (1987) described the use of geophysical techniques such as seismic, GPR and electrical resistivity for the detection of mineshafts. From table 4.5 it can be seen that GPR gives the best combination of penetration resolution and speed of operation. The advantages of GPR are described in more detail below.

Inspection Method	Parameter Measured	Advantage	Disadvantage	Cost
Visual	Surface condition	Quick; modest skills required	Superficial, subjective, slow & dangerous	Low
Coring	Specific depth & condition of ballast	Definitive dimensions	Measurement only at test points.	Moderately High
Ultrasonic NDT	Wave velocities through ballast.	Relatively quick	Poor contact with surface of ballast.	Moderate
Sonics	Wave velocity; Tomographic cross-sections	Moderately slow; Gives useful information on major elements	Poor contact with surface of ballast, requires skill to interpret data	Moderately High
Conductivity	Relative conductivity	Quick; Gives relative conductivities over a large area to a maximum depth of 1.5 m	The metal with the sleepers and the rails make conductivity impossible	Low
Infra-red	Thermal Radiation	Quick, Able to conduct survey from a distance.	Measures only the surface temperature	Low to Medium
Gamma Ray Spectrometer	Gamma Radiation	Identifies presence of fertilisers with in the fines.	Slow, needs contact with the surface, assumes presence of radioactive material	Low
Falling Weight Deflectometer	Track stiffness	Identifies areas of potential geometrical anomalies.	Slow, the sleepers need to be unclipped another method need to be used to identify the ballast deterioration.	Moderately High
Radar	Electromagnetic wave velocity	Quick; can give good penetration; can give good image of depth and condition of the ballast	May have interference from sleepers and rails.	Moderately High

Table 4.5: NDT Tests for Track bed (based on McCann. & Forde (2000))

4.8.1 Advantages Of GPR

GPR systems are relatively lightweight and easily manoeuvrable, allowing inaccessible areas to be investigated rapidly and non-intrusively. It can also be used to complement other non-destructive test procedures. Potentially large savings can be made using GPR due to the minimal disruption caused, its ability to detect structural faults early (i.e. before visual inspections or failure would lead to detection) and its high productivity. Since GPR systems do not rely on any consumables, other than batteries for field operation, they are portable and do not require a large number of operators. GPR results can be analysed and used in real time in the field through the use of dedicated computer systems. GPR has already been used on ballast previously in Germany (Gobel, Hellmann & Petzold (1994), in the UK (Jack & Jackson (1999)) and in Switerland (Hugenschmidt (1999)) with favourable results indicating that GPR is a suitable tool for use on the railway ballast. McCann, Jackson & Fenning (1988) showed that radar and seismic are appropriate tools to use on granite as thier study focused on the use of these techniques on rock, this study also gives values for the dielectric constant for granite and similar materials. No one has conducted a GPR survey of the railway ballast at speed.

4.8.2 Problems With GPR

At present, GPR systems are expensive, and therefore will not prove to be a cost-effective investment if they are used occasionally, unless a system was rented, which would reduce the initial cost. To fully utilise the system, skilled personnel are required, both to operate the system and to interpret the results accurately.

As mentioned in section 4.1.1, GPR technology is not perfect and often suffers from interference. This interference can take the form of background noise, multiple reflections and "ringing" effects between the ground surface and the antenna. Averaging the number of signals obtained in a given time without moving the antenna can sometimes reduce the effects of this interference.

GPR antennae experience "ringing" due to internal reflections, a result of the broad waveband used. This "ringing" tends to obscure later time signals recorded from buried objects. The ringing duration can be minimised by system design thus reducing the clutter in the recorded signal.

One of the major drawbacks of GPR is when there are reinforcing bars set in concrete (Bungey, Millard & Shaw (1993)) or where there is a metal plate below the surface of the structure in question. In these cases when the concrete structure is being investigated it is possible to receive no meaningful data as the radar signal would get reflected back from the metal plate or reinforcing bars if they are set close together.

The signals detected by the receiver are subject to various losses in their path from the transmitter to the receiver. The most predominant losses are detailed below (Daniels (1994) & Daniels (1989)).

- The antennae are not 100% efficient and are therefore subject to losses.

- Transmission losses can occur between the air and the material on entry.
- Retransmission losses can also occur between the material and the air on exit.
- Loss of energy due to signal spreading.
- Attenuation losses.
- Energy losses due to scattering by the target.
- Internal reflections within the antenna.

4.8.3 Advantages And Disadvantages Of Conductivity

The mapping of conductivity using the EM-38 equipment is a very quick and cost effective means of locating regions where anomalies exist. In terms of identifying regions of spent ballast in the field this technique may suffer from the fact the equipment must be regularly calibrated due to frequent changes in climatic conditions and nearby objects e.g. bridges. Furthermore, it is not yet clear whether a large enough current can be induced in the ballast to produce a detectable magnetic field at the receiver coil. Additionally the large amount of metal present in the sleepers and rails will affect the results.

4.8.4 Infra-Red Thermography

Since there are other more direct methods of measuring temperature differences such as temperature sensors and thermocouples, it is useful to consider some of the advantages provided by thermography as well as some of its limitations. Thermography has been used and proved extensively before for different applications (Donnelly &McCann (2000)).

4.8.4.1 Advantages Of Thermography.

- Remote Sensing 1. No direct contact is required between the camera and the object under investigation. Camera and object separation can range from a few millimetres to several kilometres thus allowing measurements to be made identifying potentially hazardous areas. As no external source of illumination is necessary, both day and night operation is possible.
- Remote Sensing 2. Due to the separation between camera and object, measurement by thermography should not cause interference with the object and, hence, acquired data. In reality, some interference will be caused by the camera shielding the object from some radiation which would otherwise be incident upon it and by the radiation reflected and emitted from the camera itself. These effects can normally be assumed to be negligible.
- Large Monitoring Capacity. Thermal imaging cameras are capable of monitoring temperature at many different points within a scene simultaneously.
- Visibility. Since thermal radiation can penetrate smoke and mist more readily than visible radiation, visually obscured objects can be detected readily.
- Range of Measurement. By altering the camera lens aperture and by introducing various filters, the sensitivity of the system and its response to thermal radiation can be altered to suit. Typical temperature ranges are of the order of -20 to 1600°C.
- Fast Response Rate. Thermal imaging equipment is capable of detecting and monitoring rapid temperature fluctuations to an accuracy of +/- 0.01°C.

- Portability. Thermal imaging equipment is lightweight and can be easily transported. It is also possible to use the equipment whilst mobile.
- Data Manipulation. The recorded data can be monitored and processed on a standard PC running dedicated imaging software.

4.8.4.2 Problems In Applying Thermography.

- From section 4.5.3, the radiation reaching a thermal imaging system is not only a function of the temperature of the object but also of its emissivity. Since emissivity varies from material to material, the brightnesses of different objects within a scene do not necessarily give a clear indication of their relative temperatures.
- Since the reflectivity of any surface can be taken as $(1-\varepsilon)$, any material with emissivity less than one will reflect radiation from surrounding objects as well as radiating its own radiation. Thus the temperature obtained for an object may be influenced by surrounding objects.
- Attenuation of radiation in the atmosphere caused by the absorption of energy by suspended particles and subsequent re-radiation in random directions can affect the obtained results. These effects can be assumed negligible for cases where camera-object separation is small.

There are additional problems when applying thermography to the railway track bed. The external presence of items such as bridges, trees, embankments and sewers, will affect the temperature of the ballast. Other factors that may affect the temperature of the ballast are the time of the day and whether the ballast is heating or cooling also affects the results. Also, the overhead electric lines limit the height from which a

survey can be conducted. However the thermographic survey can be conducted at speed, as no contact is needed.

Radar and infra–red thermography have been used together on a number of occasions for different applications - concrete structures (Büyüköztürk (1998)) and on highway bridges in the USA (Washer (1998)). Weil (1992, 1993 &1995) has shown that bridges, highway and airport pavement have been tested with both infra-red and radar finding a variety of faults ranging from cracks on airport pavements, to delaminations on bridges.

4.9 Conclusions

The main methods discussed to determine the state of the ballast on the track bed were - radar, infra-red thermography and conductivity. The limitations of the methods were discussed but each of these methods have different advantages for the use in the railway industry.

The falling weight deflectometer is the current method used by the industry for testing the stiffness of the ballast. This was not investigated further as part of this work.

From section 4.5 it was decided that for use on the railway it would be necessary to perform a rapid, cheap, non contact reconnaissance assessment of the ballast in-situ.

Conductivity was found to be of little use to determine the condition of the ballast due to the presence of rails and sleepers. Without these metallic elements conductivity would be an ideal method and has been used in other similar circumstance.

This thesis will therefore concentrate on both the radar and infra-red methods, as there has been limited research into these methods on railway track bed. The fact that the rails and sleepers have limited adverse effect on the techniques and both were capable of continuous, non-contact, high-speed recording, make them ideal for use on the railway. Also from the literature it can be seen that these two techniques can be used on railway track beds.

Chapter 5:

Laboratory Modelling of Radar and Infra–Red Thermography

5.1 Radar Laboratory Set-up and Results

Ground penetrating radar (GPR) may provide a possible means of determining the condition of the track bed since it can produce a cross-section view of the material underlying the surface of the track bed. This technique is cost effective and large surveys can be undertaken rapidly. It is also non-intrusive and causes no environmental impact compared with the current investigation technique of trial pit digging and visual inspection. Before GPR could be used as a tool for ballast characterisation intensive laboratory work had to be undertaken. The objectives of the laboratory work were:

- To investigate whether the dielectric constant, ε_r or the velocity of propagation of electromagnetic waves, can classify the condition of the railway ballast.
- To investigate the suitability of the 500 MHz or 900 MHz GPR antennae in providing adequate penetration and producing clear images at acceptable resolution.
- To investigate whether simple targets buried in the ballast could be indentified.

The laboratory experiments were conducted in a brick tank (figure 5.1 & figure 5.2), which provided a means of constructing a prototype track bed so the depth of ballast could be varied quickly and easily. Two different types of ballast were used in the laboratory experiments; clean and spent. The clean ballast was unused, whilst the spent ballast had been taken off the track bed, and was considered to be at the end of

its life span. The ballast was compacted in layers as it was placed into the tank to simulate the conditions found on site. The laboratory conditions of the ballast, therefore, can be thought to be near to the natural 'on rail' condition of ballast, as can be seen in figure 5.3.

The antenna acting as a transmitter/receiver was dragged along the top surface of the ballast layer as shown in figure 5.4. To reduce the vibration of the antenna caused by the slight differential settlement in the surface layer, downward pressure was used when necessary. This procedure was carried out with both the 500 MHz and the 900 MHz antennae. This technique is illustrated by figure 5.5.

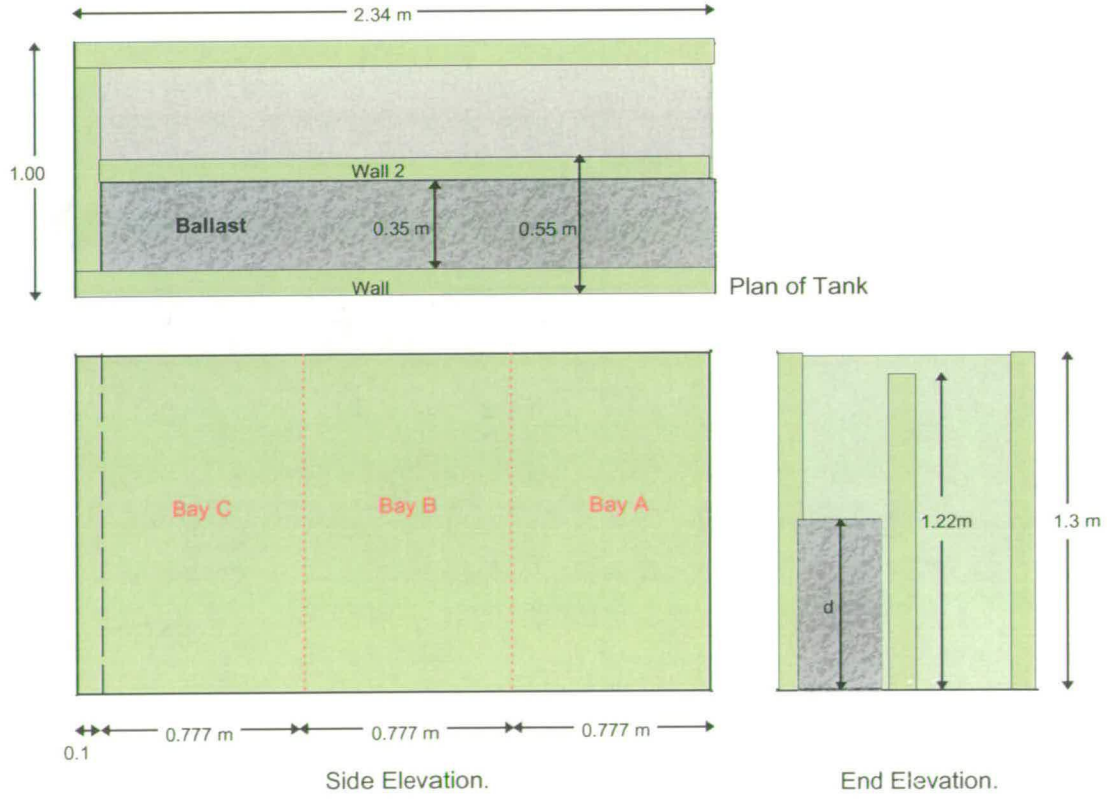

Figure 5.1: Tank Dimensions.

Figure 5.2: Elevation of Masonry Test Rig used for Ballast Experiments

Figure 5.3 Tank Containing 0.75m of Spent Ballast

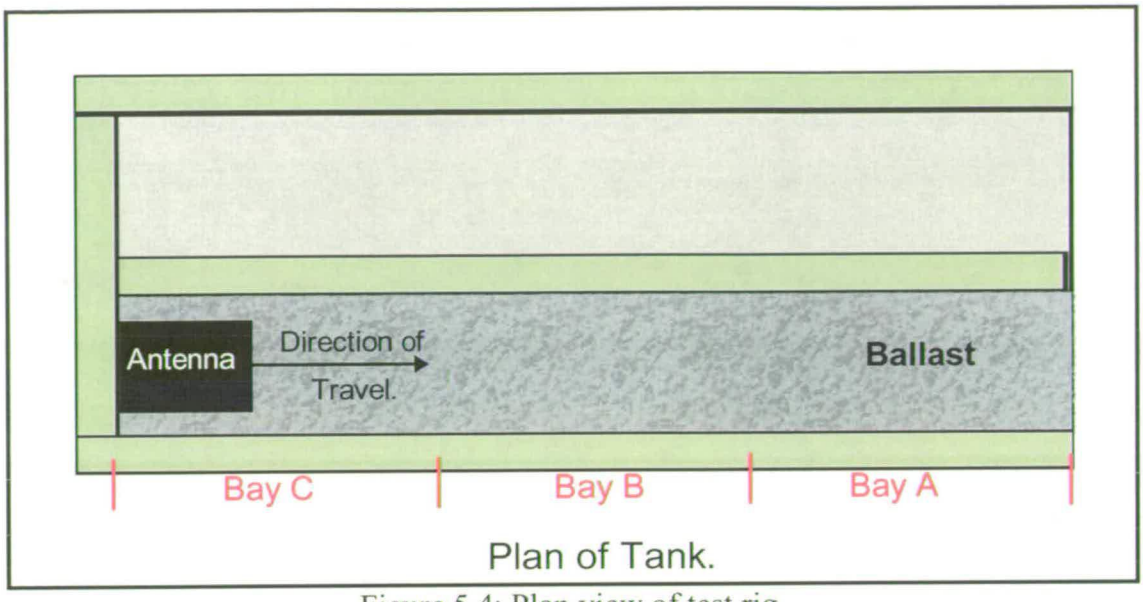

Figure 5.4: Plan view of test rig

Figure 5.5 - Surface Drag Method using 500 MHz Antenna.

5.2 Dielectric Constant

From the experiments undertaken the dielectric constant for the different types of ballast, was found using the equation:

$$\varepsilon_r=(ct/2d)^2 \qquad (5.1)$$

Where:

c = Velocity of light = 3×10^8 (m/s)

ε_r = Dielectric constant of a material

t= Time taken for electromagnetic wave to travel distance, d (s)

d = Depth of material layer (m)

The equation was used because ballast was assumed to be a low loss medium.

Material	ε_r	velocity (m/s)	Density (Mg/m^3)
Air	1	$3.00x10^8$	
Water	81	$0.33x10^8$	1
Dry Clean Ballast	3.0	$1.73 x10^8$	1.6
Wet Clean Ballast (5% water *)	3.5	$1.60 x10^8$	
Saturated Clean Ballast	26.9	$0.48 x10^8$	
Dry Spent Ballast	4.3	$1.45 x10^8$	1.8
Wet Spent Ballast (5% water *)	7.8	$1.07 x10^8$	
Saturated Spent Ballast	38.5	$0.58 x10^8$	

* 5% water by volume added

Table 5.1. List of electromagnetic properties for various materials

It can be seen that from table 5.1 that the dielectric constant for spent ballast is much higher than that for clean ballast. These results for the dielectric constant are comparable with the results for ballast found by Gobel, Hellmann & Petzold (1994) which are in the range of 4-6 – apart from the high values for saturated ballast. Although the conditions are not specified the results from table 5.1 are comparable.

5.3 Suitability of Various Antennas

To show the suitability of various antennae for ballast classification, the 500 MHz and 900 MHz antennae were dragged along the surface of the ballast in the tank. The aim of the experiment was to identify the interface between the ballast and the concrete floor. Figure 5.6 and figure 5.7 show the raw radar plots of the ballast using both antennas. Figure 5.8 shows the effect of introducing a metal object (in this case a metal plate) below the radar antenna, making it impossible to see any detail below the metal plate as there is "ringing" off the metal plate.

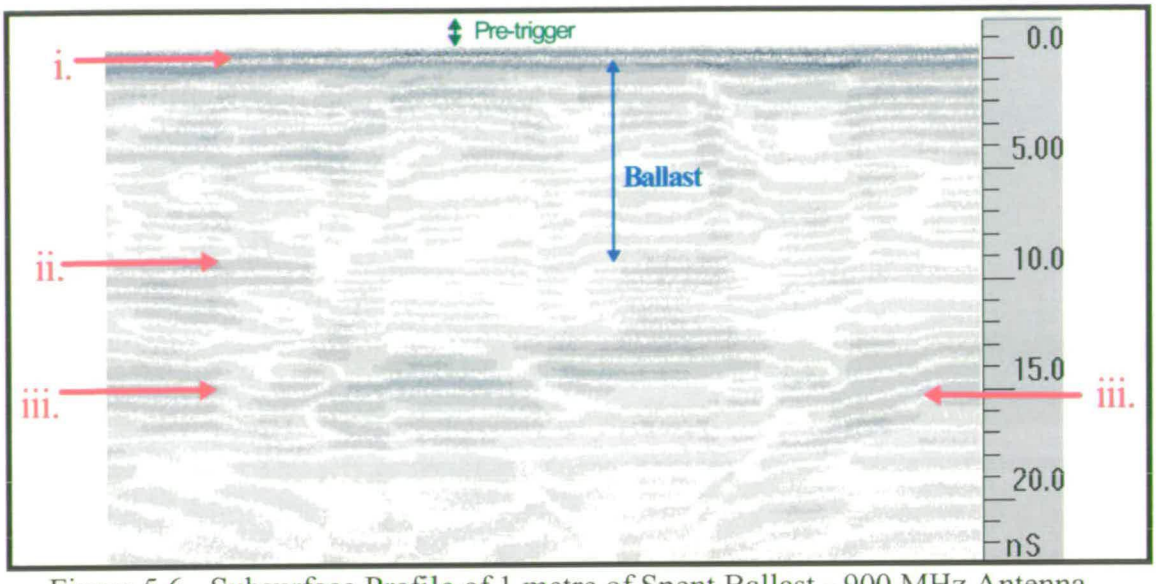

Figure 5.6 - Subsurface Profile of 1 metre of Spent Ballast - 900 MHz Antenna

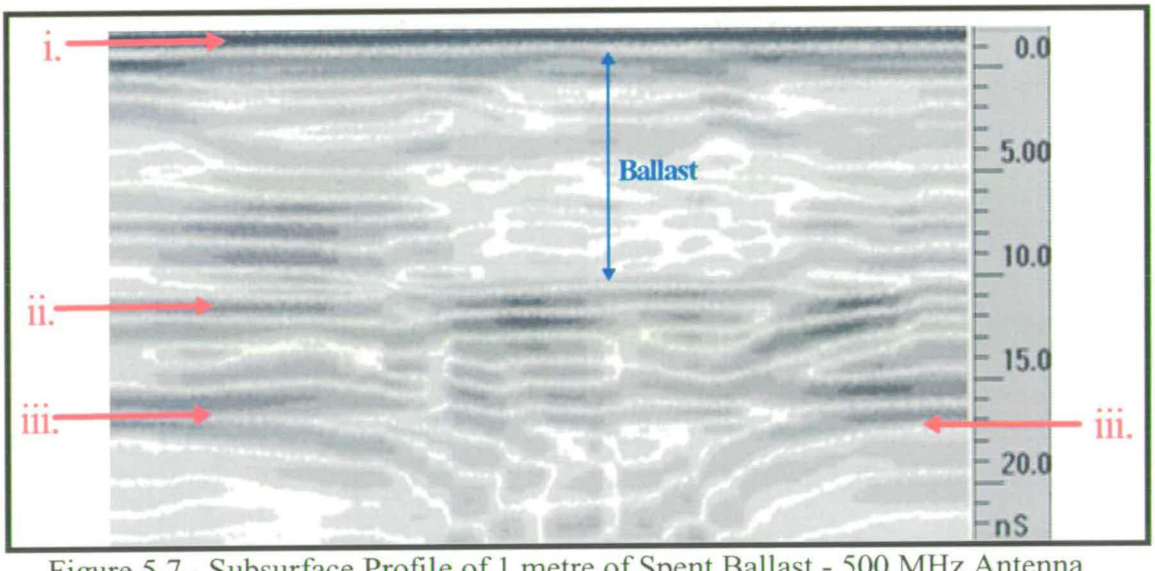

Figure 5.7 - Subsurface Profile of 1 metre of Spent Ballast - 500 MHz Antenna

Where:

i. Electromagnetic wave enters the ballast surface.

ii. Wave reflection from base of tank.

iii Diagonal "swipe signatures" are caused by reflections from the tank walls.

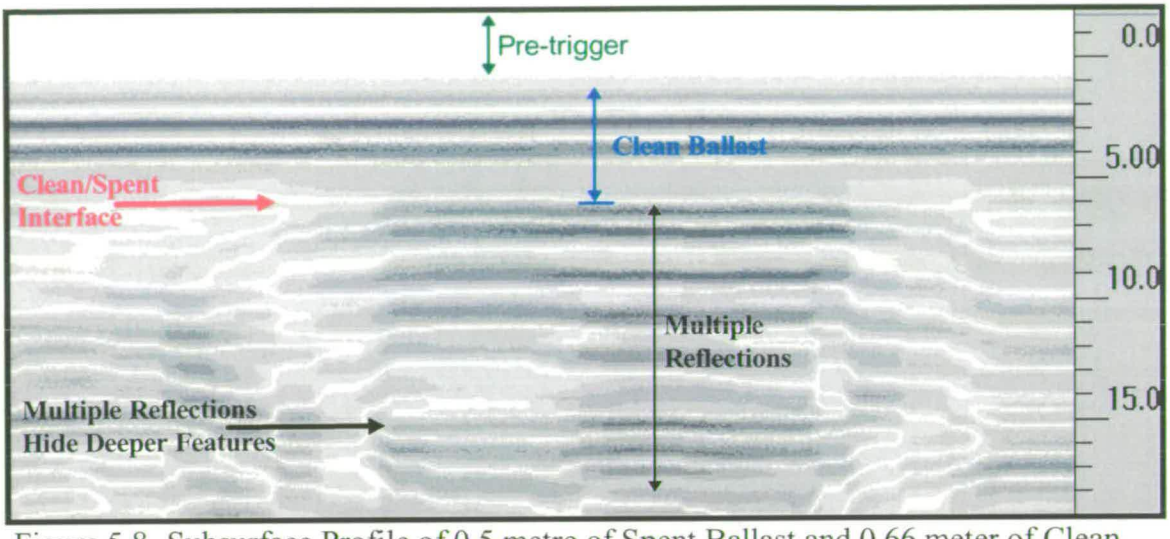

Figure 5.8- Subsurface Profile of 0.5 metre of Spent Ballast and 0.66 meter of Clean Ballast: 500 MHz Antenna - Metal Sheet at Interface

5.4 Discussion of GPR Laboratory Work

5.4.1 Dielectric Properties and Electrical Conductivity

The dielectric constant of the clean ballast was lower than that of the spent ballast. The clean ballast is uniformly graded and regardless of how well it is compacted it will always have more air voids than the spent ballast. The dielectric constant of air is 1 (velocity of 3.00 x10^8 m/s), which, as a result, allows the electromagnetic wave to propagate through it at a higher velocity compared with the ballast aggregate. The spent ballast had a gap-graded particle size distribution, presenting less air voids. As a result, it has a higher dielectric value and lower velocity of propagation than that of the clean ballast.

The dielectric constant of the wet ballast was higher than that of the dry ballast. This was due to the fact that the speed of the electromagnetic wave through water was

slow (0.33 x10^8 m/s) compared to that of the ballast or air. Thus, with the wet ballast the characteristics of the water will predominate, as water replaces air in the voids. The 17% increase of the dielectric constant (7.5% decrease in the velocity of the electromagnetic wave) showed that water was filling the air voids when it was added to the clean ballast. When water was added to the spent ballast there was a 81% increase in the dielectric value indicating that spent ballast holds water. The increase of the dielectric value was higher than that of the clean ballast because the spent ballast has a higher capacity for water retention due to the high fines content. Looking at the saturated results it can be seen that the difference of the dielectric constant increases as the water content increases. Therefore, a high moisture content in clean and spent ballast increases the difference between their dielectric constants, and thus when ballast is wet it is easier to tell the difference between clean and spent ballast.

The electrical conductivity of the ballast is affected by the presence of the fines and water. The fines are created by the factors outlined in the Introduction and Chapter 2. As the dielectric constant of the ballast increases so does the electrical conductivity. As the electrical conductivity increases the attenuation of the signal increases. This can be seen in figure 5.6 and figure 5.7 as the interface between the spent ballast and the concrete floor is not well defined.

5.4.2 Suitability of Various Antennas

Figure 5.6 and figure 5.7 show the interface between the ballast and the concrete floor of the laboratory for the same experimental set up but with different antennae. This clearly indicates that by using 500 MHz antenna it is easier to pick out the

interface between the ballast and the concrete floor than by using the 900 MHz antenna. Additionally it identifies other objects of interest on the radar plot more easily than the 900 MHz antenna; e.g. the sideswipe of the edges of the tank. This is due to the 900 MHz antenna experiencing more clutter (Padaratz, I.J. & Forde, M.C. (1995)) - the scattering of the signal. The differential compaction and irregular size and shape of grains within the ballast caused this scattering of the signal. Making the signal wavelength larger than the average dimension of the ballast can reduce the clutter effect. From the theoretical relationship, the best frequency commercial antenna is the 500 MHz. This result was confirmed by the experimental results.

5.5 Infra–Red Laboratory Experimental Set-Up

A thermal imager can only measure the surface temperature of an object. This depends on many variables, such as the temperature of the surrounding materials, the atmospheric temperature, the ambient temperature, the weather, the object properties (i.e. the rate of conductivity, convection, the thermal heat capacity), stress-induced temperature change and absorption of infra red radiation. The advantages of using a thermal imager to measure the surface temperature are: remote sensing, 2-dimensional data acquisition, rapid response, non-contact, high resolution, large temperature range, post-processing versatility and portability.

The thermal imager used was the Agema Thermovision 900 infra-red camera system. This is a long wave camera, which detects small temperature differences. The camera captures the thermal information and relays it through the PC card interface to the laptop computer for data storage and processing. By measuring the emitted

infra-red radiation from an object this camera can measure differences in temperature up to Γ 0.01°C. Radiation is a function of an object's surface temperature, which makes it possible for the camera to calculate and display the temperature. The radiation measured by the camera does depends not only on the object surface temperature but is also a function of the emissivity. Emissivity is a measure of the efficiency of a surface to act as a radiator. The equation for the radiation of an object according to the Stefan-Boltzmann equation is (Drysdale (1997), Schmidt, Henderson & Wolgemuth (1993) & Yang (1989)):

$$E = \varepsilon \sigma T^4 \tag{5.2}$$

Where:

E= radiation (W/m^2)

T= temperature (K)

σ= Stefan Boltzmann constant (5.67×10^{-8} W/m^2K^4)

ε = emissivity.

Other potential problems can occur when the object reflects radiation originating from the surroundings. Atmospheric absorption of radiation will also affect the measured temperature.

Before any experiments were conducted, the emissivity of the ballast was determined. A reference point was selected and its temperature was measured using a thermocouple. The emissivity value in the post-processor was altered until the temperature measured by the infra-red camera was identical to the temperature

measured by the thermocouple. As emissivity is a function of radiation emitted from a surface it was necessary to have a temperature difference between the ballast and the atmospheric temperature to measure the emissivity.

It was found that these values did not change if the ballast became wet unlike some materials such as sand, as the colour changes when the sand become wet. The emissivity of the ballast was found not to vary over a range of temperatures. Emissivity values range from 0.1 to 1: for a highly polished (mirror) surface the emissivity would be 0.1 while human skin exhibits an emissivity close to 1. The calculated emissivities from the experiments as well as other typical values of emissivity are shown in table 5.2. :

Material	Temp (°C)	Emissivity
Water (Distilled)	20	0.96
Water (Frost Crystals)	-10	0.98
Soil (Dry)	20	0.92
Soil (Saturated with water)	20	0.95
Brick (Common red)	20	0.93
Concrete (Dry)	35	0.95
Clean Ballast	20	0.98
Dirty Ballast	20	0.98

Table 5.2 Emissivity values of ballast and other typical materials.

The experiments were undertaken on ballast in two different states, clean and spent. Spent ballast has more fine particle as well as oils and other fouls, which fill the air voids that are present in the clean ballast. Similar experiments have been conducted (Rantala, Wu and Busse (1998)) on PVC plates to find delaminations using a similar camera and experimental set-up. Theoretically, the clean ballast, when heated or cooled, will be able to use convection in the air voids as a mechanism of heat exchange to a greater extent than the spent ballast. The spent ballast will be able to use conduction as a mechanism of heat transfer more than clean as a greater number of particles are in contact with each other and the air voids are filled with fines. The radiated heat from the spent ballast will be greater than that from clean ballast as there is more surface area exposed on the spent ballast as the air voids are filled with fines. Equation 5.2 indicates the radiated heat of a point on an object, and hence as spent ballast has a greater surface area exposed due to the presence of the fines it will then have a high amount of radiated heat. Therefore spent ballast should heat up or cool down to an equilibrium temperature at a different rate to clean ballast.

5.6 Infra–Red Theoretical Discussion

The simple steady-state heat transfer equations were used to theoretically investigate the ballast. Some of the assumptions used were:

- The ballast was of an infinite cross sectional length.
- The ballast was of a thickness (L).
- The soil or clay temperature (T_c) (i.e. the temperature below the ballast) and air temperature (T_a) were constant.
- The clay temperature was hotter than the air temperature.

- The spent ballast had a constant k (thermal conductivity).
- Clean ballast is made up of 0.05m ballast particles and 0.005m air voids.
- The heat flow is unidimensional.

The thermal conductivity (k) of ballast was taken to be 1 W/mK. As concrete is in the range 0.8-1.4, brick 0.69 and steel (mild) 45.6 W/mK, air was taken to have a thermal conductivity of 0.026 W/mK.

The rate of heat transfer (q) is onbtained by using Fourier's Law of Heat Conduction (Drysdale,D. (1997), Schmidt, Henderson & Wolgemuth (1993) & Yang (1989));

Where: $T_x > T_y$

$$q = -k\frac{dT}{dx} \tag{5.3}$$

Gives $$q\int_0^L dx = -k\int_{Tx}^{Ty} dT$$

Provided that k is independent of temperature, gives:

$$q = \frac{k}{L}(T_x - T_y) \tag{5.4}$$

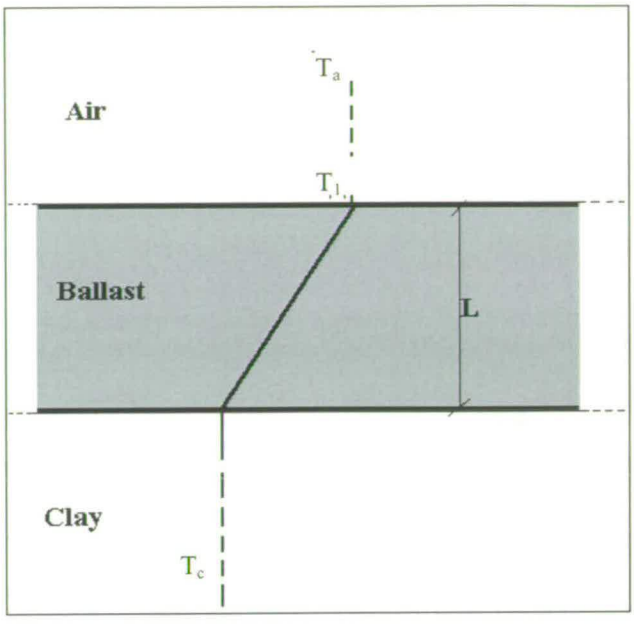

Figure 5.9 Theoretical Model of Spent Ballast

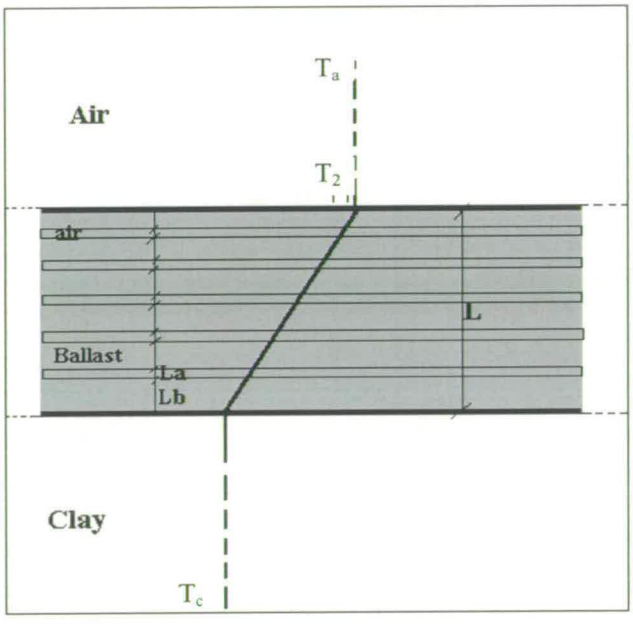

Figure 5.10 Theoretical Model of Clean Ballast

Figure 5.9 and figure 5.10 show figuratively the theoretical models from which the equations for heat transfer were derived. T_1 and T_2 are the surface temperature of spent and clean ballast respectively. Spent ballast was assumed to be homogenous,

as the fines would fill the air voids. The clean ballast was assumed to contain air voids. To simplify, it was assumed that there was a layer of air between each piece of ballast. The ballast was assumed to be 0.05m thick and the air voids 0.005m thick, and hence there would be 9 ballast particles and 8 air voids to total 0.5m. A convection factor was placed into the equation to take into consideration the air currents, h_a (convection heat transfer coefficient) the quoted value for air is 10 W/m^2K (Drysdale (1997)).

Rate of heat flow through dirty ballast.

The introduction of h_a (Drysdale (1997)) gives:

$$q = \frac{T_c - T_a}{\frac{1}{h_a} + \frac{L}{k}} \tag{5.5}$$

Using; $h_a = 10\ W/m^2K$, L=0.5 m, k = 1W/mK

$$q = \frac{T_c - T_a}{\frac{1}{10} + \frac{0.5}{1}}$$

$$q = \frac{5}{3}(T_c - T_a) \tag{5.6}$$

Rate of heat flow through clean ballast

The introduction of the ballast and air layers (Drysdale (1997)) gives :

$$q = \frac{T_c - T_a}{\frac{1}{h_a} + 9\frac{L_b}{k_b} + 8\frac{L_a}{k_a}}$$

Where; $h_a = 10\ W/m^2K$ $L_b = 0.05m$, $k_b = 1\ W/mK$, $l_a = 0.005m$, $k_a = 0.026W/mK$

$$q = \frac{1}{2}(T_c - T_a) \tag{5.7}$$

This gives an equation showing the heat flux through the different types of ballast, but does not involve the surface temperature of the ballast which can be detected with the infra-red camera. The heat flux through the whole plane is the same as that through any part, so the heat flux through the entire ballast is the same as that from the surface to the air:

Surface temperature of dirty ballast T_1

$$q = \frac{5}{3}(T_c - T_a) = h_a(T_1 - T_a)$$

Therefore: $$T_1 = T_a + \frac{5(T_c - T_a)}{30} \tag{5.10}$$

Surface temperature of clean ballast T_2

$$q = \frac{1}{2}(T_c - T_a) = h_a(T_2 - T_a)$$

Therefore: $$T_2 = T_a + \frac{(T_c - T_a)}{20} \tag{5.11}$$

A similar theoretical discussion of heat transfer has been explored in Niliot & Gallet (1998) but rather than ballast they concentrated on the boundary conditions that are evolved in various structures such as walls and hollow square bars. From equations 5.10 and 5.11 it is possible to predict theoretically the surface temperature of spent and clean ballast from a knowledge of the ground temperature and the atmospheric temperature. Both of these temperatures can be measured. The greater the

temperature difference between clean and spent ballast, the better the conditions are to conduct an infra-red survey. Figure 5.11 shows the surface temperatures of clean and spent ballast in relation to the soil temperature at an atmospheric temperature of 6°C. The linear relationship of the gradient of the lines in figure 5.11 is constant and if only the atmospheric temperature changes-only the intersection point of the lines changes; this can easily be observed in figure 5.12 and figure 5.13. The temperature difference between the atmospheric temperature and the soil has to be over 5°C to obtain a 2°C difference between the two types of ballast from figure 5.11. Figure 5.11 shows both the spent and clean ballast data for when the atmospheric temperature is 6°C while figure 5.12 and figure 5.13 shows separately the clean and dirty ballast temperature change for the total range of atmospheric temperatures. The importance of these figures is that it is possible to predict, before going on site, whether it would be possible to tell the difference between clean and spent ballast, from the atmospheric temperature and the soil temperature. With this information it is possible to timetable the field survey of ballast for when there is maximum contrast between clean and dirty ballast. This optimum time would be in early evening when the ballast has started to cool when the atmospheric temperature has dropped rapidly and the soil temperature is higher as it has a higher thermal mass.

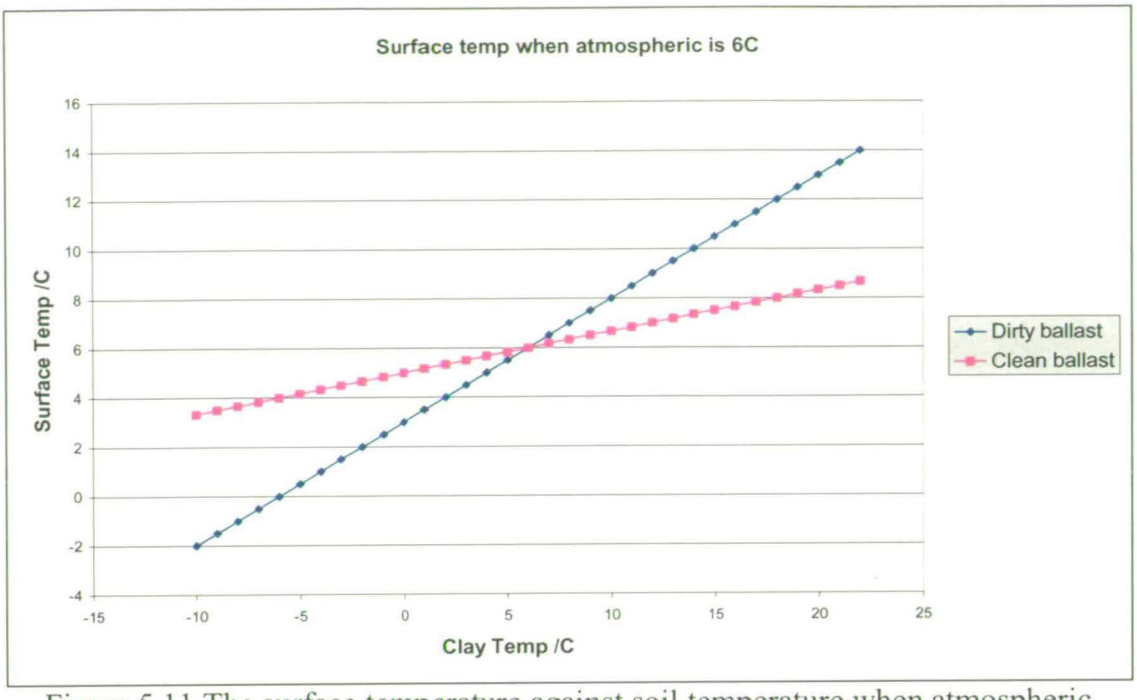

Figure 5.11 The surface temperature against soil temperature when atmospheric temperature is 6°C

Figures 5.12 and figure 5.13 show 3-D plots of the clean and spent ballast against the soil temperature, for the complete range of atmospheric temperatures.

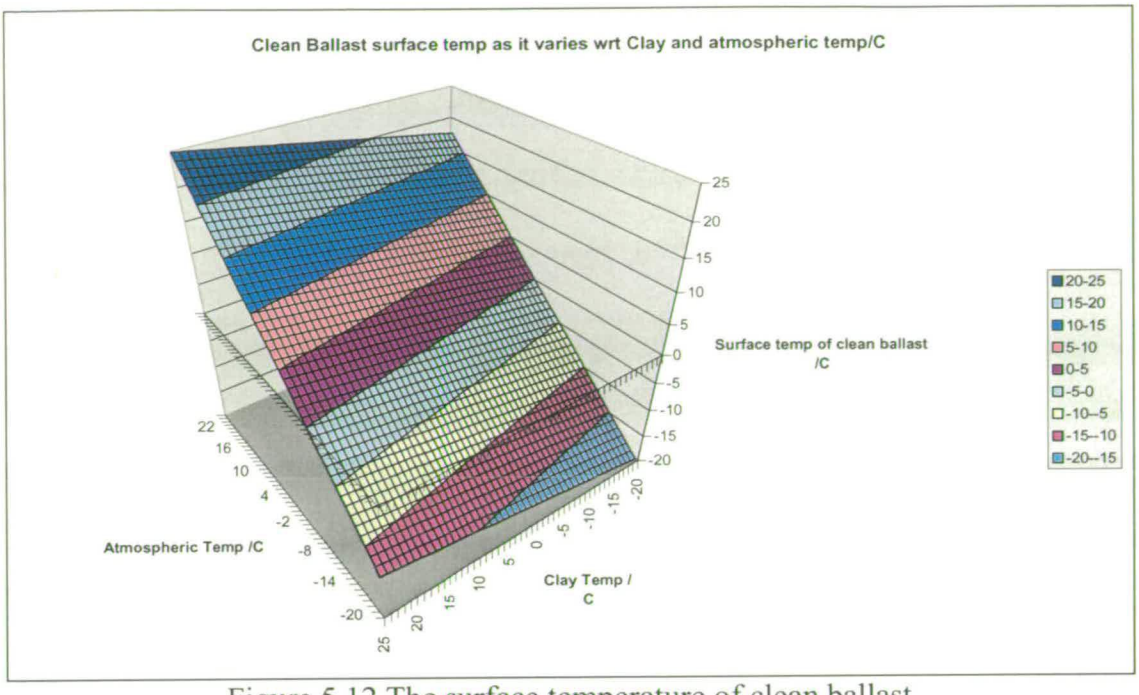

Figure 5.12 The surface temperature of clean ballast

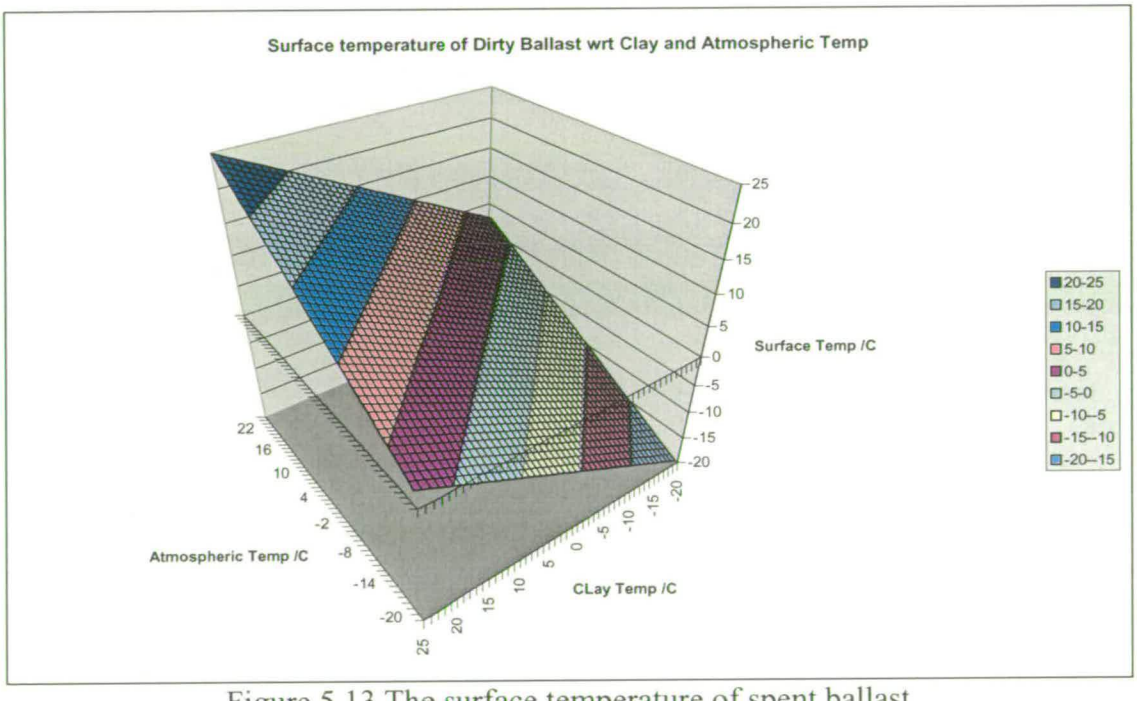

Figure 5.13 The surface temperature of spent ballast

5.7 Infra–Red Laboratory Experiment

Before any experiments could be undertaken the aperture of the infra-red camera had to be calculated. This was calculated to be 10° by 20°, giving information on the distance at which the camera had to be placed to observe the ballast.

All the experiments were conducted to the infra-red thermography standards for non-destructive testing (Bruening & Mordfin (1994)), and the procedures of Türler, Griffith and Arasteh (1997) for infra–red thermography testing to validate heat transfer models were taken into consideration.

An experiment was conducted to determine whether the clean and spent ballast samples heat and cool at different rates. If this was proved it would be useful to know if these rates of heat transfer could be calibrated and could be used in the field to identify types of ballast. An experimental set-up was devised so many of the conditions that determine surface temperature, as discussed above, could be controlled. The experimental set-up can be seen in figure 5.14, it shows the infra red camera and two trays of ballast as well as the room in which the experiments took place.

Figure 5.14 The experimental laboratory set-up

The experiment was conducted in a room where both the through flow of air and the temperature of the room could be controlled. The two ballast types were placed in equal sized containers, filled to the same level. The containers were raised off the floor so that convection through the floor could not be an influencing factor. The containers had drainage holes so that when water was added, the excess could drain off. The infra-red camera was placed as high as possible above the ballast to give a near vertical view of the ballast over the largest possible area and to avoid parallax

errors as well as localised hot and cold spots. Each experiment was run over a period of hours to allow the ballast to reach a uniform temperature.

Figure 5.15 shows the camera view, while figure 5.16 shows a generated image. This generated image is of two trays of clean ballast, the scale signifying the temperature in degree Celsius. Each colour in the diagram represents a different temperature, where the dark colour shows lower temperatures. The infra red image indentifies that concrete is hotter than ballast. The edges of the container of ballast are warmer than the main area of ballast, shown by the difference in colour.

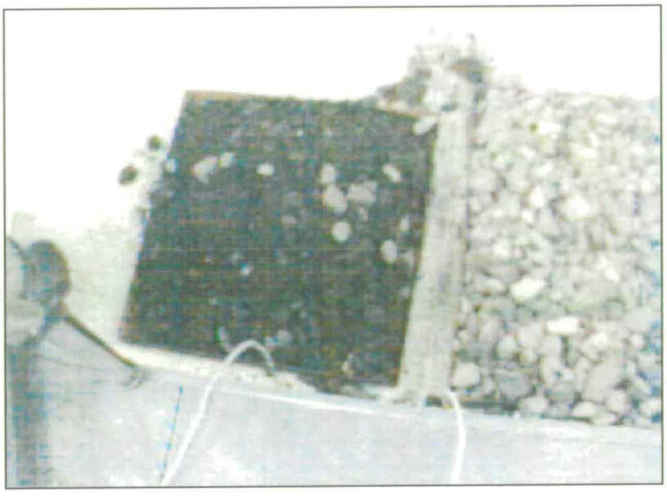

Figure 5.15 Visual image of what is seen by the infra-red camera

Figure 5.16 An infra-red image of spent and clean ballast (spent ballast on the left).

Figure 5.17 and figure 5.18 show the infra-red images of a tray of clean ballast and a tray of spent ballast heating up to room temperature. The clean ballast is on the right of the picture. The visual image (figure 5.15) shows the differences between clean and dirty as seen by naked eye, while the infra red image (figure 5.16) shows the same area with the differences between the ballast magnified. Figure 5.17 shows two trays of spent ballast with the one on the left hand side colder than room temperature. This tray was left till it reached room temperature. Figure 5.18 shows the same experiment but over 2 hours later. The spent ballast temperature has risen towards the equilibrium temperature. This experiment was repeated with clean ballast. The experiments shown in figure 5.21, figure 5.22 and figures 5.23 show that spent ballast takes a longer time than clean ballast to reach an equilibrium (atmospheric) temperature.

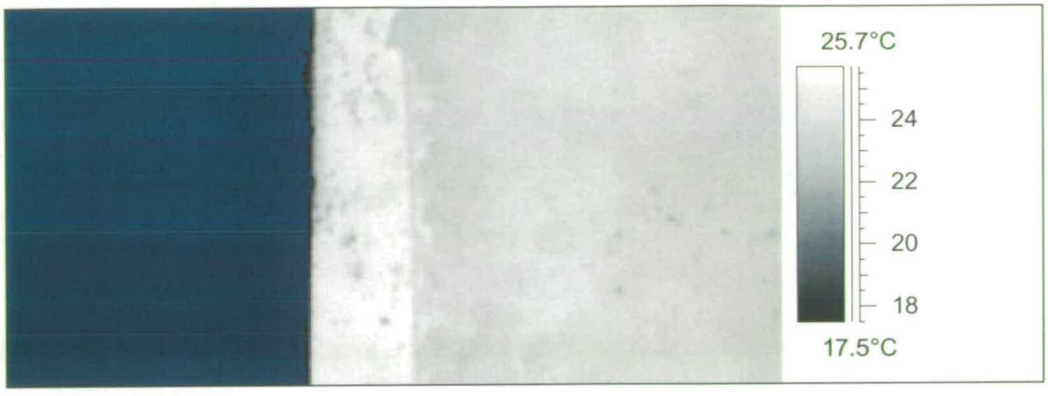

Figure 5.17 Infra-red image at the beginning of the experiment

Figure 5.18 Infra-red image of when the ballast has heated to room temperature.

Additionally an experiment was undertaken to compare the heating of spent ballast with clean ballast, and spent and clean ballast saturated to 2.5% (by mass) with water. The trays of ballast were chilled for the same time. The infra red camera recorded the trays of ballast heating up, the data was then analysed using the post-processing software for the infra-red camera as well as Excel.

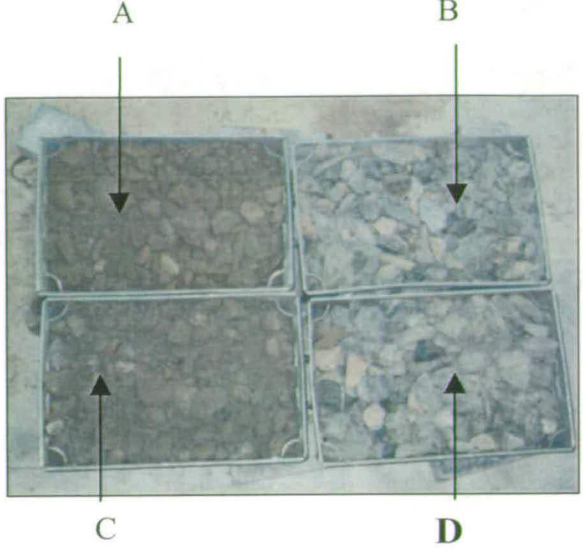

Figure 5.19 Visual of the trays of ballast shown in figure 5.19. Where A is a tray of spent ballast with 2.5% water, B a tray of clean ballast with 2.5% water, C a tray of spent dry ballast, and D a tray of clean dry ballast.

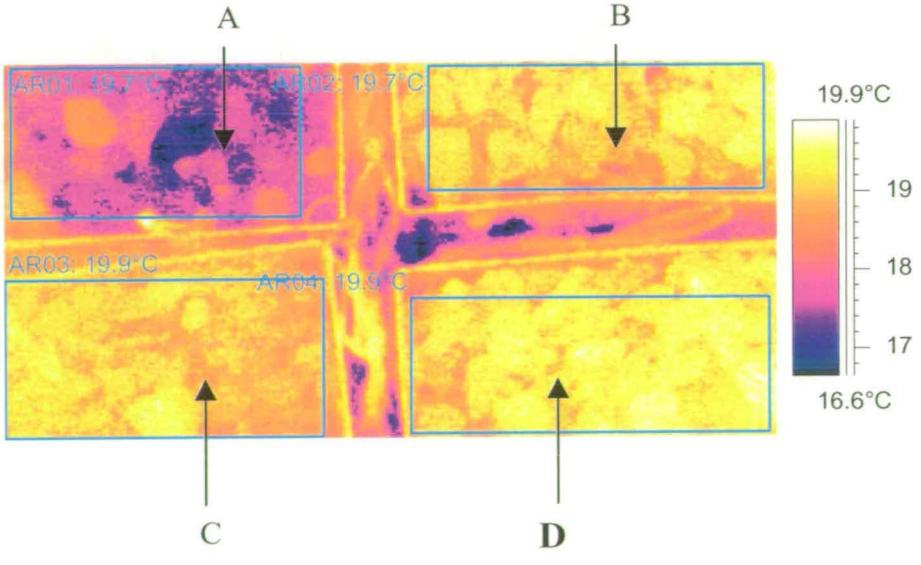

Figure 5.20 Infra red image of the trays of ballast shown in figure 5.19. Where A is a tray of spent ballast with 2.5% water, B a tray of clean ballast with 2.5% water, C a tray of spent dry ballast, and D a tray of clean dry ballast as shown in figure 5.19

Figure 5.20 shows an infra-red image of four trays of ballast, (a tray of spent ballast with 2.5% water, a tray of clean ballast with 2.5% water, a tray of spent dry ballast, and a tray of clean dry ballast in order from top left to bottom right). Figure 5.19 shows a visual image of the same area, this demonstrates the differences between the information about the state of the ballast obtainable from the naked eye and from the infra red camera. Areas were drawn around each of the portions of ballast of interest excluding the edges where the temperature was governed by external factors. From the data obtained from the software a macro was written to export it to Excel where running averages were taken as well as further analysis of the data. The results can be seen in figure 5.21, figure 5.22 and figure 5.23.

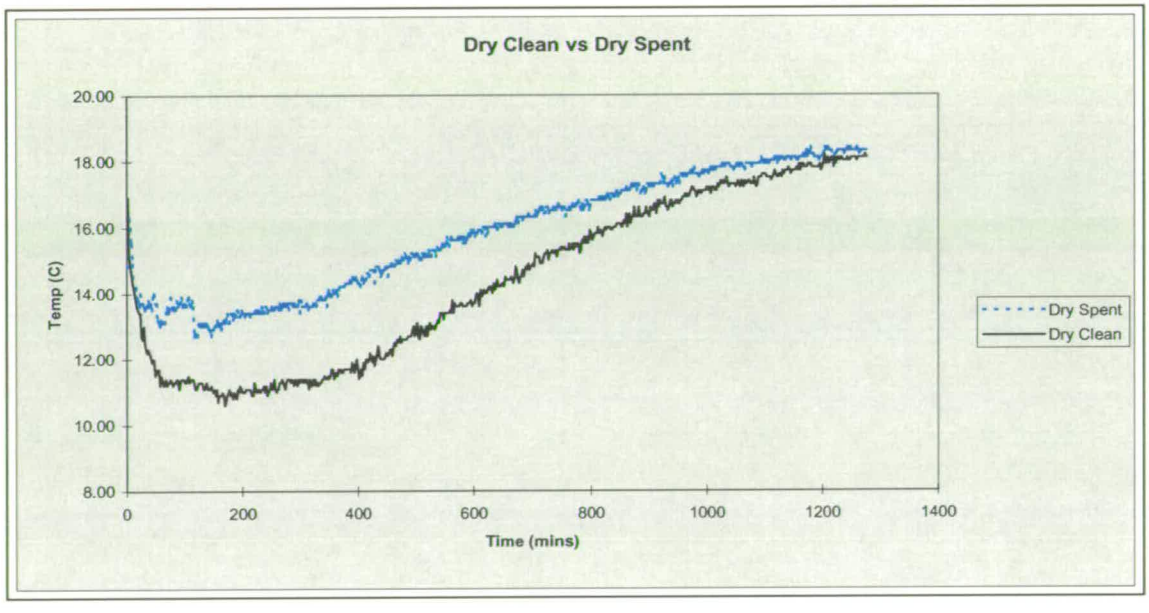

Figure 5.21 A graph of clean and spent ballast heating up to room temperature over time.

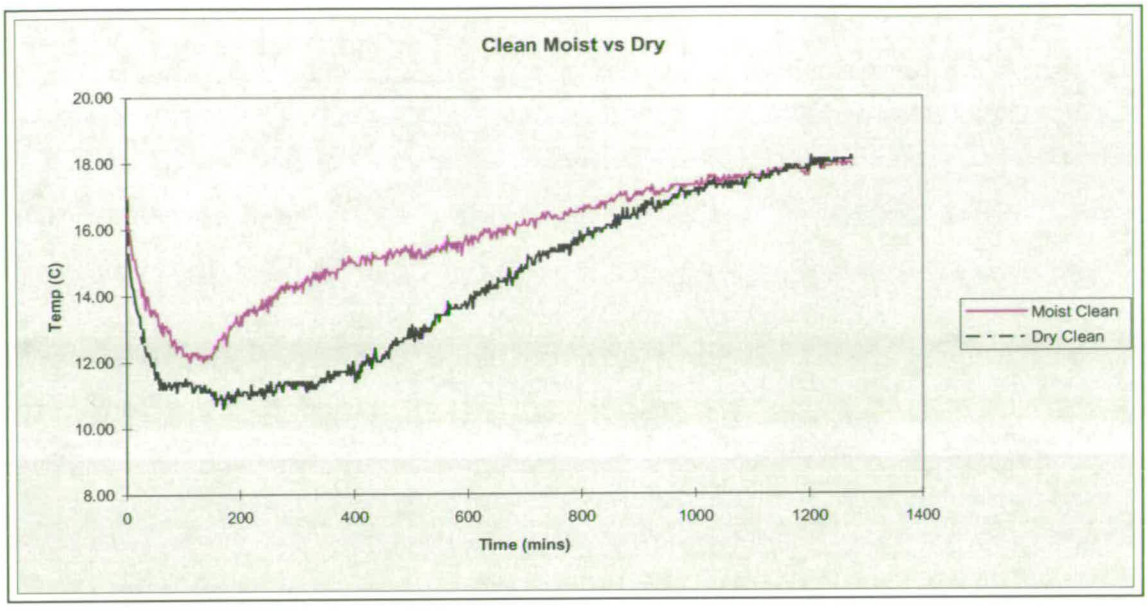

Figure 5.22 A graph of clean ballast wet and dry heating up to room temperature over time.

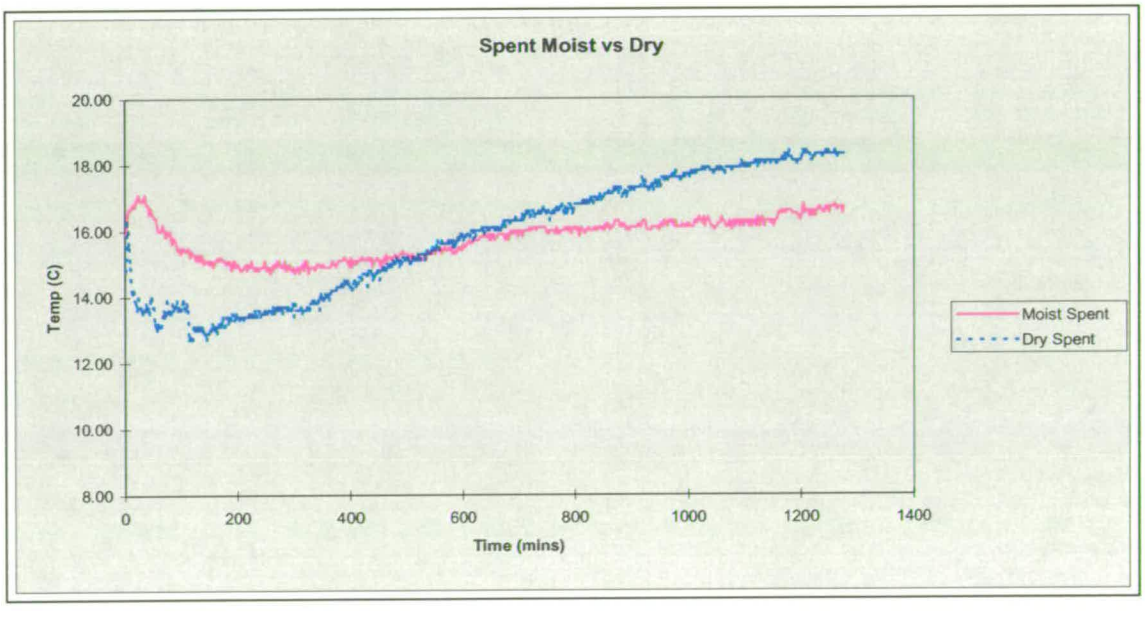

Figure 5.23 A graph of spent ballast wet and dry heating up to room temperature over time.

5.8 Discussion of Infrared Thermography Laboratory Work

From the above graphs it can be assumed that given time some of the lines will converge to a uniform temperature. All the experiments involved initially cooling the ballast down to below room temperature, making it harder to accurately compare the rate of heating of the two types of ballast. However it was possible to see the rate of cooling of the different types of ballast as each type of ballast was exposed to the same amount and time of cooling.

In figure 5.21 dry clean and spent ballast are plotted against each other while they heat up to room temperature after being artificially cooled. It is shown that the clean ballast has a lower heat capacity as it reached a lower temperature when cooled initially and warmed more quickly (shown by the angle of the graph).

Figure 5.22 shows the results for moist and dry clean ballast, where the dry clean ballast both cooled down and heated up the fastest. As a result of evaporation there was a quick temperature increase in the results from the moist ballast. This is due to clean ballast having no fines so water will drain or evaporate quickly and will not be held within the fines.

Figure 5.23 shows the results for moist and dry spent ballast. The dry spent ballast cooled quicker and thus reached a lower minimum temperature, but since the moist spent ballast retained the water for longer it was slower heating up.

5.9 Conclusions:

The dielectric constant for clean and spent ballast was determined as well as those for dry and wet ballast. The ideal antenna to use on ballast is the 500 MHz. The initial testing of GPR showed that GPR is a suitable technique for use on the railway track bed ballast. As clean and spent ballast has different dielectric constants it is possible to identify the type of ballast from a GPR survey.

From the infra–red laboratory testing it was found that there is a difference between the rate of heat transfer of spent and clean ballast. The theoretical models predicted this result. Water has an effect on the rate of heat transfer. The infra–red camera is an effective method of determining the state of the ballast, as long as there is atmospheric temperature gradient either heating or cooling the ballast.

Following the laboratory tests it was decided that, the techniques should be evaluated on a test track so that the effects of the rails and sleepers could be taken into consideration.

Chapter 6:

Model Railway Line Testing of Radar and Infra–Red Thermography

6.1 Introduction

Gaining sole access to a section of working railway in Great Britain is extremely difficult. The limiting factors are:

- The railway authorities have strict health and safety procedures relating to working on a live railway.
- The railway industry does not have calibrated ballast or formation depths.
- All work must be conducted within the hours of possession. (0030 hrs to 0600hrs).
- Possession work requires a substantial number of safety personnel.
- Twelve-week lead-in period for possession requests to be approved.
- Research work can only be undertaken on sites where contractors are already working, leading to the possible clashes with the operator.

Due to the many constraints on fieldwork a realistic stretch of track was built at Edinburgh University.

6.2 Test-Rig.

It was essential for the test-rig to have the same design criteria as a fully working permanent way. The test track was designed to the same specification as that required by the fastest lines in the UK. This was the worst case scenario in relation to both the GPR and infra–red thermography. The design requirements for the test track are outlined below.

- Must represent a live track.
- Dimensions, ballast material, sleeper dimensions and construction sequence as per Railtrack Line Specification (1988).
- Incorporate common ballast anomalies into the track bed; i.e. varying degrees of track bed deterioration.
- Deteriorated ballast must be deemed spent as taken from a track bed.
- Include both timber and concrete sleepers, as both remain in service. Tests will be required to determine the effect, if any, that sleepers have on the GPR plot.
- Incorporate geotextiles and a sand blanket to determine effect, if any, upon the GPR plot.
- Construct a test-rig in a location where weathering would be similar to the conditions found on site.
- Fully compact ballast so the density of the in-situ material is close to that of a live track bed.

The test-rig allowed the calibration of the GPR and infra-red equipment under controlled conditions, where location, degree and depth of ballast deterioration were

known. The test-rig also allowed the initial work to be conducted safely without the need to go on site and incur the associated problems.

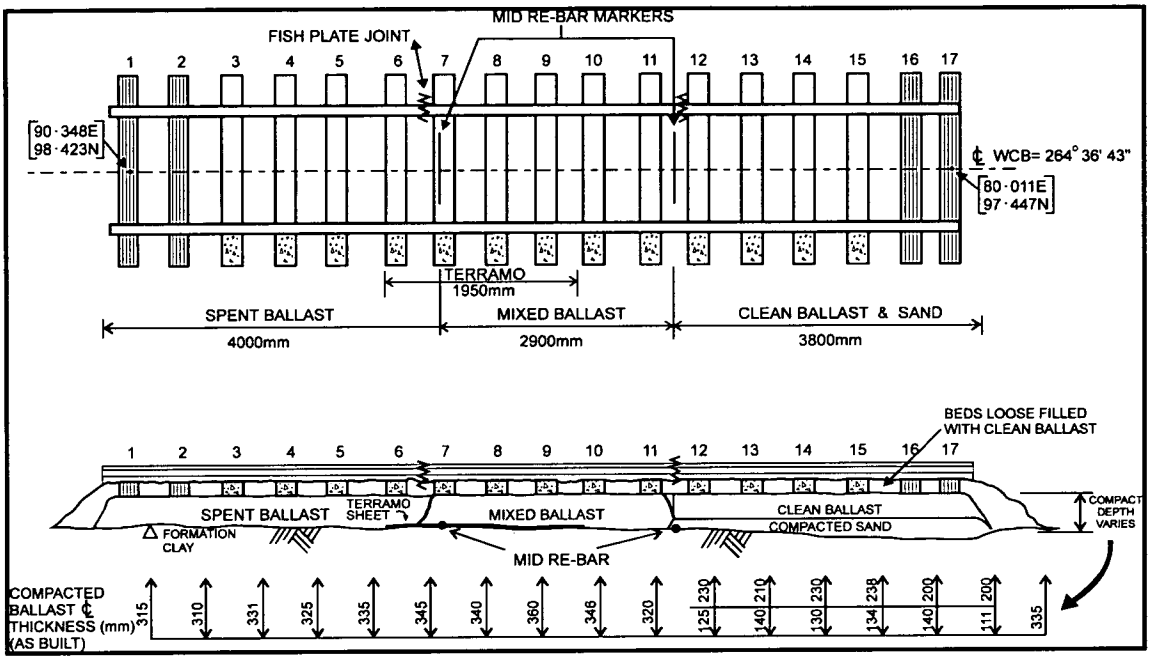

Figure 6.1 Schematic track bed built at Edinburgh University

Figure 6.1 shows the position of the sleepers and rails, as well as the depth of ballast. The track was split into three sections, clean ballast with a sand blanket, mixed ballast, and spent ballast with a Terram sheet to allow drainage. Reinforcement bars (re-bars) were placed at the bottom of the ballast layer where the different types of ballast change, so that the interface between the ballast types can be seen between them. Figure 6.2 shows the completed track.

Figure 6.2 Completed railway track at Edinburgh University.

6.3 Radar Tests on Test-Rig

The radar experiments on the test-rig were designed to:

- Compare the different antenna frequencies and orientations to determine which is most suited to railway application.
- Determine what effect, if any, the sleepers and rails have on the GPR trace.
- Determine if GPR can determine the depth of ballast.
- Ascertain if GPR can detect the varying degrees of ballast deterioration.
- Compare laboratory velocity values to the velocity on the test-rig.

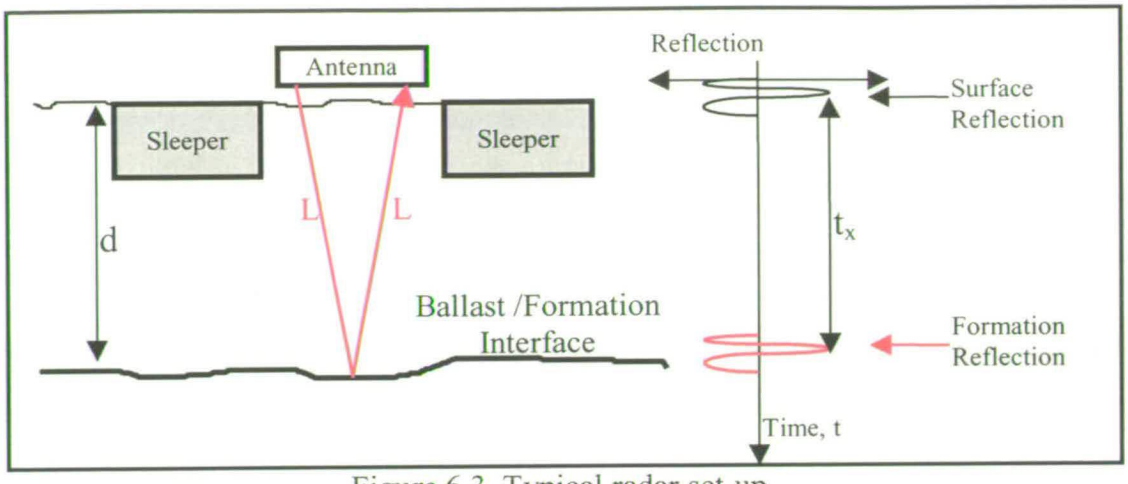

Figure 6.3. Typical radar set-up.

Figure 6.3 shows how the radar was used. The radar was used monostatically, where the antenna was used as a transmitter and receiver and t_x is the two-way travel time of the electromagnetic wave. On the test track both the 900MHz antenna and the 500 MHz antenna were used to check the results from the laboratory. Also both antennas were used so that the 500 MHz antenna could identify the bottom of the formation layer, and the 900 MHz could identify any anomalies within the ballast structure.

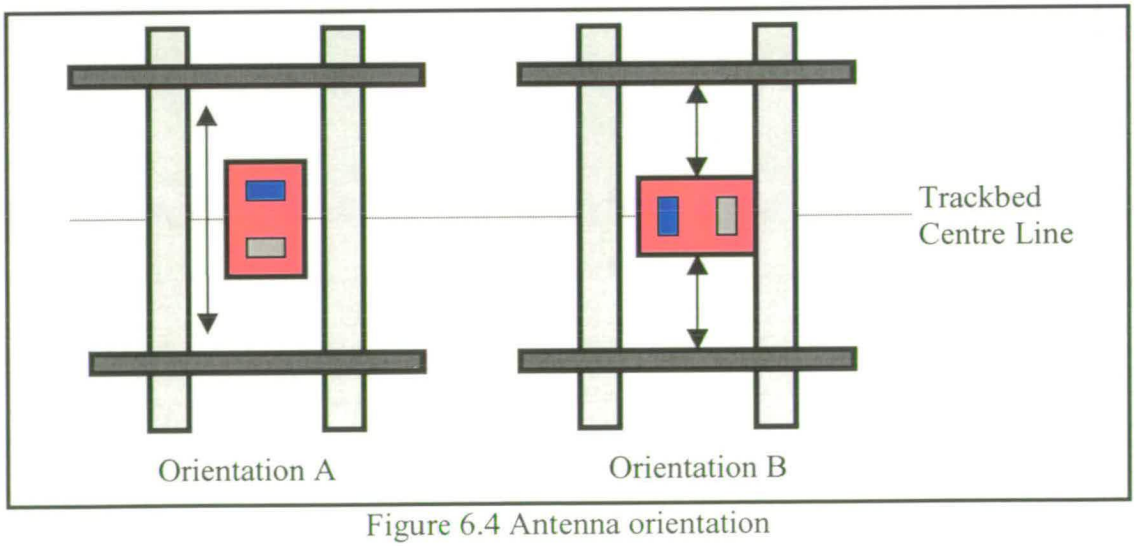

Figure 6.4 Antenna orientation

Figure 6.4 shows the experiment undertaken to determine the correct positioning of the radar antenna on the ground to obtain the best results. Figure 6.5 and figure 6.6 show the radar image for both of these tests. The radar signal is not equal for both orientations of the antenna, as the electromagnetic waves are emitted at a wider angle from the two longer sides of the antenna.

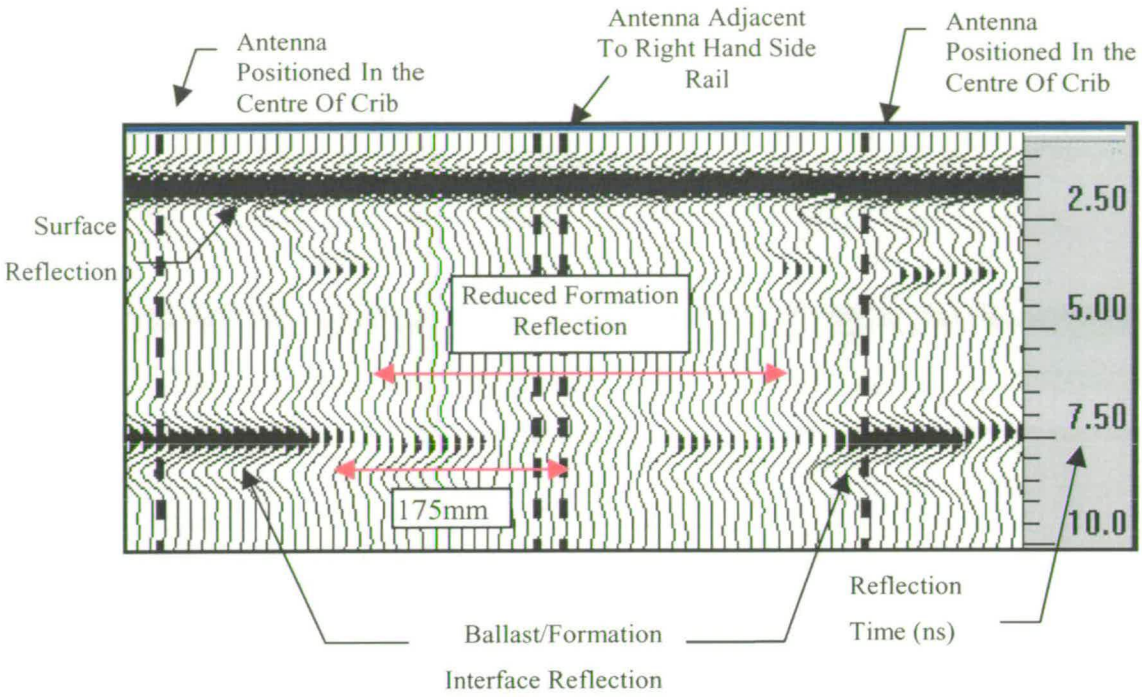

Figure 6.5 Orientation A.

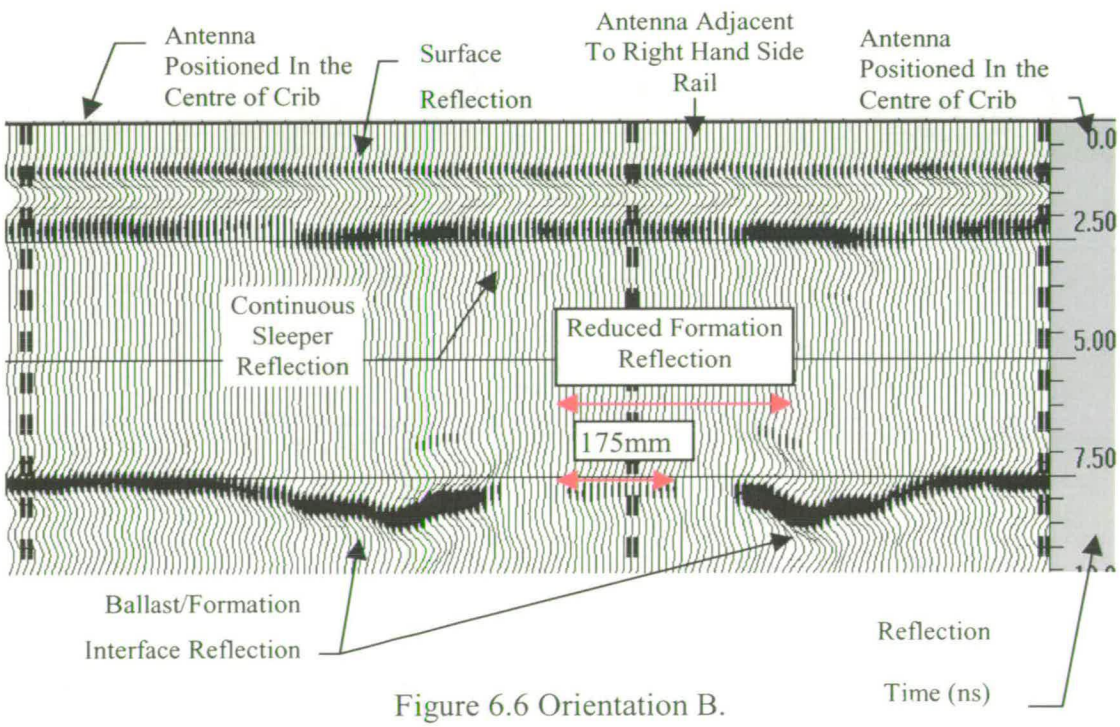

Figure 6.6 Orientation B.

In figure 6.5, as the antenna moves towards the rail, the amplitude of the reflection from the interface between the ballast and the clay formation decreases. This occurs about 175mm from the rail. This can also be seen from figure 6.6, however there is a continuous reflection throughout the radar survey. The position of this reflection does not change, as the antenna moves along, so the reflection must be from a continuous object. It was deduced that this effect was caused by reinforcing in the concrete sleepers, running parallel with the direction of survey. When the antenna was placed in orientation A the transverse electrical field was parallel to the line of the sleepers so it would, not pick up the reinforcing bars compared with position B. In position B the orientation was turned 90°, so the electrical field was perpendicular to the sleepers and picked up the reinforcing bars within the sleepers, producing a continuous reflection on the radar plot.

From this initial experiment it was deduced that for future radar experiments the antenna should be placed in the middle of the crib orientation A. This would reduce the amount of sideswipe the antenna picked up from the rails and sleepers.

The following experiment compared the laboratory results for the dielectric properties of ballast with those from the test-rig. The radar antenna was dragged along the surface of the ballast as shown in figure 6.7. The reflection caused by the interface between the ballast and clay formation was identified from the radar plot and the two-way time calculated from that. Equation 5.1 can be used to calculate the dielectric constant, as it was in the laboratory work, since the depth of the ballast layer was known.

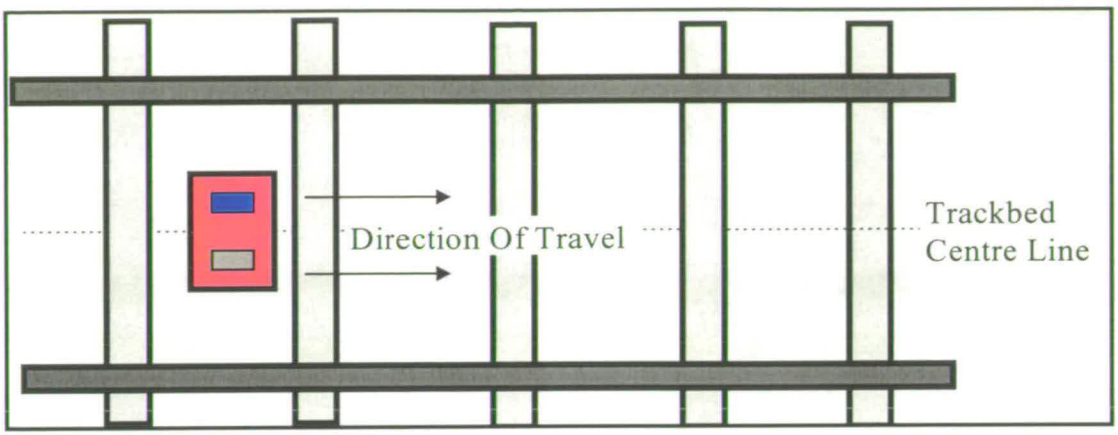

Figure 6.7 Direction of radar survey.

Figure 6.8 shows a wiggle plot through the clean ballast with a 900MHz antenna showing how the two-way travel time was identified. Figure 6.9 shows a grey scale plot of the 900 MHz antenna being dragged over the clean ballast. From the grey scale plot the effects of the reinforced concrete sleepers, which restrict the penetration of the electromagnetic wave, can be seen. Also shown is the effect a wooden sleeper has on penetration. The electromagnetic wave has no significant penetration below either of the sleepers.

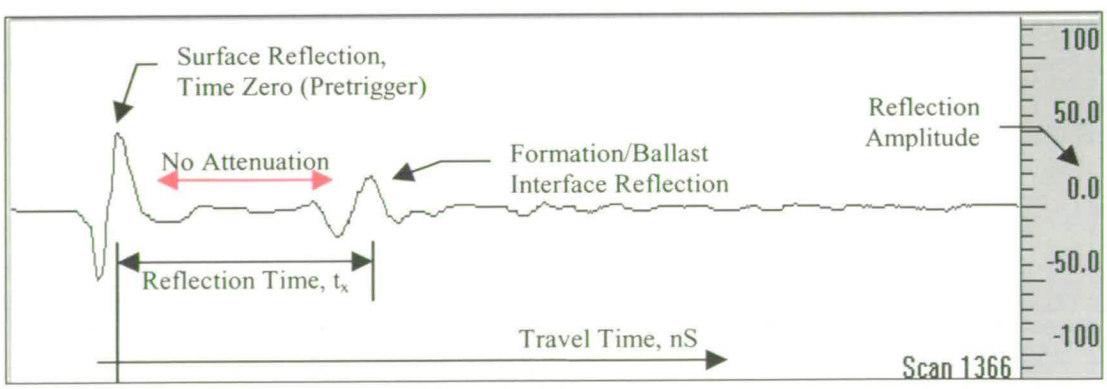

Figure 6.8 Wiggle plot from 900 MHz antenna over clean ballast.

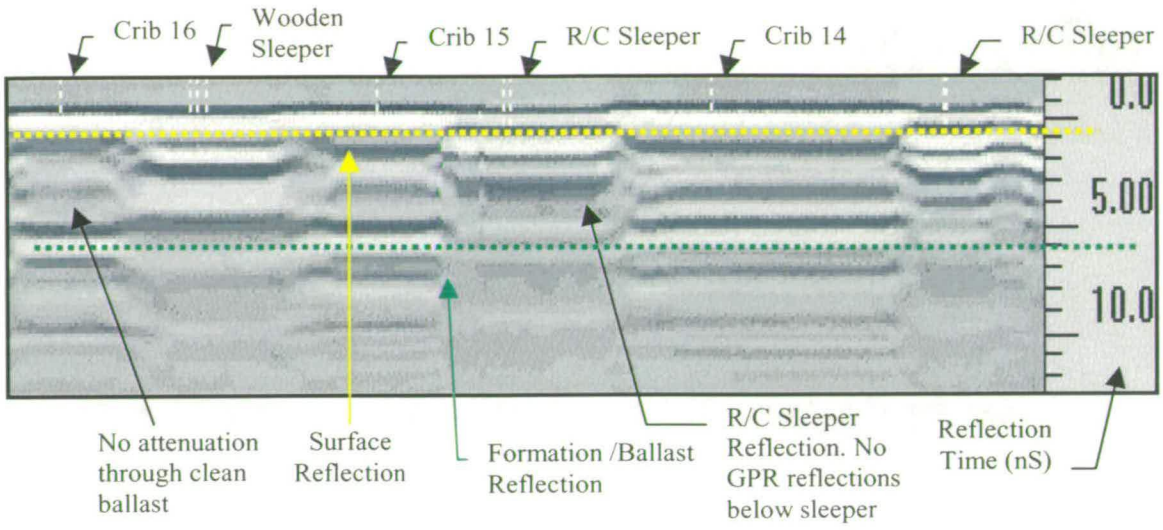

Figure 6.9 Grey Scale plot over clean ballast.

Figure 6.10 shows the section of the radar plot between the clean/mixed ballast interface, (i.e. Sleepers 10 to 12). The double line represents the centres of the reinforced concrete sleepers and the single line marker represents the centre of the crib.

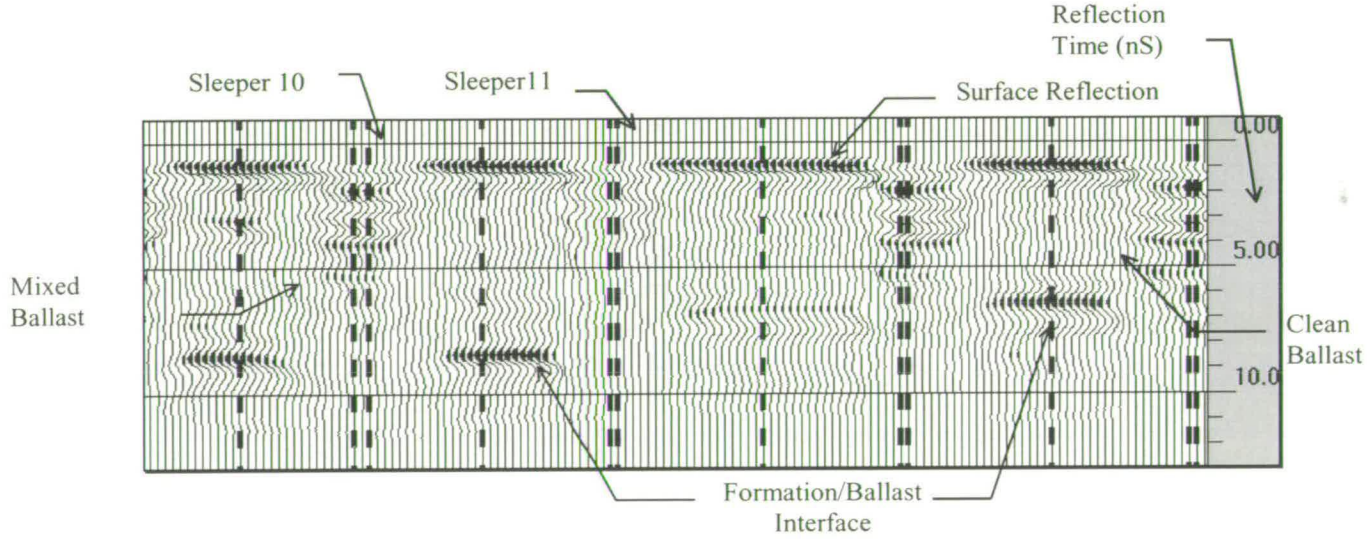

Figure 6.10: GPR Plot along Test-rig Centre Line

Figure 6.10 shows that the radar does not penetrate through the reinforced concrete sleeper. This is the result of almost all the emitted electromagnetic waves being

reflected by the reinforcing bars within the sleeper. A reflection time-step can be identified between the mixed and clean ballast. This is also the case between the spent and mixed ballast. GPR can detect clean, spent or moderately deteriorated ballast. The test-rig can be used to accurately determine dielectric constants for certain types of ballast with different moisture contents. There are strong reflections from the formation/ballast interface. From the theory and the application of radar, the depth of the formation/ballast interface can be calculated using equation 5.1. Using crib eleven as an example and 3.5 (Table 5.1) as the dielectric constant for clean ballast with a 5% moisture content, the depth to the formation is calculated as 0.441m. The actual depth to the formation is 0.445m, resulting in an error of less than 1%.

Figure 6.11 shows a wiggle plot of the electromagnetic wave through spent ballast from a 900 MHz antenna. This shows that, since the material is spent ballast, the dielectric constant has increased, and the loss of electromagnetic energy due to scattering and clutter has increased. This results in identification of the interface between ballast and clay being difficult as the amplitude of the reflected signal reduces and blurs in with the scattering and clutter. However, it is possible to identify the reflection and identify where the interface occurs

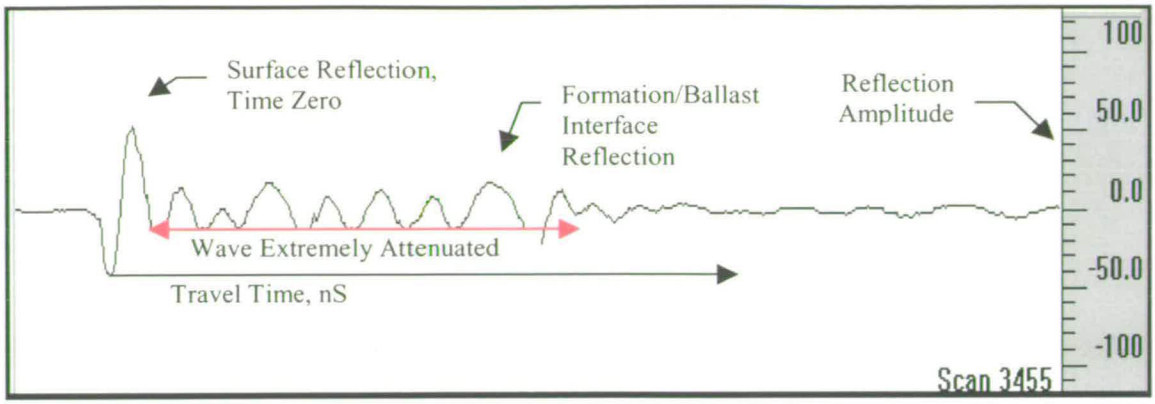

Figure 6.11 Wiggle plot from 900 MHz antenna passing through spent ballast.

Using a 500MHz antenna it can be seen that the identification of the interface (figure 6.12) is made easier as the wavelength is longer, so that the wave is not attenuated or scattered by small particles of ballast. As a result the reflected signal from the interface between ballast and clay has a greater magnitude. This is because the 500MHz signal has a wavelength twice that of the 900 MHz signal, which reduces the scattering but also reduces the resolution by about a half. This situation is similar to the problem described in table 4.2 with the different wavelength and velocities of different antennae.

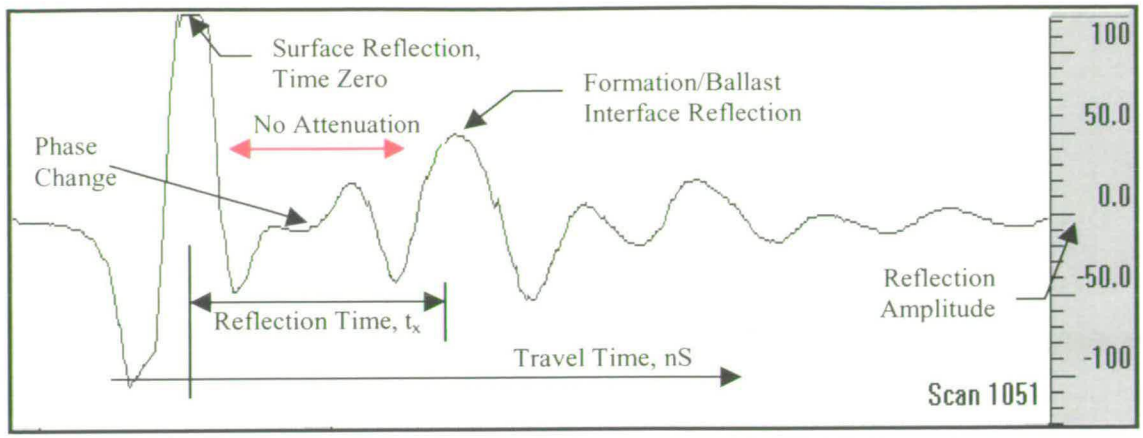

Figure 6.12 Wiggle plot from 500 MHz antenna

The dielectric constant was calculated for the spent, mixed and clean ballast from the test-rig, in the same way as it was calculated for the laboratory work. Since the depth was known as it was measured when the track was laid, the two-way travel time can be taken from the radar plot using equation: 4.2.

As shown in figure 6.1 the test–rig cribs: 1 to 6 contained clean ballast, 7-10 mixed ballast and 11-16 spent ballast. Figure 6.13 shows the comparison between the dielectric results from the test-rig and the laboratory experiments. It can be seen from the values obtained for the dielectric constants from the test-rig are similar to the results from the laboratory work. The unknown water content in the test-rig causes the differences observed. The water content at the time of testing on the test-rig appeared to be in the range 7-10%. The difference between the laboratory and the test-rig results for spent ballast are greater than the difference between the results for clean ballast. This can be explained by spent ballast having more fines that retain water, due to capillarity or soil suction (Lambe & Whitman (1979)), than the clean ballast which drains water away. From Lane & Washburn (1946) a capillary head of

about 106 cm (when saturated) and 68 cm (maximum capillary rise from free water) for particles of a similar size to the fines can be achieved. Therefore all the fines could be saturated due to capillary action and not just due to rainfall. Water has a dielectric constant of 80, which will dominate the results for spent ballast. The presence of water, which has high conductivity value, will attenuate the electromagnetic signal. This does not occur if water is not present. This is reinforced by the fact that the tests were repeated and the clean ballast results varied by 5-7% whilst the results for the spent ballast varied by 25 %. These variations are due to the test-rig being open to the atmosphere, so the weather (rainfall) affects the dielectric constants. The clean dielectric constants are similar to those of 0% moisture content from the laboratory work. This was due to the clean ballast having the ability to drain effectively, and is not greatly affected by rain.

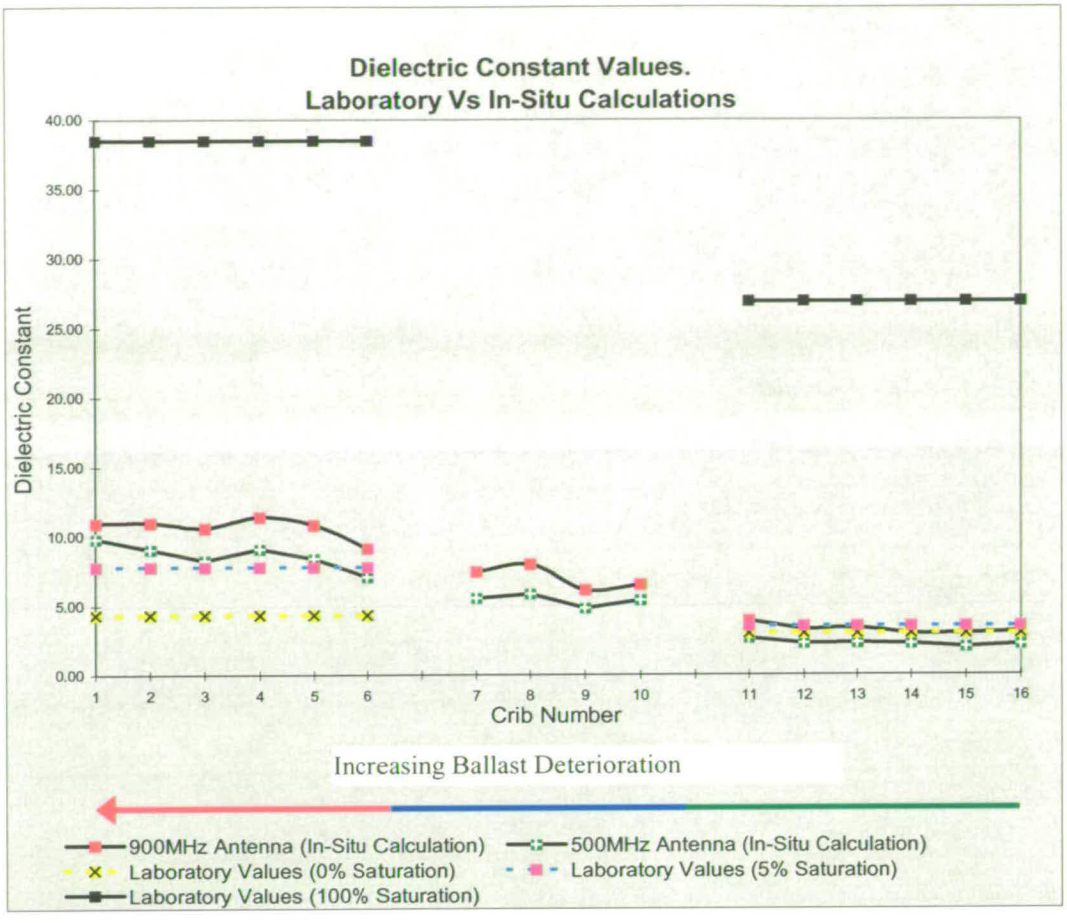

Figure 6.13 Dielectric Constants from Both Laboratory and Test-Rig

The results from the test-rig confirm the results obtained from the laboratory work as well as the theory, i.e. that the 500MHz antenna is more effective than the 900MHz antenna for radar testing ballast. This was due to the fact that the electromagnetic signal from the 500MHz antenna was not scattered or attenuated by the ballast particles.

6.4 Depth Calibration

Before any fieldwork commences the value of the dielectric constant needs to be calculated at the beginning of a survey. Two methods were investigated:

- Common Mid-Point Method (CMP)
- Wide Angled Reflection Refraction Method (WARR)

Both velocity (dielectric) calibration techniques use geometrical manipulation to calculate propagation velocity. Both of these methods use two antennae.

6.4.1 Common Mid Point Test

Positioning two antennae side-by-side on the ground and pulling them evenly away from each other carries out CMP tests. Figure 6.14 shows the layout for a typical CMP survey. The transmitting (T) and receiving (R) antennae are positioned an equal distance (X) from a common mid-point. The wave is then transmitted from T_1 to R_1. The antennae are moved to position two. A second reading is taken. By comparing the reflection times, the in-situ propagation velocity can be calculated. A minimum of two readings is required to make this calculation. Using geometric manipulation the propagation velocity can be calculated. Equation 6.1 shows how the in-situ velocity can be calculated from the CMP method.

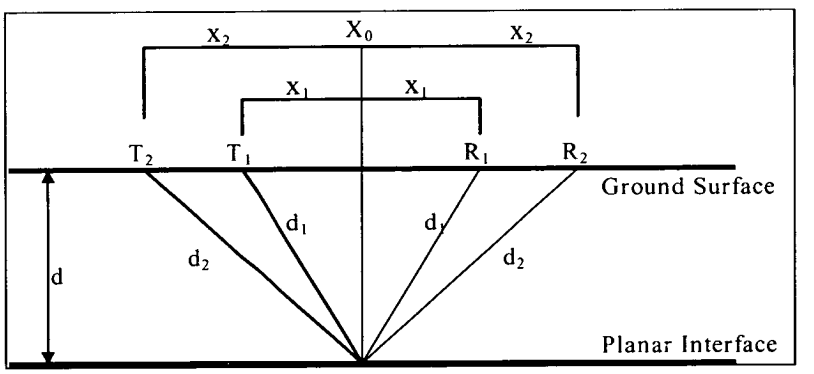

Figure 6.14 Common mid-point technique. (antennae arrangement)

d_n Path Length (m) for set-up n.

t_n, Travel time (s) for set-up n.

T_n, Position of antenna for set-up n.

R_n, Position of antenna for set-up n.

x_n, Antenna distance (m) from CMP for set-up n.

This gives equation 6.1 for the depth in terms of separation and two-way travel time only:

$$d = \sqrt{\frac{(t_2^2 x_1^2 - t_1^2 x_2^2)}{(t_1^2 - t_2^2)}} \tag{6.1}$$

6.4.2 Wide Angled Reflection Refraction Analysis

Similar to the CMP method, the WARR method manipulates antenna geometry to obtain in-situ propagation velocity and depth. Unlike the CMP method, the transmitting antenna remains stationary throughout the WARR survey, with only the receiver moving as seen in figure 6.15. Equation 6.2 shows how the in-situ velocity can be calculated from the WARR method.

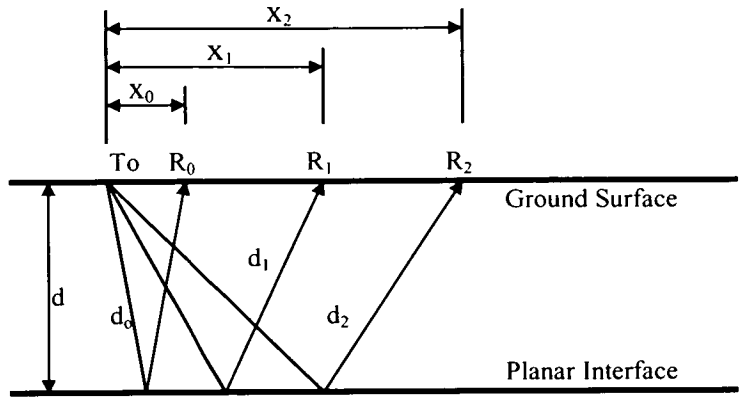

Figure 6.15 WARR antenna set-up

d_n, Path Length (m) for set-up n.

t_n, Travel time (s) for set-up n.

T_n, Position of stationary transmitter.

R_n, Position of antenna for set-up n.

x_n, Separation between receiving and transmitting antennas (m) for set-up n.

This gives equation 6.2 for the depth in terms of separation and two-way travel time only:

$$d = \sqrt{\frac{(t_1^{\,2}\frac{x_2^{\,2}}{4} - t_2^{\,2}\frac{x_1^{\,2}}{4})}{(t_2^{\,2} - t_1^{\,2})}} \qquad (6.2)$$

6.4.3 Depth Calculation Discussion

Using these methods an accurate ballast depth profile can be achieved. There are dangers associated with using calibration trial pits on changeable sections of tracks. By their nature, trial pits give a snapshot of the ballast conditions. They are also expensive and time consuming to excavate

The two antennae methods discussed set out to achieve velocity calibration without excavating trial pits. The two velocity calibration techniques were performed on the prototype test-rig. Using the test-rig allowed the depth calculations from the CMP and WARR survey to be validated against the known depth.

6.5 Further Radar Testing on the Test-Rig

The experiments undertaken on the test-rig were realistic although controlled. The next stage in the research was to carry out a field survey on a live working railway. Before starting the fieldwork on live track, the health and safety issues had to be dealt with. These included making the radar system so it could be removed from the track by 2 people, all users had to obtain Personal Track Safety training and the work had to be conducted while there were no trains running. To help with this transfer to a live track a trolley system was made to transport the radar system. The antennae were hung from the trolley so the radar survey could be conducted at speed. The trolley system was designed and built at Edinburgh University. It was important to reference the survey such that the position of the trolley was accurately known and related to the marks on the radar sections.

The trolley is shown in figure 6.16 and figure 6.17.

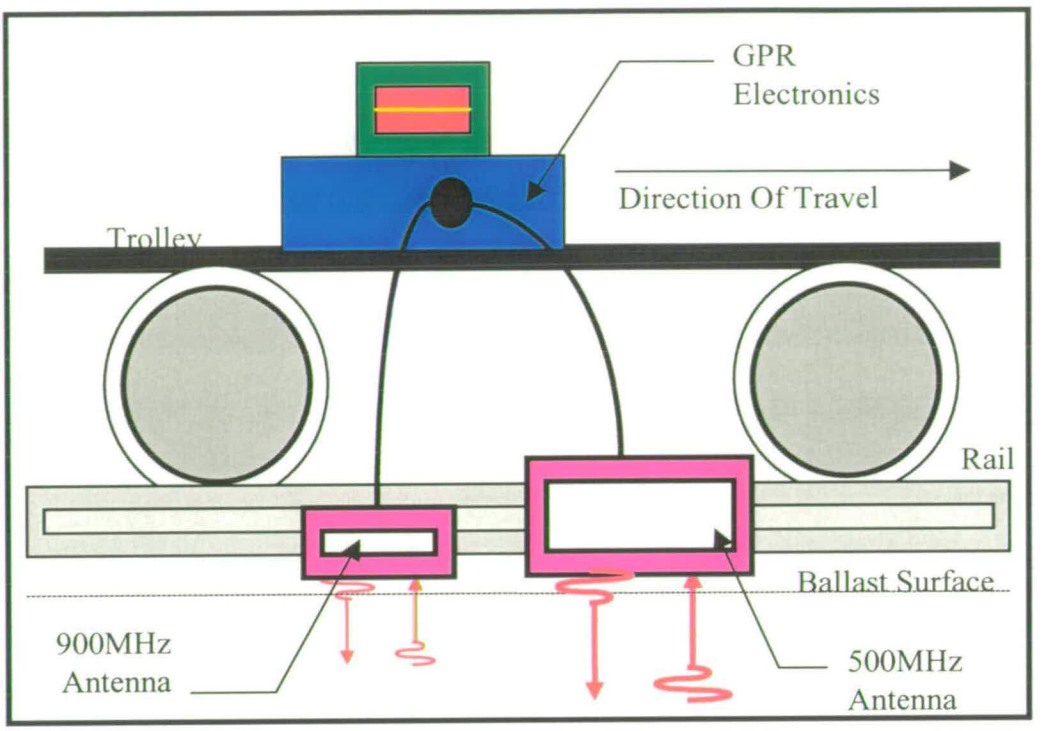

Figure 6.16 Trolley with antennae

Figure 6.17 Trolley mounted Radar System on a field trial.

Figure 6.16 shows the trolley. The trolley was made as non-metallic as possible, to reduce the effect of unwanted electromagnetic reflections from the trolley. The antennae had to be raised above the surface of the ballast to allow the trolley to move along the track. It was possible to find a ballast heap of nearly 20cm above the height of the sleepers.

During the field trial the non metallic Edinburgh University trolley was easily damaged by the heaps of ballast and the work had to be completed using a standard railway trolley - figure 6.17. No adverse data collection problems were encountered.

Figure 6.18 shows typical conditions on site and shows some heaped ballast.

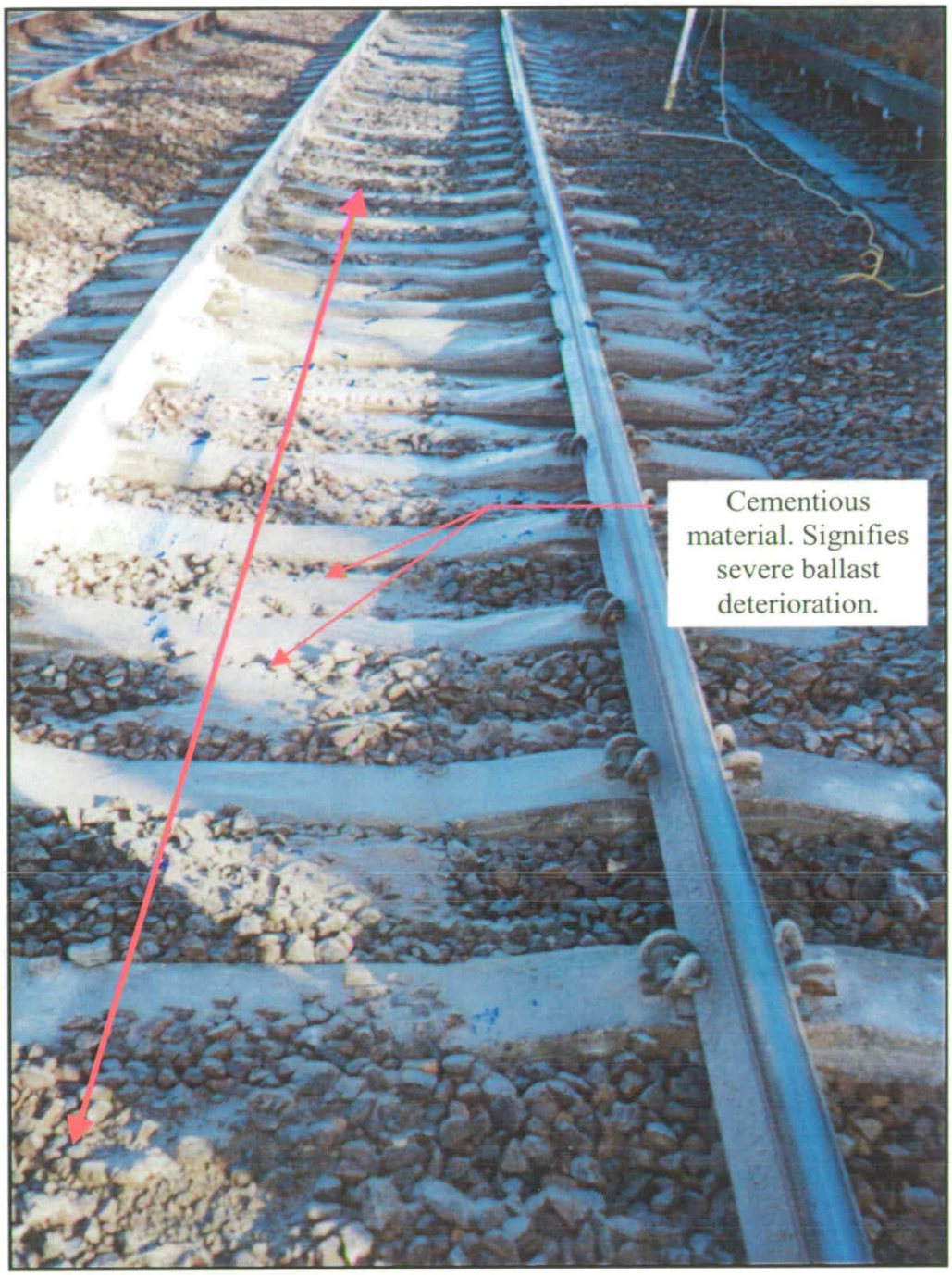

Figure 6.18 A picture of heaped ballast as well as spent ballast.

Raising the antenna above the ground has a dramatic affect on the propagation capacity of GPR antennae. The performance of antennae raised above a target surface was discussed by Davidson, & Forde, (1996) and Smith, (1984) concluding that increasing the distance between the antenna and target surface reduces the

magnitude of the reflected signal which limits the system's ability to detect sub-surface features. The results obtained from the research demonstrated a substantial reduction in reflected magnitude when the antenna was raised to a height equivalent to $1/10^{th}$ of the centre frequency wavelength (λ).

More specifically, the reflection magnitude obtained from a 900MHz antenna reduces by 50% at a height of λ/10m above the target surface. The reflection magnitude associated with the 500MHz antenna reduced by 30% at a height of λ/10m above the target surface. In real terms, given the wavelengths, the 900MHz and 500MHz antennae should not be separated from the ground by more than 4cm and 6cm respectively.

The above antenna/target height separation is easily achieved on a flat surface, such as a road pavement, while it is hard to achieve this result on the railway where the surface can be highly irregular.

The problem associated with raising the antennae above the target surface was solved by physically reducing any ballast which would obstruct the passage of the antennae to a maximum height of 5cm above the sleeper. From further laboratory experiments it was demonstrated that a vertical separation of 5cm achieved acceptable sub-surface reflections, as seen in figure 6.19. Figure 6.19 shows the 500MHz antenna being lowered towards the ballast. It can been seen when the bottom of the ballast layer disappears. At a height of 5cm the magnitude of the reflected signal is significantly reduced.

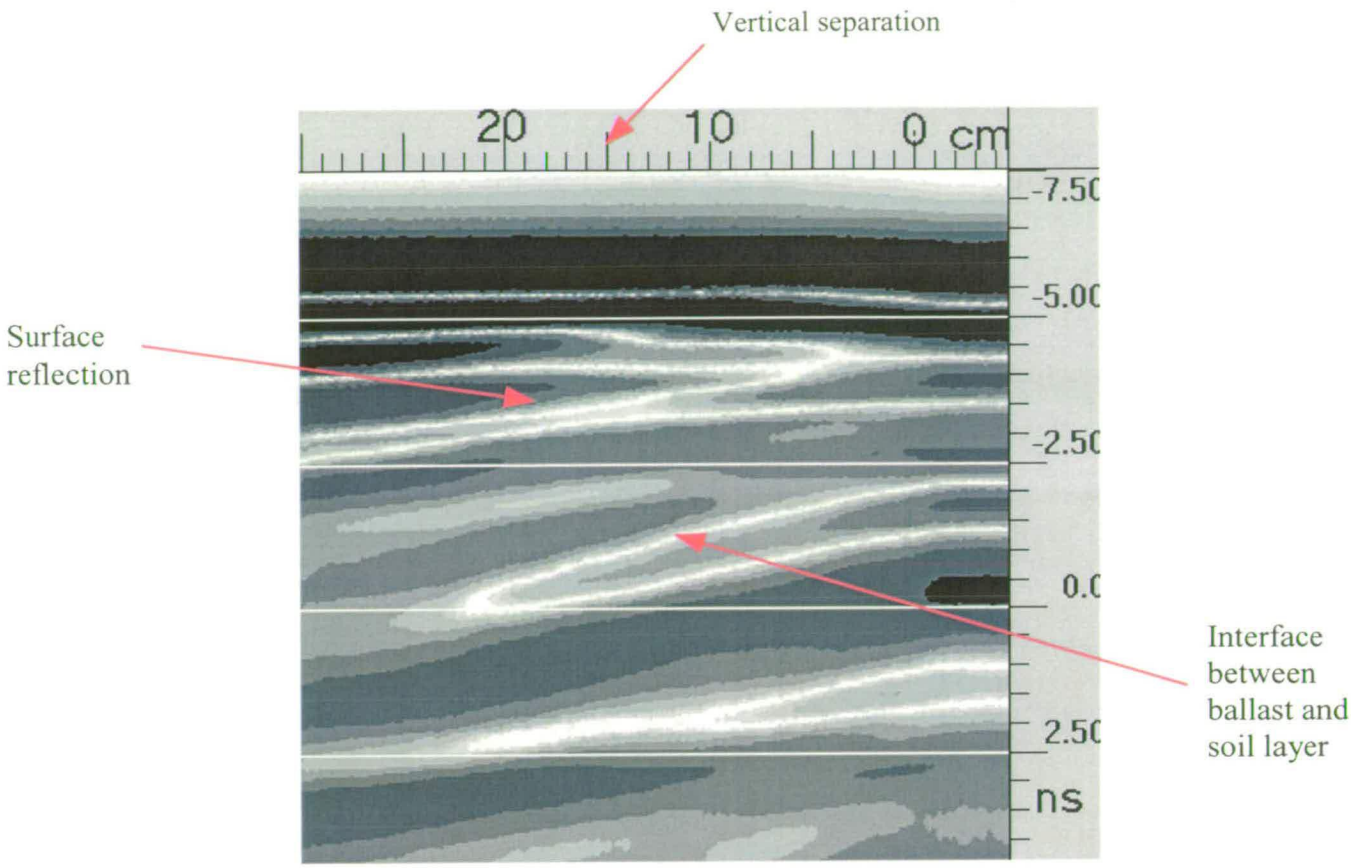

Figure 6.19 Radar image of ballast soil interface

6.6 Infra–Red Tests on Test–Rig

The purpose of the test track experiments was to test the camera and theory obtained in the laboratory in a real environment on a pseudo track. In this manner it can be shown how practical it is to use infra–red thermography for outdoor testing.

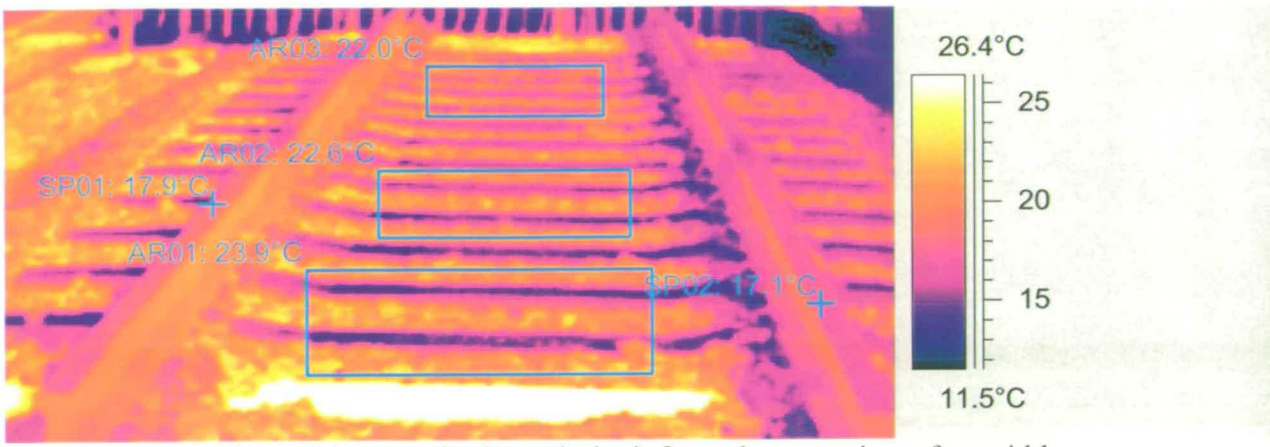

Figure 6.20 View of the test-rig through the infra-red camera just after midday.

Figure 6.20 is the infra–red image of the track bed, viewing the track bed where the clean ballast is closest to the camera and the spent ballast furthest away from the camera. Using the software supplied with the infra–red camera the three areas of different ballast, clean mixed and spent ballast are highlighted. Two spot temperatures of the rails shown can be used as reference temperatures. Figure 6.20 shows the raw data acquired form the infra–red camera, the data acquired from the infra–red pictures was exported into Excel, as in the laboratory experiments. The data shown in figure 6.21 and figure 6.22 are from the ballast filmed cooling over a 2 hour period. Figure 6.21 shows the results from all three areas of ballast and it shows the maximum, average and minimum temperature from the areas. Figure 6.22 shows just the spent and clean results. From these results it can be seen that there is a difference between the two types of ballast. This temperature difference is due to the different rates of heating and cooling between spent and clean ballast. From this relative difference in temperature it is possible to determine where ballast in-situ changes from clean to spent.

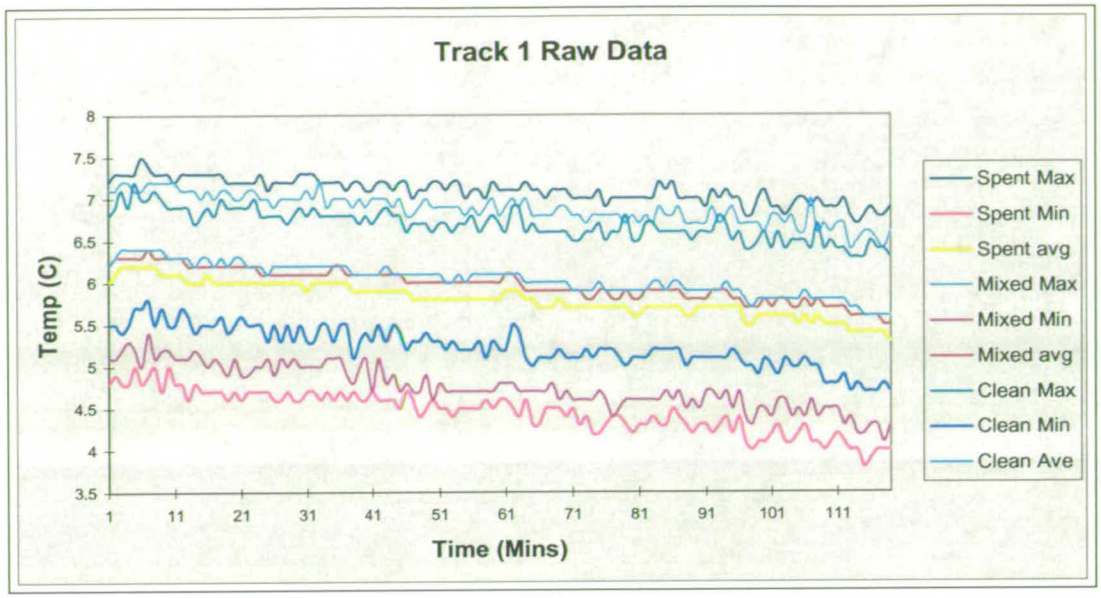

Figure 6.21 Graph showing the raw data obtained from the track bed.

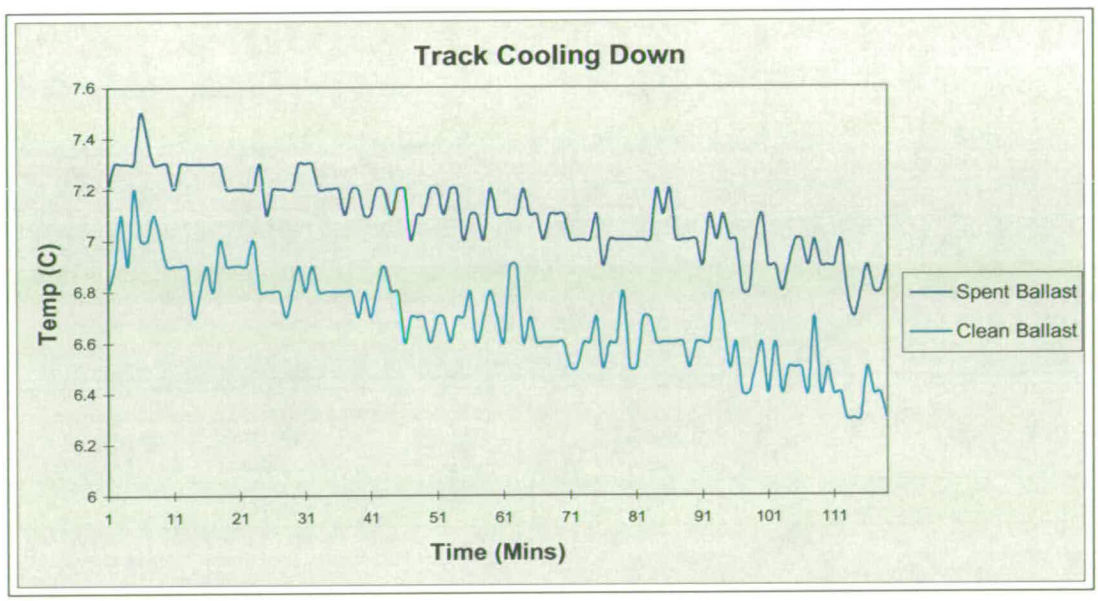

Figure 6.22 Cooling of spent and clean ballast on the test-rig.

6.7 Conductivity.

The conductivity of the test-rig was measured, to completely discount this method for the identification of the condition of ballast. The Geomics EM-38 conductivity metere was used. Figure 6.23 shows data recorded. The initial readings and end readings where taken from off the track, away from the influence of the metal rails. The measurements were then taken as the EM-38 travelled over the length of the track. Figure 6.23 shows that due to the influence of the metal rails there was very little difference along the length of the track. Form this result it can be clearly seen that conductivity is not a suitable technique to measure the condition of the ballast.

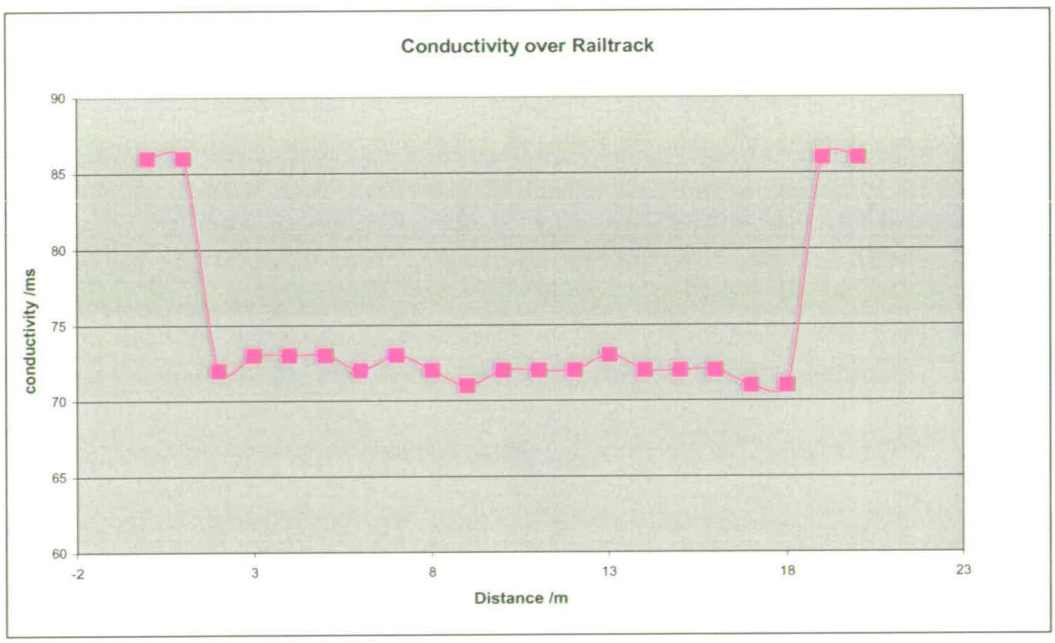

Figure 6.23 The conductivity measurements over the test-rig.

6.8 Conclusions from the Test Track

- Radar can detect the varying degrees of ballast deterioration,
- Attenuation increases with ballast deterioration,

- Dielectric constant increases with ballast deterioration,
- Formation reflections can be identified by both antennas for clean and partially deteriorated ballast,
- The 500MHz antenna is more effective than the 900MHz antenna, for both penetration and attenuation.
- Reinforced concrete and wooden sleepers do not allow the penetration of electromagnetic waves below the sleeper.
- The velocity for spent ballast on the test-rig is highly dependent on prevailing weather conditions,
- The velocity for clean ballast is less dependent on prevailing weather conditions,
- The CMP and WARR ballast depth calculations are independent of weather conditions, moisture content, ballast deterioration and attenuation.
- The depth profiles calculated from each method were compared to the physical measurements of the test-rig. The difference was very small.
- Both methods can accurately determine ballast depth.
- These two antennae methods cannot identify the ballast condition, just depth. The optimum survey set-up would be to use the WARR method to calculate ballast depth, with the monostatic antenna locating ballast deterioration.
- Both the CMP and WARR methods remove the need to excavate expensive and time consuming velocity calibration trial pits.
- The dielectric constant and thus the velocity of the ballast can be calculated by using either the WARR or CMP method and the knowledge of the dielectric constant from table 5.1, removing the need for a trial pit.

- The infra–red thermography trial on the test-rig proved that this method can detect the difference between clean and spent ballast.
- Conductivity is not a suitable method to measure the condition of the in-situ ballast.

Chapter 7

Field Trials of Radar and Infra–red Thermography

7.1 Introduction

There are several problems involved with working on live track. There are both general problems involved with any field-work and specific problems involved with working on live railway track.

The general considerations to be considered before field work is undertaken are:

- A qualified first aider must be available.
- The Edinburgh University's Risk assessment form must be completed.
- Transportation of equipment
- Access to the area.

The limitations that are specific to working on live railway track are:

- Work can only be conducted at night.
- Every person on the track needs a valid Personal Track Safety Card.
- There is limited access and care has to be taken when travelling down the railway line.
- Any work on the railway track needs a Picow (a person in charge of work), Lookout and Site Foreman, all supplied by Railtrack.

Figure 7.1 shows a quiet railway line where some of the above issues were not such a problem, (e.g. night work - there was 1 train a week travelling on this line). Other

issues still had to be addressed e.g. holding a Personal Track Safety Card, as the property is owned by Railtrack plc and access is granted with the same restrictions as any other line.

Figure 7.2 shows a busy InterCity electrified rail track at Ingatestone, East Anglia. This image shows some of the problems associated with work on the railway track. For example, there are over-head electrified lines and by Railtrack plc rules, to prevent electrocution nothing can enter a nine foot no-go zone around the lines. Trains run along this line for 20 hours a day, leaving only a 4 hour period to conduct a survey. The survey time also includes the travel time to and from the survey site from the access point, which may be up to 2 miles away. With the work being undertaken at night, a generator and spot lights need to be taken with the surveying team as seen in figure 7.3.

Figure 7.1 A quiet non-electrified track

Figure 7.2 A busy high speed electrified track

Figure 7.3 Night work at Ingatestone showing the spot lights

7.2 Field Test of Radar

The fieldwork was carried out at Ingatestone, East Anglia. A distance of 1 km was surveyed either side of a ballast renewal project. A velocity calibration method (CPR) was undertaken next to a trial hole so the ballast condition was known at one point. The velocity from the calibration method was used to calculate the depth for the radar plots, (figure 7.4 and figure 7.5).

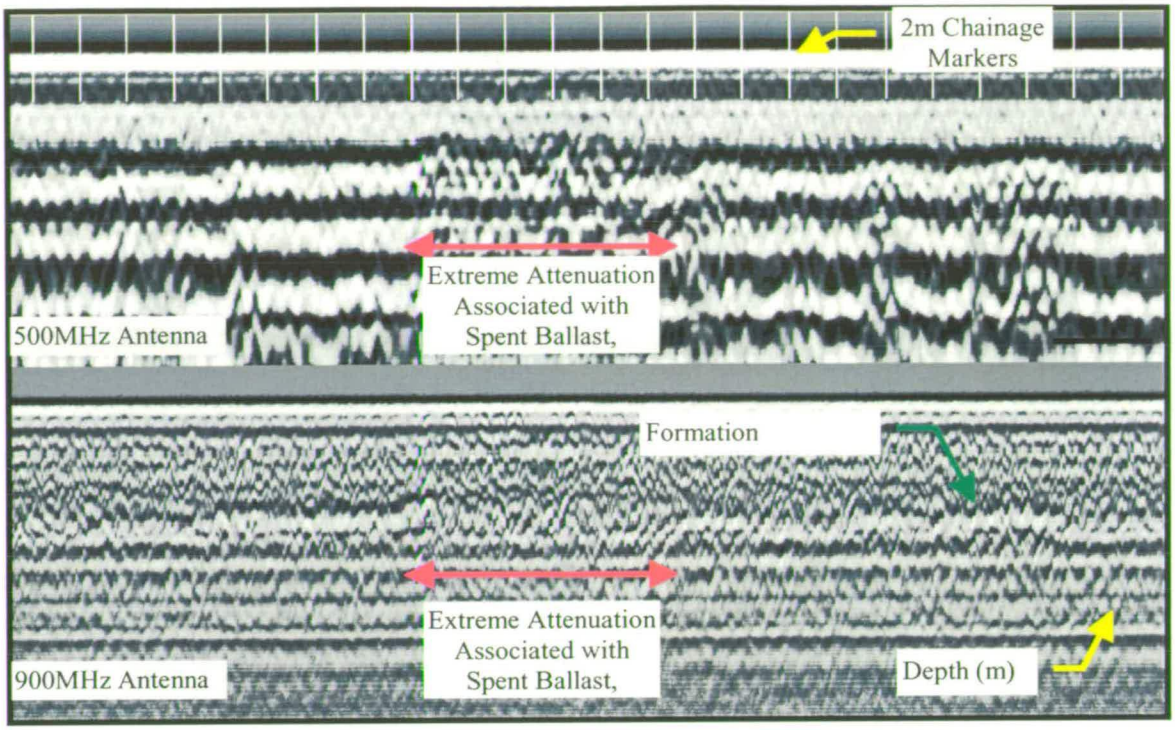

Figure 7.4 Ingatestone field trial, GPR grey scale plot

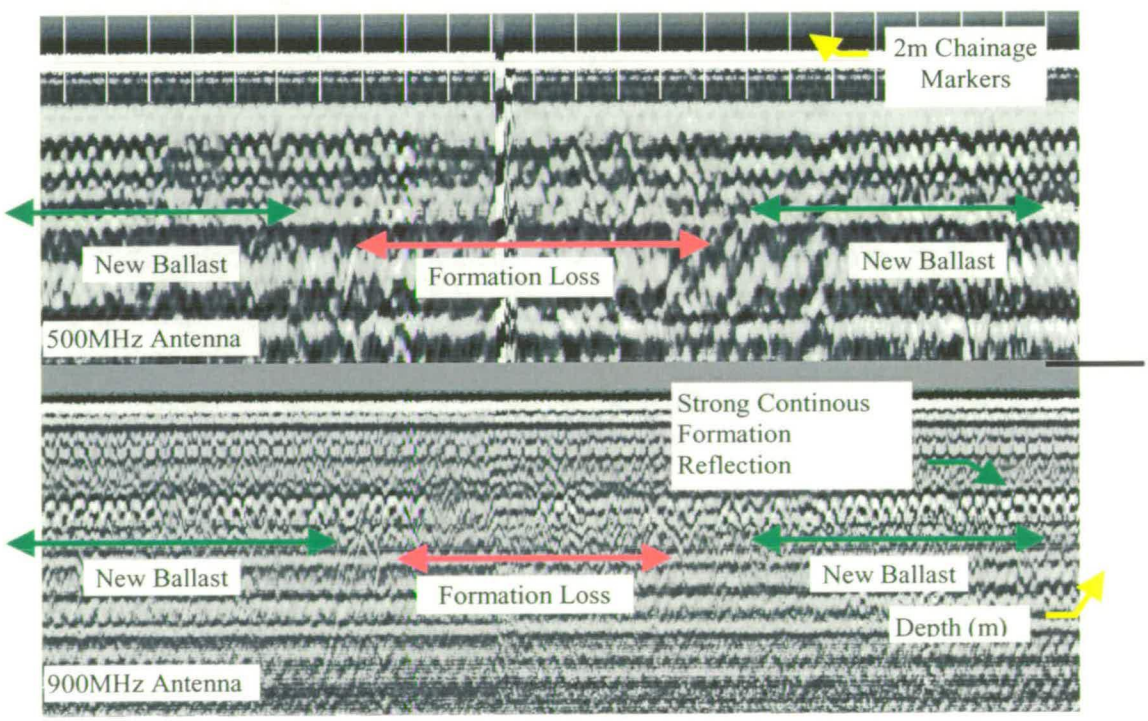

Figure 7.5 Ingatestone field trial, GPR grey scale plot

Figure 7.4 and figure 7.5 shows different track sections. The section of ballast in the centre of figure 7.4 suggests a problem with the continuity of the replaced material. Such a relative increase in scattering was evident on both frequencies. It was concluded that the ballast returned to this section of track did not have the same material properties as clean ballast. A trial hole concluded that a portion of the old ballast was unknowingly placed into this section of track. It can be seen from figure 7.4 and figure 7.5 that the conclusions from the laboratory results that an increase of the fines in the ballast causes an increase of dielectric properties and attenuation are shown to hold true on the live track.

7.3 Practical Implications of the Radar

From the work undertaken in the laboratory it was possible to characterise ballast quantitatively using GPR. This work was the first of this type, as seen from the literature survey in Chapter 2. This work has been presented at a number of conferences and the results (table 5.1) are currently being used by the industry, as the standard to assess the characteristics of ballast (Czech Railways, AREMA).

From the pilot scale experiments on the test track, it was possible to confirm the laboratory results. The test track enabled testing and optimisation of the trolley. This enabled problems encountered on the test track to be solved before the field trials. It also proved that GPR was a successful tool in determining the characteristics of ballast.

7.4 Field Test of Infra-red Thermography

At the Ingatestone site (the same site as the radar field trial – see section 7.1) an infra-red thermography field trial was conducted to assess its performance on a real track. The trial was conducted on an operational track and at night. Figure 7.6 shows a typical infra-red image of the track at Ingatestone. It can be seen from the image that the rails running north/south are at a lower temperature (-1°C to –2°C) than the ballast or sleepers. The sleepers can just be seen as the lighter stripes of colour across the image. The scale on the right-hand side shows the temperature range of the image.

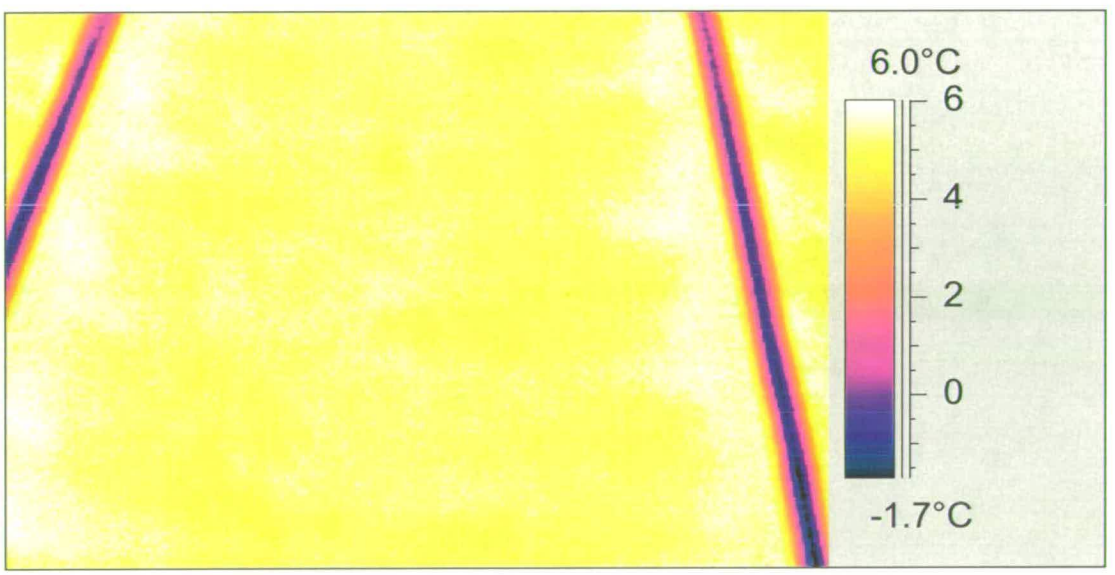

Figure 7.6 An infra-red image of the Ingatestone track.

The infra-red camera was mounted on the same trolley as the radar and both systems recorded as the trolley moved along the track. The survey was conducted at night so the temperatures were low. The temperature of the track was measured and all data converted to Excel format and plotted. Figure 7.7 shows the raw data (every data

point that was recorded) with temperature (°C) on the y-axis and time on the x-axis. At that time there was no way of telling the position of the camera apart from the time the frame was taken.

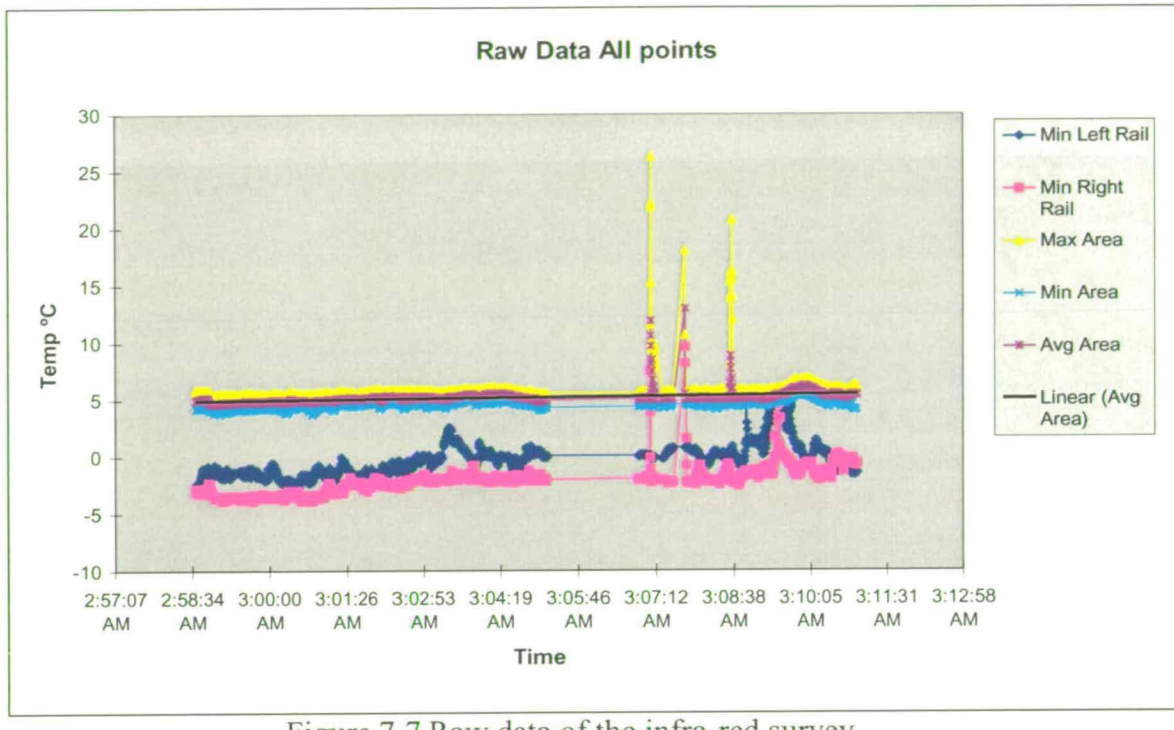

Figure 7.7 Raw data of the infra-red survey

The data was processed by taking an area of ballast and sleepers in-between the rails and the average, minimum and maximum temperatures were plotted, as well as the temperature of the rails. It can be seen from just the temperature of the track bed, that there are anomalies. These are indicated by the peaks in the yellow, red and light blue lines. All the plotted lines spike at the same time signifying that it is an extreme temperature change (such as a plant) but in actual fact the spikes are due to people walking in front of the camera. The measured temperatures of the ballast were compared with those of the rails, which can be considered as atmospheric temperature (the rails are made from steel which has a lower heat capacity and will fluctuate with the air temperature). Figure 7.8 show the relative temperature of the

track bed with respect to the rails. This shows a large dip in the relative track bed temperature. This relates to the area of track bed that was not re-ballasted. This correlates with the same area that was found using the radar.

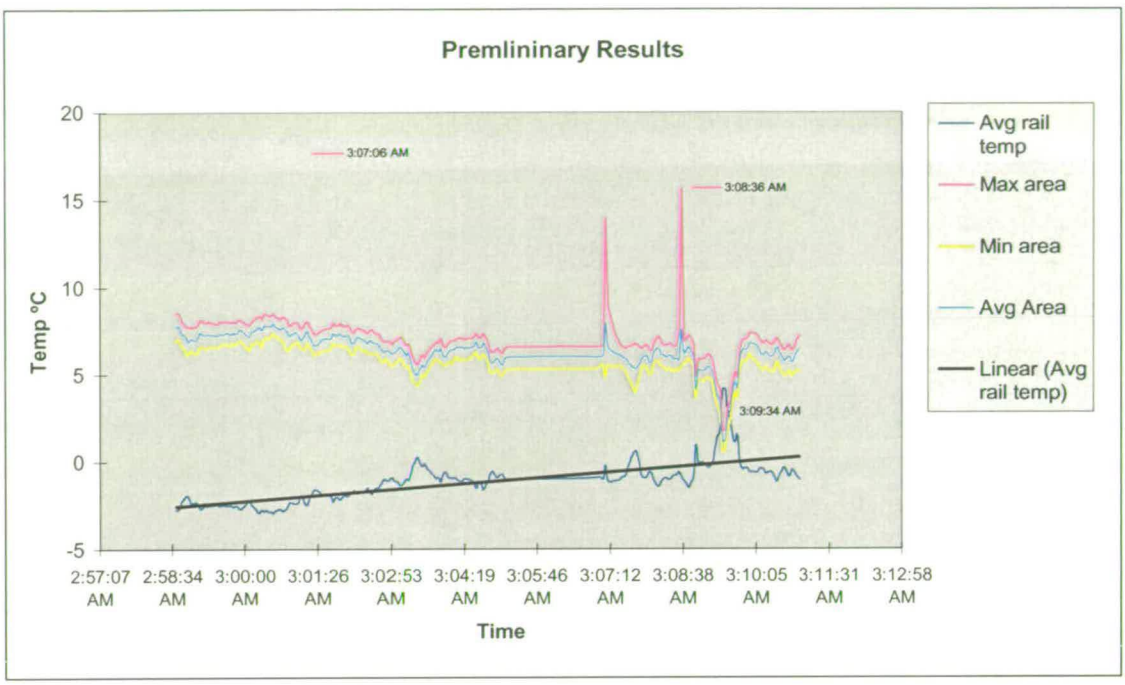

Figure 7.8 Filter results of the Infra red survey.

7.5 Speed Of Radar and Infra-red Thermography

Radar

The governing factors of the speed that the radar can record data are the number of scans per second the radar can record and the level of detail required. There are other factors such as the transmit rate, speed of antenna and the frequency of pulse, but these factors are not as decisive as the level of detail required. Figure 7.9 shows the relationship between the speed of the recording vehicle and the required detail

(distance between data points), depending upon the scans/second which is set by the number of channels being used. The required detail for the classification of ballast is a maximum of 1 m. If the radar is only recording on 1 channel, the maximum speed is 25 kph which is slow. The survey would not be detailed so data would be missed. If the radar was recording on 2 channels, (as it was in the field survey), and a high level of detail was needed (e.g. 0.25 m to guarantee a scan line between every sleeper) the speed would then be limited to under 10 kph (walking pace).

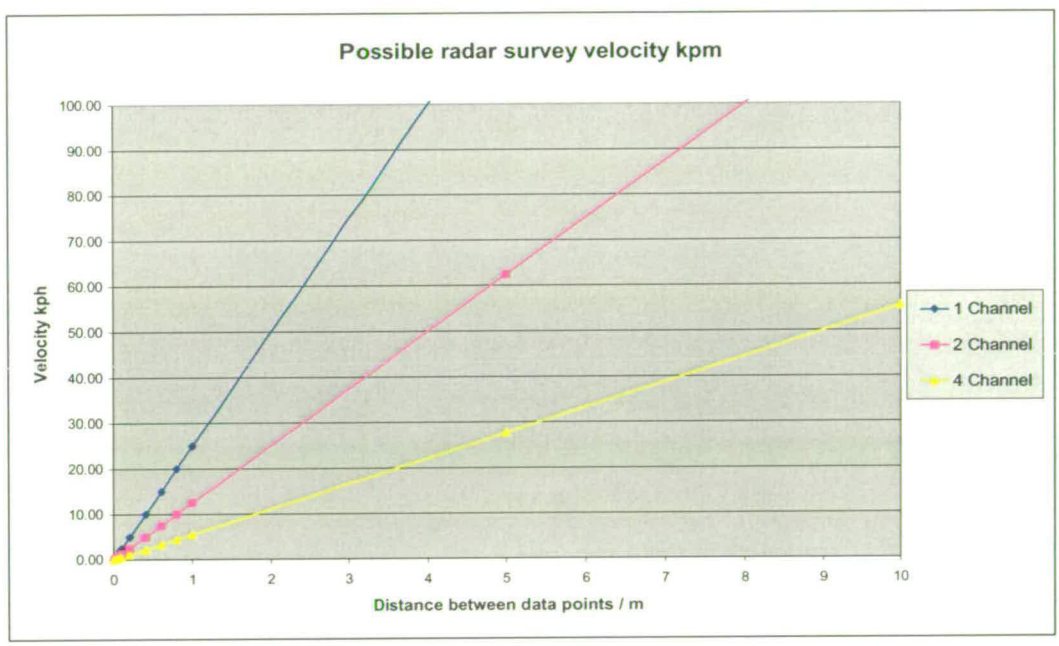

Figure 7.9 Speed of the recording vehicle based on the level of detail and number of channel.

Infrared Thermography

Figure 7.10 shows the relationship between the speed of the vehicle and the level of detail (in this case represented by the degree of the camera from the vertical). Further constraints are the height of the camera and recording frame rate, these are

set at 3m and a frame rate of 2.9 in figure 7.10. The level of detail reduces as the camera angle increases because the amount of data in each image increases for the same number of pixels in each image. Figure 7.10 shows that if a low level of detail (e.g. just over one pixel per third of a metre), is required a speed of over 100 kph can be achieved.

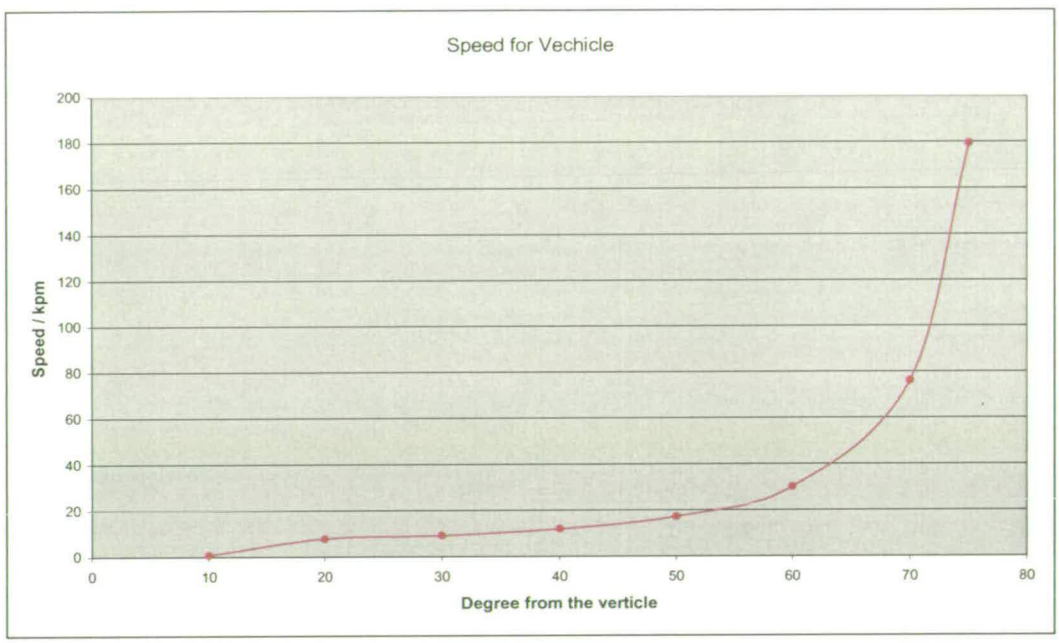

Figure 7.10 Speed of the recording vehicle if the infra-red camera is mounted at a height of 3m.

From figure 7.9 and figure 7.10 it is proposed that when undertaking a survey of the ballast, an infra-red high speed survey should be undertaken in the first instance followed by a more detailed, slower survey of problem areas by a GPR survey.

7.6 Field Test Conclusions

1. Ingatestone GPR field trial proved successful in:
    - Identifying varying degrees of ballast deterioration.
    - Locating sections of track that had not been replaced.
    - Providing continuous depth profiles for old and new track bed.
    - By applying velocity calibration techniques, an accurate depth calculation was obtained
2. There is a difference between the rate of heat transfer of spent and clean ballast.
3. The infra-red camera is an effective method of determining the state of the ballast.

The Ingatestone field trails have proved that both of the techniques were able to identify the same anomaly, which proved to be a change in ballast properties from clean to spent.

Chapter 8

Conclusion and Further Work

8.1 Conclusion

- In the UK railway track consists of various components; subgrade, subballast, ballast, sleepers, rail fasteners and the rail. This thesis has only investigated the ballast. As described in Chapter 3 the ballast was found to be granodiorite. This thesis has shown that deterioration of ballast depends on many factors; mechanical wear, vibration caused by the train, chemical wear, weathering and infiltration of fines from the surface.
- The difference between clean and spent ballast has been demonstrated with particle size distribution charts. Clean ballast was uniformly graded whilst spent ballast was 'gap-graded'. The spent ballast contained fines while clean ballast did not. This was confirmed by spent ballast having a higher density than that of clean ballast.
- There are various methods of track maintenance; tamping, stoneblowing or by using a ballast cleaner. The advantages and disadvantages have been outlined for these methods. The ballast cleaners have not been fully approved by Railtrack plc at present for use in the UK. These methods of maintenance are not compatible; it is not possible to tamp a stone blown track, therefore, once it is decided to maintain a route with one method, it is not possible to change.
- There are many British and American Standards that are used to categorise aggregates. Only a few of these standards are used for the British Railway Standards for ballast. These standards were compared in this thesis against the railway standards of other industrialised countries. It was found that all the

countries' standards were intrinsically similar, but some countries had their own specific tests, (e.g. Finland and the Nordic have the ball mill test which was similar to the Los Angeles abrasion test).

- This thesis investigated, in depth, a number of non-destructive techniques; radar, infra-red thermography and conductivity. A number of other techniques were discussed and explanations offered as to why they were not suitable for use on railway track beds. Radar, infra-red thermography, conductivity and the falling weight deflectometer all have several limitations, but also advantages for railway track bed use. These have been explained.
- The falling weight deflectometer is the current method used by the industry for testing the stiffness of the ballast. This was not investigated further as part of this thesis.
- Conductivity was found to be of little use to determine the condition of the ballast due to the presence of the rails and sleepers. Without these metallic elements conductivity would be an ideal method and has been used in other similar circumstances.
- This thesis has concluded that radar and infra-red thermography were two methods with many positive factors. The fact that the rails had a limited adverse effect on the techniques and that both were capable of continuous, non-contact, high-speed recording, make them ideal for use on railway track beds.
- Theoretically the ideal conditions for a radar survey are when the spent ballast is saturated. The clean ballast will drain and thus there will be the greatest difference between the two types of ballast in a radar survey.

- The ideal conditions for an infra-red survey are when the clean and spent ballast have different thermal gradients, in early morning or late afternoon.
- The Railtrack plc ballast standards have been examined in depth and the ballast used in the laboratory experiments was subject to the ballast standard tests. These tests showed that spent ballast met some of the ballast standards. This revealed that the ballast standards were insufficient to identify spent ballast. The spent ballast could have failed some of the tests due to stress fractures, which occurred whist it was on the track bed. Also Railtrack plc ballast standards could be specific to particular rail routes, which is not the case at present. For example the ten-percent fines test is a more suitable test for a freight line than high-speed lines.
- The lack of a current durability test for ballast was considered to be an oversight. The Slake Durability Test was thought to be a suitable test. It was undertaken and the results compared with other rock types, such as Portland Limestone. Ballast (granodiorite) was found to be a very durable material.
- It was found from the Slake Durability Test that sea spray (salt water) adversely affected the durability of ballast.
- A new standard was drawn up for the use of new and recycled ballast using the test data found in this thesis as its basis.
- The work on infra-red thermography showed theoretically that there was a difference in the heat transfer through the two different types of ballast (clean and spent). Thorough laboratory tests were undertaken to see if the theoretical model was accurate. It was found that there was a difference in the rate of temperature change within the different types of ballast, i.e. that they had different thermal

properties. Additionally water had an effect on the rate of heat transfer. This effect was to enlarge the differences between the types of ballast. These differences in thermal properties were due to the fines, which were found within the spent ballast. The fines filled the air voids, creating different heat transfers through the ballast. The fines also soaked up water, which drained through the clean ballast. Water affected spent ballast to a greater extent than clean ballast.

- The ideal conditions for an infra-red survey were found to be when there is a 5°C temperature difference between the soil and the air temperature, and the ballast is wet.
- This theory was also found to hold true when the field trial was undertaken. The infra-red thermography correctly identified an area of spent ballast, proving that infra-red thermography is an effective method of determining the condition of the ballast.
- One of the major advantages of an infra-red survey is that it is a quick, non-invasive method.
- Ballast was subjected to laboratory tests using radar. The clean and spent ballast's dielectric constants were found. This is useful when a survey attempts to identify the type of ballast under investigation. The dielectric constant was found for dry and wet clean and spent ballast. In the radar tests, the 500 MHz antenna was found to be suitable for use on the railway track bed as the signal from the 900 MHz scattered.
- From the test-rig built at Edinburgh University, it was found that radar could identify the interface between the ballast and formation layers and that the rails

and sleepers did not adversely affect the signal if the antenna was held within 10 cm of the track bed surface.

- The field trial was successful in showing that radar can be used on live track to detect changes in the characteristic of the ballast; i.e. it distinctly differentiated between clean and spent ballast.
- The ideal conditions for a radar survey are when the rail track bed is wet, so the greatest difference between the clean and spent ballast occurs. From the research undertaken in this project the ideal way to conduct a survey is to conduct a high speed survey using infra-red thermography and then a slower more detailed radar survey on problem areas.
- The most important result from the work undertaken in this thesis was that both radar and infra-red thermography found the same anomaly, an area of spent ballast within an area of clean ballast in the field trial. This proves that both techniques satisfy the requirement set out at the beginning of the thesis to identify the difference between clean and spent ballast.

8.2 Further work

Certain areas should be followed up and explored. The issue of speed limitations for both the radar and infra-red should be further field investigated, as this project has shown that these techniques work, as the operating speed at the moment is too slow for use on live track. Eventually these techniques should be undertaken using an intercity train, so they can record track data whilst the train is running at operating speed. Before this can be achieved further field trials on other lengths of track need to be undertaken to confirm the findings in this thesis, as well as automating the

processing of the radar and infra–red data, perhaps using an application such as Matlab.

The research completed so far has shown that as the deterioration increases (amount of fines within the ballast), the dielectric constant and attenuation increases as well. Future work in this area should concentrate on identifying the level of deterioration from the attenuation and dielectric constant.

Another area of future research is the Slake Durability Test. Future research in this area should reveal how the Slake Durability Test models the action of trains passing over ballast, as well as comparing the lifetime predictions of the ballast from the Slake Durability Test to results from the track.

References:

Adams, A.K., Gill, A.S., Ek, J.R., & Nelson, R.A., 1998,

Contribution of Conduction to Total Infant Energy Expenditure, *Journal of Thermal Biology*, Vol. 23, No. 5, pp 267-272

Agema Infrared Systems,

Irwin Research 1.1, Operating Manual.

Annan, A.P. & Cosway, S.W., (1992),

Ground Penetrating Radar Survey Design, *J SAGEEP*, Vol. 1, pp 329-351.

Anonymous, (1994*),*

Use and Limitations of Ground Penetrating Radar for Pavement Assessment, HA 72/94, Design Manual for Roads and Bridges, London: HMSO, 1994

AREA (1990).

Manual for Railway Engineering. American Railway Engineering Association , Washington, D.C.

American Standard Test Method, 1997a

Accelerated Polishing of Aggregates Using the British Wheel, D3319, Vol. 4.03, pp 300 – 303

American Standard Test Method, 1997b

Aggregate Durability Index, D3744, Vol. 4.03, pp 374 – 381

American Standard Test Method, 1997c

Bulk Density, C29/29M, Vol. 4.02, pp 1- 4

American Standard Test Method, 1997d

Degradation of Fine Aggregate Due to Attrition, C1137, Vol. 4.02, pp 591 – 593

American Standard Test Method 1997e

Detecting Delamination in Bridge Decks Using Infrared Thermography, D4788, Vol. 4.03, pp 474 – 475.

American Standard Test Method, 1997f

Index of Aggregate Particle Size and Texture, D3398, Vol. 4.03, pp 317 – 320

American Standard Test Method, 1996a

Lightweight Particles in Aggregates, C123, Vol. 4.02, pp 58 – 60

American Standard Test Method, 1996b

Resistance to Degradation of Large-Size Coarse Aggregate by Abrasion and Impact in the Los Angles Machine, C535, Vol. 4.02, pp 278 – 279.

American Standard Test Method, 1996c

Sieve Analysis of Fine and Coarse Aggregates, C136, Vol. 4.02, pp 78 – 79

American Standard Test Method, 1994

Surface Moisture in Fine Aggregate, C70, Vol. 4.02, pp 28 – 70

American Standard Test Method, 1993

Specific Gravity and Absorption of Coarse Aggregate, C127, Vol. 4.02, pp 64 – 65

Banverket, (1996),

Makadamballast förJjärnväg (Ballast for railways), Foreskrift BVF 585.52, 1996-03-01

Bell, F.G., 1992,

Engineering Properties of Soils and Rocks third edition, Butterworth Heinmann, Oxford, pp 207-228

Bell, F.G., Culshaw, M.G. & Cripps, J.C., 1999,

A Review of Select Engineering Geological Characteristics of English Chalk, *Engineering Geology*, Vol. 54, pp 237 – 269,

Bell, F.G., Entwisle, D.C. & Culshaw, M.G., 1997,

A Geotechnical Survey of Some British Coal Measures Mudstones, with Particular Emphasis on Durability, *Engineering Geology*, Vol. 46, pp 115-129

Binda, L., Saisi, A. & Tiraboschi, C., 2000,

Investigation Procedures for the Diagnosis of Historic Masonries, *Construction and Building Materials*, Vol. 14, No. 4, pp 199 – 233.

Bishop, A.W. & Henkel, D.J., 1962

The Measurement of Soil Properties in the Triaxial Test, 2nd Edition, Edward Arnold (Publishers) Ltd, London.

Bonnett, C.F., (1996)

Practical Railway Engineering; Imperial College Press.

Brewer, P., (1999)

Private conversion.

British Standards Institution, 1951,

BS 812 Wet Attrition Value Clause 25

British Standards Institution, 1981,

Code of Practice for Site Investigation, pp 147

British Standards Institution 1985

BS 812 Particle Size Distribution part 103.

British Standards Institution 1988a

BS 812 Sulphate Content part 118.

British Standards Institution 1988b

BS 812 Water Soluble Chlorides part 117.

British Standards Institution 1989a

BS 812 Elongation Index part 105.

British Standards Institution 1989b

BS 812 Flakiness Index part 105.

British Standards Institution 1989c

BS 812 Frost Heave part 124

British Standards Institution 1989d

BS 812 Polished Stone Value part 114.

British Standards Institution 1989e

BS 812 Soundness part 121.

British Standards Institution 1990a

BS 812 Aggregate Abrasion Value part 113

British Standards Institution 1990b

BS 812 Aggregate Crushing Value part 110.

British Standards Institution 1990c

BS 812 Aggregate Impact Value part 112.

British Standards Institution 1990d

BS 812 Moisture Content part 109.

British Standards Institution 1990e

BS 812 Ten-percent Fines Value part 111.

British Standards Institution 1995

BS 812 Density and Absorption part 2.

British Standards Institution 1999

BS 5930 *Classification of weathering tests*

Brown, E.T., 1981,

Rock Characterization Testing and Monitoring, ISRM Suggested Methods, Pergamon Press

Bruening, R & Mordfin, L 1994,

Infra red Thermography Standards for Nondestructive Testing *Thermosense*, Vol. 2245 pp 220-221

Bungey, J.H., Millard, S.G. & Shaw, R.M., 1993,

The Influence of Reinforcing Steel on Radar Survey of Concrete Structures, *Proc. 5th International Conference on Structural Faults and Repairs*, Vol. 3, pp 43-50, Engineering Technics Press, London

Burnay, SG, Williams, TL & Jones, CH, 1988,

Applications of Thermal Imaging, Adam Hilger.

Büyüköztürk, O., 1998

Imaging of Concrete Structures, *NDT & E International*, Vol. 31, No. 4, pp 233-243

Can, M., 1998,

Simultaneous Convective Heat and Mass Transfer in Impingement Ink Drying, *Int. Comm. Heat Mass Transfer*, Vol. 25, No. 6, pp 863-874

Colla, C., Burnside, C.D., Clark, M.R., Broughton, K.J. & Forde, M.C., 1998,

Comparison of Laboratory and Simulated Data for Radar Image Interpretation, *NDT & E International*, Vol. 31, No. 6, pp 439 – 444.

Colla, C., McCann, D.M., Forde, M.C. & Das, P.C., 1997,

Radar Imaging in Composite Masonry Structures, *Proc. 7th Int. Conf. Structural Faults and Repairs – 97*, Vol 3, Engineering Technics Press, Edinburgh.

Collinson, R., 1998,

Ballast Life & Maintenance, *Proc. 1st Int. Conf. Railway Engineering 2000*, Engineering Technics Press, London.

Coombs, D.H., 1971,

British Railway Track Design, Construction and Maintenance; The Permanent Way Institution.

Cox, K.G., Bell, J.D. and Pankhurst, R.J., 1979,

The Interpretation of Igneous Rocks Unwin Hyman, London, England.

CP Rail specification for ballast, 1987,

Performance of aggregates in railroads and other track performance issues, Transportation Research Record1131, Washington, D.C..

Daniels, D.J. 1994,

Developments in Impulse Radar Technology for Surface Penetrating Radar, ERA Technology.

Daniels, D.J. 1994,

Radar for Non Destructive Testing of Materials, ERA Technology.pp1-3.

Daniels, J.J., 1989,

Fundamentals of Ground Penetrating Radar, *Symposium on the application of geophysics of Engineering And Environmental Problems*, PP 62 - 141

Davidson, N.C. & Forde, M.C. 1996,

A laboratory appraisal of GPR over water. *Non-Destructive Tesing Evaluation,* Vol. 12, pp 219-242.

Dearman, W.R., 1959,

The Geology of the Devonian and Carboniferous Rocks of the North-West Border of the Dartmoor Granite, Devonshire, *Proc. Geol. Assoc.*, Vol. 70, pp 51-92

Dearman, W.R., 1960,

Bavenite from the Meldon Aplite Quarries, Okehampton, Devonshire, *Miner Mag.*, Vol. 32, pp 577 – 578

Dearman, W.R., 1962,

Dartmoor : the North-west Margin and Other Selected Areas, *Geologists' Association Guides, No. 33*, Benham and Company Limited, Colchester.

Bruening, R & Mordfin, L 1994,

Infra red Thermography Standards for Nondestructive Testing *Thermosense*, Vol. 2245 pp 220-221

Bungey, J.H., Millard, S.G. & Shaw, R.M., 1993,

The Influence of Reinforcing Steel on Radar Survey of Concrete Structures, *Proc. 5th International Conference on Structural Faults and Repairs*, Vol. 3, pp 43-50, Engineering Technics Press, London

Burnay, SG, Williams, TL & Jones, CH, 1988,

Applications of Thermal Imaging, Adam Hilger.

Büyüköztürk, O., 1998

Imaging of Concrete Structures, *NDT & E International*, Vol. 31, No. 4, pp 233-243

Can, M., 1998,

Simultaneous Convective Heat and Mass Transfer in Impingement Ink Drying, *Int. Comm. Heat Mass Transfer*, Vol. 25, No. 6, pp 863-874

Colla, C., Burnside, C.D., Clark, M.R., Broughton, K.J. & Forde, M.C., 1998,

Comparison of Laboratory and Simulated Data for Radar Image Interpretation, *NDT & E International*, Vol. 31, No. 6, pp 439 – 444.

Colla, C., McCann, D.M., Forde, M.C. & Das, P.C., 1997,

Radar Imaging in Composite Masonry Structures, *Proc. 7th Int. Conf. Structural Faults and Repairs – 97*, Vol 3, Engineering Technics Press, Edinburgh.

Collinson, R., 1998,

Ballast Life & Maintenance, *Proc. 1st Int. Conf. Railway Engineering 2000*, Engineering Technics Press, London.

Coombs, D.H., 1971,

British Railway Track Design, Construction and Maintenance; The Permanent Way Institution.

Cox, K.G., Bell, J.D. and Pankhurst, R.J., 1979,

The Interpretation of Igneous Rocks Unwin Hyman, London, England.

CP Rail specification for ballast, 1987,

Performance of aggregates in railroads and other track performance issues, Transportation Research Record1131, Washington, D.C..

Daniels, D.J. 1994,

Developments in Impulse Radar Technology for Surface Penetrating Radar, ERA Technology.

Daniels, D.J. 1994,

Radar for Non Destructive Testing of Materials, ERA Technology.pp1-3.

Daniels, J.J., 1989,

Fundamentals of Ground Penetrating Radar, *Symposium on the application of geophysics of Engineering And Environmental Problems*, PP 62 - 141

Davidson, N.C. & Forde, M.C. 1996,

A laboratory appraisal of GPR over water. *Non-Destructive Tesing Evaluation,* Vol. 12, pp 219-242.

Dearman, W.R., 1959,

The Geology of the Devonian and Carboniferous Rocks of the North-West Border of the Dartmoor Granite, Devonshire, *Proc. Geol. Assoc.*, Vol. 70, pp 51-92

Dearman, W.R., 1960,

Bavenite from the Meldon Aplite Quarries, Okehampton, Devonshire, *Miner Mag.*, Vol. 32, pp 577 – 578

Dearman, W.R., 1962,

Dartmoor : the North-west Margin and Other Selected Areas, *Geologists' Association Guides, No. 33*, Benham and Company Limited, Colchester.

Dearman, W.R., 1974,

Weathering Classification in the Characterisation of Rock for Engineering Purposes in British Practice, *International Assoc. Eng. Geol.*, Vol. 9, pp 33 - 42

Dearman, W.R., 1986,

State of Weathering: The Search for a Rational Approach, *Engineering Geology Special Publication No. 2*, Ed. Hawkins, A.B., Geological Society, London, pp 193-198

Dearman, W.R., 1995,

Description and Classification of Weathered Rocks for Engineering Purposes: the Background to the BS5930:1981 Proposals, *Quarterly Journal of Engineering Geology*, Vol. 28, pp 267 - 276

Dearman, W.R., & El Sharkawi,M.A.H, 1965,

The Shape of the Mineral Deposits in the Lower Culm Measures of North-West Dartmoor, *Trans. Roy. Geol. Soc. Corn.*, Vol. 19, pp 286 – 296.

Denton, G. 1995,

Final Year Honours Project, University of Edinburgh.

Donnelly, L.J. & McCann, D.M. 2000,

The Location of Abandoned Mine Workings Using Thermal Techniques. Engineering Geology, Elsevier, Vol 57, pp 39-52.

Duffin, W.J., 1990

Electricity and magnetism, London, McGraw-Hill, pp 322-331.

Drysdale, D. 1997,

An Introduction to Fire Dynamics A Wiley-Interscience Publication. pp32-33

Ehara, G., 1999,

The Development of the Guiling Method for Tamping Machine's Lining Work Under the High Speed Operation At Shinkansen line and Ordinary line. *Proc. 1st World Congress on Railway Research 1999*. Toyoko, Japan.

Engelbert, P.J., Hotchkiss, R.H. & Kelly, W.E. 1997

Integrated Remote Sensing and Geophysical Techniques for Locating Canal Seepage in Nebraska, *Journal of Applied Geophysics*, Vol. 38, pp 143 -154

Flint, R.C., Jackson,P.D. & McCann, D.M., 1999,

Geophysical Imaging Inside Masonry Structures, *NDT & E International*, Vol. 32, pp 469 - 479

Forde, M.C. & McCavitt, N., 1993,

Impulse Radar Testing of Structures, *J Institute of Civil Engineers Structures and Buildings*, pp96-99

Fortin, J.P., 1983,

Dymnaic Track Deformation, *French Railway Review*, Vol. 1, No. 1.

Giannopoulos, A., 1997

The Investigation of Transmission-Line Matrix and Finite-Difference Time-Domain Methods For the Forward Problem of Ground Probing Radar, University of York, UK, D.Phil Thesis.

Gobel, C., Hellmann, R. & Petzold, H., 1994,

Georadar – Model and In-situ Investigation for Inspection of Railway Tracks, *Proc. 5h International Conference on Ground Penetrating Radar*, Vol. 3, pp 1121- 1133, Canada

Göttel, R., & Flohrer, C., 1999,

Investigation with Radar on Concrete Bridges in Combination with a Forward Simulation Program, *8th Internation Conference Srtuctural Faults and Repair-1999*, London.

Greaves, R.J., Lesmes, D.P., Lee, J.M. & Toksöz, M.N., 1996,

Velocity Variations and Water Content Estimated From Multi-Offset, Ground-Penetrating Radar, *Geophysics*, Vol. 61, No. 3, pp 683 - 695

Gordon, M.O., Broughton K. & Hardy, M.S.A., 1998,

The Assessment of the Value of GPR Imaging of Flexible Pavements, *NDT & E International*, Vol. 31, No. 6, pp 429 - 438

Goodman, D. & Nishimura, Y., 1992,

2-D Synthetic Radargrams for Archaeological Investigation, *4th Int. Conf. On Ground Penetrating Radar*, Rovaniemi Finland, Special paper 16, pp 339 – 343.

Hall, A. 1987,

Igneous Petrology. Longman Scientific and Technical, London.

Hobbs, C.P., Temple, J.A.G., Hillier, M.J., Silk, H.G. & Tattersall, M.G., 1993,

Radar Inspection of Civil Engineering Structures, *International Conference on Non – Destructive Testing in Civil Engineering*, The British Institution of NDT, Liverpool, April, Vol. 1, pp 79 - 96

Holman, J.P., 1992,

Introduction to Heat Transfer, Heat Transfer, McGraw Hill, 7th edition.

Hugenschmidt, J., 1999

Ballast Inspection Using Ground Penetration Radar, *Proc 2nd International Railway Conference*, Engineering Technics Press, London.

Hugenschmidt, J., Partl, M.N. & De Witte, H., 1998,

GPR inspection of a mountain motorway in Switzerland, *Journal of Applied Geophysics*, Vol. 40, pp 95 - 105

Huille, J-P. and Hunt, G.A., 2000,

Track Stiffness: A Tool for Maintenance. *Proc. 3rd Int. Conf. Railway Engineering 2000*, Engineering Technics Press, London.

ICE report, 2000,

"The State of the Nation" *New Civil Engineer*, 9th November 2000, pp 20-21

Institute of Geological Sciences, 1976,

An Investigation into the Geological Feasibility into the Geological Feasibility of Storing Crude Oil in Unlined Caverns in the Hunterston Peninsula, Ayrshire, London.

Kulkarni, VK, 1996,

Use of Infra-Red Thermography in the Restoration of a Building, *The Indian Concrete Journal* pp 323-325

Jack, R. & Jackson, P., 1999,

Imaging Attributes of Railway Track Formation and Ballast Using Ground Probing Radar, *NDT & E International*, Vol. 32, pp 457 - 462

Lambe, T.W., & Witman, R.V. 1979,

Soil Mechanics, SI Version, John Wiley & Sons, pp 225-247.

Lanaro, F., Tolppanen,P., Illerström,A. & Stephansson, O., 2000,

Characterisation of Size, Shape and Texture of Aggregates by Fourier Analysis of 3-D-laser Images, *GeoEng2000*, 19-24 November 2000, Melbourne, Australia.

Lane, K.S., & Washburn,.D.E., 1946,

Capillarity Tests by Capillarimeter and by Soil Filled Tubes, *Proc. Highway Research Board.*

Le Maitre, R.W., 1976,

The Chemical Variability of Some Common Igneous Rocks Journal of Petrologists , Vol 17, pp 589-637.

Lee, Y.G. & Suh. J.H., 1997,

Finite-Difference Time Domain (FDTD) Simulation of GPR Propagation in Disperisve Media, *Proc. Non- Destructive Testing in Civil Engineering*, Ed. Bungey, J.H., Vol. 1, pp 261 – 270

Mallinson, P., 1997,

Surface Penetrating Radar as an NDT Tool, *Insight* Vol 39 No. 12, pp 874-877.

Markine, V.L. & Esveld, C., 2000,

Determination of Track Lateral Resistance and Train Speed Limits Using Tamping Machine and Numerical Optimisation. *Proc. 3rd Int. Conf. Railway Engineering 2000*, Engineering Technics Press, London.

Martin. J, Hardy, M.S.A., Usmani, A.S. & Forde, M.C., 1995,

Quantifying the Defects in Post-tensioned Bridge Using Impulse Ultrasonics, *Proc. 6th Int. Conf. Structural Faults and Repair – 95*, Vol 1, Engineering Technics Press, London.

McCann, D.M., Culshaw, M.G. & Fenning, P.J., 1997,

Setting the Standard for Geophysical Surveys in Site Investigation, In: McCann, D.M., Eddleston, M., Fenning, P.J. & Reeves, G.M. (eds) *Modern Geophysics in Engineering Geology*, Geological Society, London, Engineering Geology Special Publication, No. 12, pp 3 – 31.

McCann, D.M. & Forde M.C. 2000,

Review of NDT Methods in the Assessment of Concrete and Masonry Structures, *To be published.*

McCann, D.M., Jackson, P.D. & Culshaw, M.G., 1987,

The use of Geophysical Surveying Methods in the Detection of Natural Cavities and Mineshafts, *Quarterly Journal of Egineering Geology*, Vol. 20, pp 59 - 73, London

McCann, D.M., Jackson, P.D. & Fenning, P.J., 1998,

Comparison of the Seismic and Ground Probing Radar Methods in Geological Surveying, *Proc. Instn. Elec. Engnrs.*, Vol 135, Part F, No. 4, pp 380 - 390

McNeil. J, D, 1980,

Elctromagnetic Terrain Conductivity Measurement at Low Induction Numbers, Geonics Ltd., pp 5-6

McNeil. J, D, 1980,

Electrical Conductivity of Soils and Rocks, Geonics Ltd., pp5-9.

Milson. J, 1996,

Field Geophysics, John Wiley and Sons Ltd, West Sussex pp 103- 118

Moropoulou, A., Koui, M., Tsiourva, Th., Kourteli, Ch., & Papasotiriou, D., 1997, Macro- and Micro- Non Destructive Tests For Environmental Impact Assessment on Architectural Surfaces, *Mat. Res. Soc. Symp.* Proc.,Vol. 462, pp 343-349.

Nelson, S.D., 1994,

Electromagnetic Modelling for Ground Penetrating Imaging Radar (GPIR) using 3-D Finite Difference Time Domain (FDTD) Modelling codes, *NDT & E International*, Vol. 6, No. 3, pp 179 – 194.

Niliot, C.L. & Gallet, P., 1998,

Infrared Thermography Applied to the Resolution of Inverse Heat Conduction Problems: Recovery of Heat Line Sources and Boundary Conditions, *Rev. Gén. Therm.*, Vol. 38, pp 629-643.

Offermann, S., Bissieux, C. & Beaudoin, J.L., 1998,

Statistical Treatment Applied to Infrared Thermoelastic Analysis of Applied Residual Mechanical Stresses, *Rev. Gén. Therm.*, Vol. 38, pp 718-724.

Olhoeft, G.R., 1993,

Processing, Modelling and Presentation of Ground Penetrating Radar Data, *2nd Government Workshop GPR – Advanced Ground Penetrating Radar: Technologies and Applications*, Ohio, pp 23

Padaratz, I.J. & Forde, M.C., 1995a,

A Theoretical Evaluation of Impulse Radar Wave Propagation Through concrete, *J.Non-destructive Testing & evaluation*, Vol. 12 pp 9-32.

Padaratz, I.J. & Forde, M.C., 1995b,

Influence of Antenna Frequency on Impulse Radar Surveys of Concrete Structures, *Proc. 6th Int. Conf. Structural Faults and Repair – 95*, Vol 2, Engineering Technics Press, London.

Padaratz, IJ, Hardy, MSA & Forde, MC (1997), Calibration of radar testing of concrete, *Proc. 7th Int. Conf. Structural Faults & Repair-97,* Edinburgh, 8-10 July 1997, Vol. 2, Engineering Technics Press, 387-393.

Phemister, J. & Markwick, A.H.D., 1946,

Roadstone:Geological Aspects and Physical Tests, Department of Scientific and Industrial Research, London, England.

Railtrack Line Specification, 1998,

Track Ballast, RT/CE/S/006, Issue 2, Railtrack.

Railtrack Line Specification, 1996,

Tack Ballast Returned by Automatic Ballast Cleaners, Issue 1, Railtrack.

Rantala, J., Wu, D. & Busse, G., 1998,

NDT of Polymer Materials using Lock-in Thermography with Water-coupled Ultrasonic Excitation, *NDT & E International,* Vol. 31, No. 1, pp 43-49

Raymond, G.P., & Diyaljee, V.A., 1979,

Railroad Ballast Load Ranking Classification, *J. Geotechnical Engineering Division*, Vol. 105, Part 105, pp 1133 - 1153

Schmidt, FW, Henderson, RE & Wolgemuth,CH., 1993,

Introduction To Thermal Sciences, John Wiley & Sons, Inc.

Selig E T and Waters J M., 1994,

Track Geotechnology and Substructure Management, Thomas Telford. pp 2.1-14.1

Selig, E. T., 1985,

Ballast for Heavy Duty Track; Track Technology, Institution of Civil Engineers. pp 245-253

Sharpe, P. 1996,

Trackbed Stiffness and Falling Weight Deflectometer, Report No. LR-MSU-206, Scientifics, Derby

Sharpe. P, & Collop, A.C., 1998,

Trackbed Investigation- a Modern Approach, *Proc. 1st Int. Conf. Railway Engineering-98*, Engineering Technics Press, London.

Shen, L.C., Savre, W.C., Price, J.M. & Athavale, K., 1985,

Dielectric Properties of Reservoir Rocks at Ultra-high Frequencies, *Geophysics*, Vol. 50, No. 4, pp 692 – 704.

Shenton, M.J., 1975,

Deformation of Railway Ballast under Repeated loading Conditions; Railroad Track Mechanics and Technology, Kerr A D, Pergamon Press.

Shenton, M.J., 1984,

Ballast Deformation and Track Deterioration; Track Technology, Institution of Civil Engineers.

Simmons, J. 1961,

The Railways of Britain, Routledge & Kegan Paul Ltd, London.

Smith, G.S., 1984,

Directive Properties of Antennas for Transmission into a Material Half-space. *IEEE Trans. Antennas and Propagation*, No 3 , pp 232-246.

Talwar, D.N., Jogai, B., & Loehr, J.P., 1998,

Novel Type II Strained Layer Superlattices for Long Wavelength Infrared Detectors, *Materials Science and Engineering*, B51, pp12-17.

Taylor-Firth, A. & Laycock, E.A., 1999,

Weathering Simulation for Durability Assessment of the In-Service Performance of Construction Materials, *Quarterly Journal of Engineering Geology*, Vol. 32, pp 291 – 301.

Terzaghi, K., 1943,

Theoretical Soil Mechanics., John Wiley and sons inc, New York.

Track Access, 1998,

Ballast- Work on Asset Specification, Issue 2.0, Australia.

Türler, D., Griffith, B.T., & Arasteh, D.K., 1997,

Laboratory Procedures for Using Infrared Thermography to Validate Heat Transfer Models, *Insulation Materials: Testing and Applications: Third Volume, ASTM STP 1320*, Graves, R.S. & Zarr, R.R., Eds., American Society for Testing and Materials, 1997.

VR, 1995,

Raidesepelin laatuvaatimukset (Quality requirements for railway ballast in Finland), Valtion Rautatiet, 30.6.1995

Waldon, M., 2000,

Personal Communication,

Washer, G.A., 1998,

Developments for the Non-destructive Evaluation of Highway Bridges in the USA, *NDT & E International*, Vol. 31, No. 4, pp. 245-249.

Weil, G. J., 1992,

Non - Destructive Testing of Bridge, Highway and Airport Pavements, *No Trenches in Town Proceedings of International Conference*, Paris, France, 12-14 Oct., pp 243 – 246.

Weil G.J., 1993,

Non- Destructive of Bridge, Highway and Airport Pavement, *International Conference on NDT of Concrete in the Infrastructure*, Deardon, Michigan, 9-11 June, pp 93 – 105.

Weil, G.J., 1995,

Non– Destructive testing of Bridge, Highway and Airport Pavements, *International Symposium on Non – Destructive Testing in Civil Engineering (NDT-CE)*, DGZfP, Berlin, Vol. 1, 26-28 Sept., pp 467 – 474.

Wensink, W.A., 1993,

Dielectric Properties of Wet Soils in the Frequency Range 1-3000 MHz, Geophysical Prospecting, Vol. 41, pp671 - 696

Yang, W.J., 1989,

Handbook of Flow Visulization, Hemisphere Publishing Corp. pp 531- 553.

Appendix A

Density

Clean Ballast

	1	2
Container (kg)	15.91	15.91
Container + Ballast (kg)	191.818	192.152
Mass of ballast (kg)	175.91	176.24
Volume (m^3)	0.1095	0.1095
Density kg/ m^3	1606.47	1609.50

Density kg/ m^3 **1605 ± 10**

Spent Ballast

	1	2
Container (kg)	15.91	15.91
Container + Ballast (kg)	212.735	213.953
Mass of ballast (kg)	196.825	198.043
Volume (m^3)	0.1095	0.1095
Density kg/ m^3	1797.49	1808.61

Density kg/ m^3 **1800 ± 10**

Aggregate Crushing Value (ACV) Testing Values

Spent Ballast

	1	2	3
Bowl (kg)	2.83	2.83	2.83
Bowl + Ballast (kg)	5.99	5.94	6.04
Mass of ballast (kg)	3.160	3.114	3.212
Mass passing 2.36mm sieve (kg)	0.700	0.622	0.676
% fines	22.2	20.0	21.0

Average % fines 21.1%

Clean Ballast

	1	2	3
Bowl (kg)	2.83	2.83	2.83
Bowl + Ballast (kg)	5.86	6.16	6.23
Mass of ballast (kg)	3.036	3.331	3.408
Mass passing 2.36mm sieve (kg)	0.538	0.587	0.587
% fines	17.7	17.6	17.2

Average % fines 17.5%

Ten percent fines value (TFV), test results

Spent Ballast

	1	2	3	4	5	6	7
F= load over 10 minutes (kN))	363	95	220	160	160	140	140
Mass of Ballast (kg)	3.16	2.85	3.11	3.07	3.12	3.15	3.15
Mass passing 2.36mm sieve (kg)	0.69	0.05	0.56	0.33	0.46	0.31	0.30
M= % fines	21.7	1.8	18.0	10.8	14.8	9.8	9.5
F=(14f)/(m+4)	197.46	229.78	140.09	151.57	118.98	141.77	144.77

Average of valid (underlined)
Values of F 146.04

Clean Ballast

	1	2
F= load over 10 minutes (kN))	250	25095
Mass of Ballast (kg)	3.42	3.46
Mass passing 2.36mm sieve (kg)	0.32	0.35
M= % fines	9.5	10.1
F=(14f)/(m+4)	259.66	248.20

Average of valid (underlined)
Values of F 253.93

Arregate Impact Value (AIV) Test Results

Spent Ballast

	1	2	3
Bowl (kg)	2.826	2.826	2.826
Bowl +Ballast (kg)	3.480	3.475	3.480
Ballast [M1] (kg)	0.654	0.649	0.654
Tray (kg)	0.454	0.454	0.454
Tray + ballast passing 2.36mm sieve (kg)	0.528	0.525	0.527
Ballast passing 2.36mm sieve [M2] (kg)	0.074	0.071	0.073
AIV %	11.3	10.9	11.2

Average AIV 11.1%

Clean Ballast

	1	2	3
Bowl (kg)	2.826	2.826	2.826
Bowl +Ballast (kg)	3.460	3.505	3.553
Ballast [M1] (kg)	0.634	0.679	0.727
Tray (kg)	0.454	0.454	0.454
Tray + ballast passing 2.36mm sieve (kg)	0.509	0.526	0.516
Ballast passing 2.36mm sieve [M2] (kg)	0.055	0.072	0.062
AIV %	8.7	10.6	8.5

Average AIV 9.3%

Sieve Analysis

Clean Ballast

Total Mass of Clean Ballast Tested = 74211g
Mass Retained on 20 mm = 73653g
Mass Passing 20 mm sieve = 558g

Sieve test 1:

Retaining Sieve Size (mm)	Mass Including Container (g)	Nett Mass (g)	Percentage Retained (%)	Percentage Passing (%)
75	1203	0	0	100.00
67	1203	0	0	100.00
50	5116	4313	5.81	94.19
37.5	37519	33504	45.15	49.04
28	28258	25046	33.75	15.29
20	12396	10790	14.54	0.75
14	1287	484	0.65	0.10
10	874	71	0.10	0.00
6.3	806	3	0.00	0.00
5	803	0	0	0.00
	Totals	74211	100	

Sieve Test 2

Retaining Sieve Size (mm)	Mass Including Container (g)	Nett Mass (g)	Percentage Retained (%)	Percentage Passing (%)
75	1203	0	0	100.00
67	1203	0	0	100.00
50	5056	4253	5.73	94.27
37.5	37603	33588	45.26	49.01
28	28316	25104	33.83	15.18
20	12330	10724	14.45	0.73
14	1285	482	0.65	0.08
10	850	47	0.06	0.02
6.3	816	13	0.02	0.00
5	803	0	0	0.00
	Totals	74211	100	

Spent Ballast

The ballast was initially cleaned with Sodium Hexametaphosphate.

Total mass of Spent Ballast = 84490 g
Mass retained on 20 mm sieve or above = 49381 g
Mass passing 20 mm sieve = 35109 g

Sieve Test 1

Retaining Sieve Size (mm)	Mass Including Container (g)	Nett Mass (g)	Percentage Retained (%)	Percentage Passing (%)
75	N/A	0	0	100.00
67	N/A	0	0	100.00
50	N/A	1300	1.54	98.46
37.5	N/A	12616	14.93	83.53
28	N/A	17292	20.47	63.06
20	N/A	18173	21.51	41.55
	Part Total	49381	58.45	
14	2879	1558	1.84	39.71
10	28592	23308	27.59	12.12
6.3	8363	5721	6.77	5.35
5	3382	972	1.15	4.20
3.35	2200	879	1.04	3.16
2	1964	643	0.76	2.40
1.18	1737	416	0.49	1.91
0.6	1400.55	1369.28	1.62	0.29
0.425	185.97	175.32	0.21	0.08
0.3	79.21	68.23	0.08	0.00
	Part Total	35109.83	41.55	
	Total	**84490.83**	**100**	

Sieve Test 2

Retaining Sieve Size (mm)	Mass Including Container (g)	Nett Mass (g)	Percentage Retained (%)	Percentage Passing (%)
75	N/A	0	0	100.00
67	N/A	0	0	100.00
50	N/A	1119	1.32	98.68
37.5	N/A	13124	15.53	83.14
28	N/A	16784	19.86	63.28
20	N/A	17546	20.77	42.51
	Part Total	48573	57.49	
14	2879	2325	2.75	39.76
10	28622	23338	27.62	12.14
6.3	7863	5221	6.18	5.96
5	3976	1566	1.85	4.10
3.35	2200	879	1.04	3.06
2	2305	984	1.16	1.90
1.18	1376	55	0.07	1.83
0.6	1356.37	1325.1	1.57	0.27
0.425	152.56	141.91	0.17	0.10
0.3	91.34	80.36	0.10	0.00
	Part Totals	35915.37	42.51	
	Total	**84488.37**	**100.00**	

List of Publications

Journal Papers:

1. Clark M. R., McCann D. M. and Forde M. C., (2000), *Dynamic Testing of Railway Ballast, Using the Slake Durability Test and Determining Ballast Life.*, Quarterly Journal of Engineering Geology (submitted and awaiting referees report)

2. Clark M. R., McCann D. M. and Forde M. C., (2000), Infra-red thermographic inspection of railway trackbed ballast, *NDT&E International* (submitted and awaiting referees reports)

3. Clark M. R., Gillespie R., Kemp T., McCann D. M. and Forde M. C., (2000) Electromagnetic properties of railway ballast., *NDT&E International* (refereed, corrected and accepted for publication).

4. Gallagher G. P., Leiper Q., Clark M. R. and Forde M. C (2000) Ballast evaluation using ground-penetrating radar, *Railway Gazette International*, Vol 156, No. 2, 101-102.

5. Forde M. C., McCann D. M., Clark M. R., Broughton K. J., Fenning P. J. and Brown A. (1999) Radar measurement of Bridge scour, *NDT&E International*, 1999, 32, 481-492.

6. Gallagher G. P., Leiper Q., Williamson R., Clark M. R. and Forde M. C. (1999) The application of time domain ground penetrating radar to evaluate railway track ballast. *NDT&E International*, 1999, 32, 463-468.

7. Colla C., Burnside C. D., Clark M. R., Broughton K. J. and Forde M. C. (1998) Comparison of laboratory and simulated data for radar image interpretation. *NDT&E International*, 1998, 31 (6), 439-444.

Conference Papers:

8. Clark M. R., McCann D. M. and Forde M. C. (2001) Infrared thermographic survey of delamination of bridge decks. *Proc. 9th Int. Conf. Structural Faults and Repair 2001,* Engineering Technics Press London 2001.

9. Clark M. R., McCann D. M. and Forde M. C. (2001) Infrared thermographic survey of tunnel linings. *Proc. 9th Int. Conf. Structural Faults and Repair 2001,* Engineering Technics Press London 2001.

10. Clark M. R., McCann D. M. and Forde M. C. (2001) Theory and applications of infrared thermographic. *Proc. 9th Int. Conf. Structural Faults and Repair 2001,* Engineering Technics Press London 2001.

11. Clark M. R., McCann D. M. and Forde M. C. (2001) Infrared thermographic survey of delamination of bridge decks. *Proc. 4rd Int. Conf..Railway Engineering 2001,* Engineering Technics Press, London 2001.

12. Clark M. R., McCann D. M. and Forde M. C. (2001) Determining Dynamically the Life-span of Railway Ballast Using the Slake Durability Test. *Proc. 4rd Int. Conf..Railway Engineering 2001,* Engineering Technics Press, London 2001.

13. Clark M. R., McCann D. M. and Forde M. C. (2000) Infrared investigation of trackbed ballast. *Proc. 3rd Int. Conf..Railway Engineering 2000,* Engineering Technics Press, London 2000.

14. Gallagher G. P., Leiper Q., Clark M. R. and Forde M. C. (1999) Laboratory and full scale prototype evaluation of ground penetrating radar on railway trackbed ballast. *Proc. World Congress on Railway Research. Japan 1999.*

15. Clark M. R. and Forde M. C. (1999) Infrared thermographic investigation of ballast. *Proc. 2nd Int. Conf. Railway Engineering-99,* Engineering Technics Press, London 1999.

16. Gallagher G. P., Leiper Q., Clark M. R. and Forde M. C. (1999) Identification of railway track bed anomalies using monostatic GPR reflection techniques *Proc.*

2nd Int. Conf. Railway Engineering-99, Engineering Technics Press, London 1999.

17. Clark M. R., Gillespie R., Kemp T., McCann D. M. and Forde M. C., (1999) Electromagnetic properties of railway ballast. *Proc. 1st Int. Conf. Railway Engineering-98,* Engineering Technics Press, London 1999, pp. 21-28.

18. Gallagher G. P., Leiper Q., Williamson R., Clark M. R. and Forde M. C., (1999) Application of ground penetrating radar in the railway industry. *Proc. 1st Int. Conf. Railway Engineering-98,* Engineering Technics Press, London 1999, pp. 33-36.

19. McCann D. M., Fenning P. J., Brown A., Clark M. R., Broughton K. J. and Forde M. C., (1998) Radar measurement of bridge scour, *Proc. 1st Int. Conf. Railway Engineering-98,* Engineering Technics Press, London 1999, pp. 179-194.

20. Davidson N. C., Forde, M. C., Hardy M. S. A., McCann D. M., Colla C., Clark M. R., Broughton K. J. and Das P. C., (1997) Field trials to establish accuracy of radar for scour detection. *Proc. 7th Int. Conf. Structural faults and repair -97, vol. 1,* Engineering Technics Press, Edinburgh 1997, pp 171 - 178.

21. Colla C., Burnside C. D., Clark M. R. and Forde M. C. (1997) Comparison of laboratory and simulated data for radar image interpretation. *Proc. 7th Int. Conf.*

Structural faults and repair -97, vol. 3, Engineering Technics Press, Edinburgh 1997, pp 523 - 528.